HANDLING QUALITY ORIENTED FAULT TOLERANT LONGITUDINAL FLIGHT CONTROL ALGORITHM DESIGN FOR A JET TRAINER AIRCRAFT

BİR JET EĞİTİM UÇAĞI İÇİN UÇUŞ KALİTESİ ODAKLI HATA DAYANIMLI BOYLAMSAL UÇUŞ KONTROL ALGORİTMASI TASARIMI

BAHADIR GÖKÇEASLAN

PROF. DR. SELAHATTİN ÇAĞLAR BAŞLAMIŞLI

Supervisor

Submitted to

Graduate School of Science and Engineering of Hacettepe University

as a Partial Fulfillment to Requirements

for the Award of the Degree of MASTER OF SCIENCE

in Mechanical Engineering

2023

ABSTRACT

HANDLING QUALITY ORIENTED FAULT TOLERANT LONGITUDINAL FLIGHT CONTROL ALGORITHM DESIGN FOR A JET TRAINER AIRCRAFT

Bahadır GÖKÇEASLAN

Master of Science, Mechanical Engineering Department

Supervisor: Prof. Dr. Selahattin Çağlar BAŞLAMIŞLI

January 2023, 124 pages

In the scope of the thesis an alternative longitudinal flight control algorithm, which satisfies predefined stability and performance requirements, in case of a specific fault is aimed for a jet trainer aircraft.

Base flight control algorithm, which is being used currently, requires CG_X position information to schedule controller parameters to achieve predefined stability and performance goals. In case of fault in CG_X position information, where current CG_X position information is not available or has low fidelity, flight control algorithm is automatically being fed with mid CG_X position parameters. According to current CG_X position, especially when current CG_X position closes to edge of CG_X range, there are significant stability and performance degradations in longitudinal flight control characteristics of the aircraft. An alternative longitudinal flight control

algorithm which does not require CG_X position information to sustain nominal stability and performance is the topic of the thesis.

Six of degree of freedom nonlinear aircraft model is constructed with sub-blocks which represents different systems, to represent jet trainer aircraft model completely. This nonlinear model is trimmed around a specific design point and linear time invariant models are generated with small perturbations around this design point, to be used in flight control algorithm design processes.

Flight control algorithm design requirements in terms of stability and performance are explained in detail to guide design process and asses the final controllers. Detailed design process of base controller and two alternate controllers are explained and applied for a specific design point. Base controller and the first alternative controllers are based on same architecture, PI with feedforward elements, but with different design methodologies. Base controller parameters are calculated via pole – zero assignment. Parameter space approach methodology for SAS and structured H_∞ synthesis methodology for CAS design are followed in the first alternative controller . The second alternative controller is based on explicit model following architecture with disturbance rejection capability. SAS feedback gains are calculated via parameter space approach methodology and structured H_∞ synthesis is used to design disturbance rejection compensator.

Base controller and two alternative controllers are assessed in terms of predefined stability and performance requirements. The second alternative controller, explicit model following with disturbance rejection, has been found as the best one. It satisfies all stability and performance requirements even tough in case of fault in CG_X position information. It has been observed that exact reference model match has been achieved with the second alternative controller with significant disturbance ejection capability. Stability has been ensured with parameter space approach which gives a 2D feedback gains basis which guarantees predefined stability requirements in Nyquist diagram. On the other hand, the first alternative controller has showed that even with a different design technique the architecture, PI with feedforward elements, is weak in terms of

disturbance rejection. The main idea in the second alternative controller architecture is that; changes in internal aircraft dynamics and uncertainties can be assumed as disturbance and exact nominal performance can be reached with a sufficient rejection of those disturbances.

Keywords: flight control, robust control, fault tolerant control, parameter space approach, explicit model following, handling qualities, structured H_∞ synthesis, disturbance rejection controller

ÖZET

BİR JET EĞİTİM UÇAĞI İÇİN UÇUŞ KALİTESİ ODAKLI HATA DAYANIMLI BOYLAMSAL UÇUŞ KONTROL ALGORİTMASI TASARIMI

Bahadır GÖKÇEASLAN

Yüksek Lisans, Makine Mühendisliği Bölümü
Tez Danışmanı: Prof. Dr. Selahattin Çağlar BAŞLAMIŞLI
Ocak 2023, 124 sayfa

Tez kapsamında, bir jet eğitim uçağı için belirli bir hata durumunda önceden tanımlanmış olan kararlılık ve başarım isterlerini sağlayan alternatif bir boylamsal uçuş kontrol algoritması tasarımı hedeflenmiştir.

Jet eğitim uçağında güncel olarak kullanılmakta olan boylamsal uçuş kontrol algoritması önceden belirlenmiş olan kararlılık ve başarım gereksinimlerini sağlayabilmek için kontrolcü parametrelerinin CG_X pozisyon bilgisine göre düzenlenmesine ihtiyaç duymaktadır. CG_X Pozisyon bilgisinde bir hata olması durumunda, hesaplanamaması ya da hesaplanan değerin düşük güvenirliğe sahip olduğu tespit edilmesi durumunda, uçuş kontrol algoritması CG_X pozisyonun ortada olduğu konfigürasyona ait olan parametreleri otomatik olarak

kullanmaktadır. Güncel CG_X pozisyonuna göre, özellikle de CG_X'in tanımlı olduğu aralığın uç noktalarına yakın bir yerde olduğu zaman, boylamsal uçuş kararlılık ve başarım oranlarında ciddi düşüşler gözlemlenmiştir. Bu sebeple nominal kararlılığı ve başarım oranını sürdürebilmek için CG_X pozisyon bilgisine ihtiyaç duymayan bir boylamsal uçuş kontrol algoritması bu tezin konusunu oluşturmaktadır.

Altı serbestlik dereceli doğrusal olmayan uçak modeli, jet eğitim uçağının özelliklerini tam olarak temsil edecek şekilde farklı sistemleri temsil eden alt bloklar ile oluşturulmuştur. Bu altı serbestlik dereceli lineer olmayan model, uçuş kontrol algoritması tasarımı sürecinde kullanılmak için belirli bir tasarım noktası etrafında denge koşuluna getirilmiş ve küçük pertürbasyonlarla bu denge noktası etrafında doğrusallaştırılarak gerekli olan zaman bağımsız doğrusal modeller elde edilmiştir. Uçuş kontrol algoritması tasarım gereksinimleri uçuş kontrol algoritması tasarım sürecini yönlendirmek ve tasarlanan nihai kontrolcüleri değerlendirmek için kararlılık ve performans başlıkları altında tanımlanmıştır. Güncel kontrolcü ve buna alternatif iki adet kontrolcü tasarımı detaylı şekilde verilmiş ve belirli bir uçuş koşulu için uygulanmıştır. Güncel kontrolcü ve birinci alternatif kontrolcü aynı ileri beslemeli PI mimarisine sahip olmakla birlikte farklı tasarım metotları ile tasarlanmıştır. Güncel kontrolcüye ait parametreler kutup – sıfır atama metodu ile hesaplanırken birinci alternatif kontrolcüde; kararlılık arttırım sistemi için parametre uzayı yaklaşımı kullanılmıştır, kontrol arttırım sistemi ise sabit bir kontrolcü mimarisi için H_∞ normu sentezi metodu kullanılmıştır. İkinci alternatif kontrolcü bozuntu baskılama ile referans model takibi tabanlı bir yapı kullanmaktadır. Stabilite arttırım sistemi için yine parametre uzayı yaklaşımı metottu kullanılmıştır. Bozuntu baskılayıcı denetleyici ise sabit bir kontrolcü mimarisi için H_∞ normu sentezine dayalı metot ile tasarlanmıştır.

Tasarlanan kontrolcüler önceden belirlenmiş kararlılık ve performans gereksinimleri doğrultusunda değerlendirilmiş ve en başarılı kontrolcünün yapısını ikinci alternatif kontrolcü, bozuntu baskılama ile referans model takibi, olduğu görülmüştür. Bozuntu baskılayıcı kontrolcünün CG_X pozisyon bilgisinde hata olması durumunda dahi tüm kararlılık ve performans isterlerini karşılamaya

devam ettiği görülmüştür. İkinci alternatif kontrolcünün bozuntu baskılama kabiliyeti sayesinde referans modeli hata durumunda dahi tam olarak takip ettiği gözlemlenmiştir. Parametre uzayı yaklaşımı sayesinde önceden belirlenmiş olan kararlılık isterlerini Nyquist diyagramı üzerinde sağlayan iki boyutlu parametre uzayı hesaplanmış ve bu sayede hata durumunda dahi kararlılık garanti edilmiştir. Birinci alternatif kontrolcü göstermiştir ki farklı bir tasarım metoduyla dahi söz konusu mimari, ileri beslemeli PI, bozuntu baskılama açısından zayıf. İkinci alternatif kontrolcü uçağın iç dinamiklerinde meydana gelen değişiklikleri ve belirsizlikleri birer bozuntu olarak algılama ve bozuntuyu baskılayarak referans model takibini sağlamak üzerine kurgulanmıştır.

Anahtar Kelimeler: uçuş kontrol algoritması, hata dayanımlı kontrol, parametre uzayı yaklaşımı, model takibi, uçuş kullanım kalitesi, H_∞ norm sentezi, bozuntu baskılayıcı kontrol

ACKNOWLEDGEMENT

First, I am grateful to my lovely family for their love, patient, and sacrifice. They have supported me through all my life.

I would like to express my special thanks to my supervisor Prof. Dr. Selahattin Çağlar Başlamışlı for his guidance and patient.

I am grateful to my friends Şahika Akdoğan, Zafer Kaçan, İrem Kırcı, and Melis Özen for their support and patient. I also want to express my special thanks to my colleagues Onur Albostan, Ayşenur Bıçakçı, Salih Volkan Özkan, Volkan Mesce, Sadettin Balcan and Mustafa Çağatay Şahin for making the work hours enjoyable.

TABLE OF CONTENTS

LIST OF FIGURES

LIST OF TABLES

SYMBOLS AND ABBREVIATIONS

Symbols

L	Lift
D	Drag
M	Aircraft body y axis moment
L	Aircraft body x axis moment
N	Aircraft body z axis moment
U	Aircraft body x axis velocity
V	Aircraft body y axis velocity
W	Aircraft body z axis velocity
p	Body axis roll rate
q	Body axis pitch rate
r	Body axis yaw rate
α	Angle of Attack
β	Side slip angle
v_s	Speed of sound
V_T	True air speed
F_X	Aircraft body x axis force
F_y	Aircraft body y axis force
F_z	Aircraft body z axis force
F_A	Aerodynamic Force
M_A	Aerodynamic Moment
F_T	Thrust
M_T	Engine induced moment
C_X, C_Y, C_Z	Nondimensionalized body axis force coefficients
C_l, C_M, C_N	Nondimensionalized body axis moment coefficients
C_{X_Q}	Contribution of pitch rate to aircraft body x axis force
$C_{X_{LEF}}$	Contribution of LEF position to aircraft body x axis force
$C_{X_{Q_{LEF}}}$	Contribution of pitch rate to aircraft body x axis force w.r.t

	LEF position
C_{Z_Q}	Contribution of pitch rate to aircraft body z axis force
$C_{Z_{LEF}}$	Contribution of LEF position to aircraft body z axis force
$C_{Z_{Q_{LEF}}}$	Contribution of pitch rate to aircraft body z axis force w.r.t LEF position
C_{Y_R}	Contribution of yaw rate to aircraft body y axis force
$C_{Y_{R_{LEF}}}$	Contribution of yaw rate to aircraft body y axis force w.r.t LEF position
C_{Y_P}	Contribution of roll rate to aircraft body y axis force
$C_{Y_{P_{LEF}}}$	Contribution of roll rate to aircraft body y axis force w.r.t LEF position
$C_{Y_{LEF}}$	Contribution of LEF position to aircraft body y axis force
$C_{Y_{FLP}}$	Contribution of flaperon position to aircraft body y axis force
$C_{Y_{FLP_{LEF}}}$	Contribution of flaperon position to aircraft body y axis force w.r.t LEF position
$C_{Y_{RUD}}$	Contribution of rudder position to aircraft body y axis force
C_{M_Δ}	Nondimensionalized body y axis delta moment coefficient
$C_{M_{LEF}}$	Contribution of LEF position to aircraft body y axis moment
C_{M_Q}	Contribution of pitch rate to aircraft body y axis moment
$C_{M_{Q_{LEF}}}$	Contribution of pitch rate to aircraft body y axis moment w.r.t LEF position
C_{N_R}	Contribution of yaw rate to aircraft body z axis moment
$C_{N_{R_{LEF}}}$	Contribution of yaw rate to aircraft body z axis moment w.r.t LEF position
C_{N_P}	Contribution of roll rate to aircraft body z axis moment
$C_{N_{P_{LEF}}}$	Contribution of roll rate to aircraft body z axis moment w.r.t LEF position
$C_{N_{LEF}}$	Contribution of LEF position to aircraft body z axis moment
$C_{N_{FLP}}$	Contribution of flaperon position to aircraft body z axis moment

$C_{N_{FLP_{LEF}}}$	Contribution of flaperon position to aircraft body z axis moment w.r.t LEF position
$C_{N_{RUD}}$	Contribution of rudder position to aircraft body z axis moment
$C_{N_{\beta}}$	Contribution of side slip angle to aircraft body z axis moment
C_{l_R}	Contribution of yaw rate to aircraft body x axis moment
$C_{l_{R_{LEF}}}$	Contribution of yaw rate to aircraft body x axis moment w.r.t LEF position
C_{l_P}	Contribution of roll rate to aircraft body x axis moment
$C_{l_{P_{LEF}}}$	Contribution of roll rate to aircraft body x axis moment w.r.t LEF position
$C_{l_{LEF}}$	Contribution of LEF position to aircraft body x axis moment
$C_{l_{FLP}}$	Contribution of flaperon position to aircraft body x axis moment
$C_{l_{FLP_{LEF}}}$	Contribution of flaperon position to aircraft body x axis moment w.r.t LEF position
$C_{l_{RUD}}$	Contribution of rudder position to aircraft body x axis moment
$C_{l_{\beta}}$	Contribution of side slip angle to aircraft body x axis moment
CG_X	Position of center of gravity along aircraft body x axis
CG_{XR}	Reference position of center of gravity along aircraft body x axis
I_X, I_Y, I_Z	Moment of inertia about aircraft body x, y, and z axes
I_{XZ}	Product of moment of inertia w.r.t aircraft body x and z axes
K_q	Pitch rate gain
H_∞	H infinity norm
W_P	Performance Weight
W_U	Uncertainty Weight

σ	Ratio of dynamic pressure to static pressure
g_d	Gravitational acceleration
B	Span of wing
S	Wing area
μ	Dynamic viscosity
S	Laplace's domain operator
θ	Pitch angle
$\emptyset$	Bank angle
ψ	Yaw angle
w	Frequency
φ	Phase angle
τ	Time constant
Λ	Eigen value
l_{chr}	Characteristic length
η_{HT}	Horizontal tail effectiveness
$H_{X_{Engine}}$	Engine angular momentum about aircraft body x axis

Abbreviations

LTI	Linear Time Invariant
LG	Landing Gear
MFW	Most Forward
NMNL	Nominal
MAFT	Most Aft
FFW	Feed forward
TPR	Transient Peak Ratio
M	Mach number
E	Error
Re	Reynolds number
Temp	Temperature
ISA	International Standard Atmosphere

LEF	Leading Edge Flap
TEF	Trailing Edge Flap
FLP	Flaperon
RUD	Rudder
PIO	Pilot Induced Oscillation
Mac	Mean aerodynamic chord
q_{er}	Pitch rate error
SAS	Stability Augmentation System
CAS	Control Augmentation System
LG	Landing Gear
GM	Gain Margin
PM	Phase Margin
SM	Stability Margin
PI	Proportional – Integrator
IMU	Inertial Measurement Unit
rps	Radian per second

1. INTRODUCTION

The first controlled, powered, and sustained flight with an aircraft heavier than air was performed on 17th of December 1903 by Wright brothers.[1] There were some difficulties that Wright brother had to encounter, such as controlling the aircraft. A biomimicking based approach, “wing – wrapping”, was followed to solve this problem. A flexible wing shaped box which can re-shaped like birds flex its wing was used to control the aircraft in roll axis during the flight. [2]

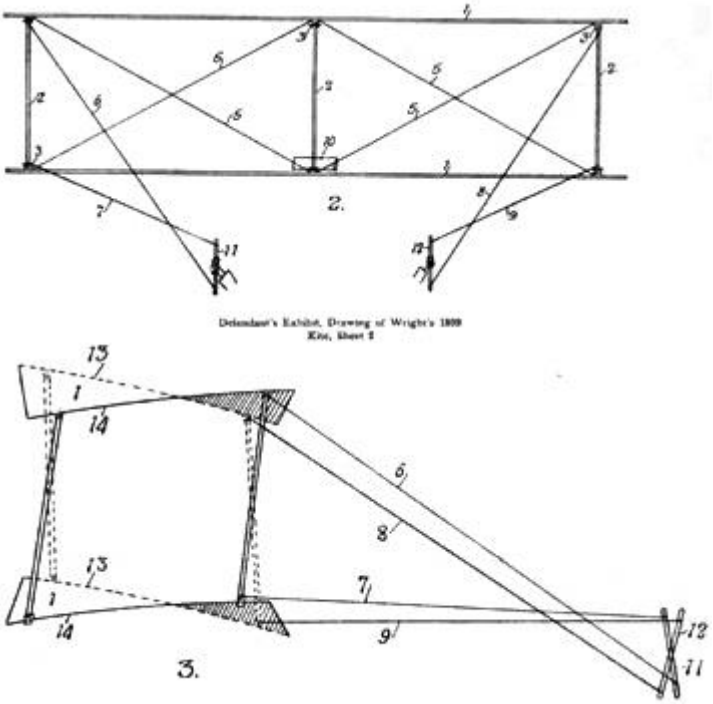

Figure 1. Wing wrapping [2]

From 1903, when the Wright brothers made the first powered and controlled flight, to time of the First World War aircrafts were designed with same configuration, a wing mounted onto fuselage, horizontal tail, and vertical tail. Control of the aircrafts were performed with design of elevator and rudder at the tail and ailerons at the wing. Elevators were used to control pitch axis; lateral and directional control was performed with ailerons and rudder; Wright brothers wing wrapping mechanism was replaced with these ailerons. Design of the control surfaces made pilots enable to control aircraft with a centered stick and pedals.[3]

Until the time of the Second World War, aircrafts were equipped with this pulley system, until the forces that pilots had to apply become so heavy because of increasing aircraft dimensions and speed. At this point “mechanical linkages which make pilot to transfer more power from stick to control surfaces” were introduced according to [3].

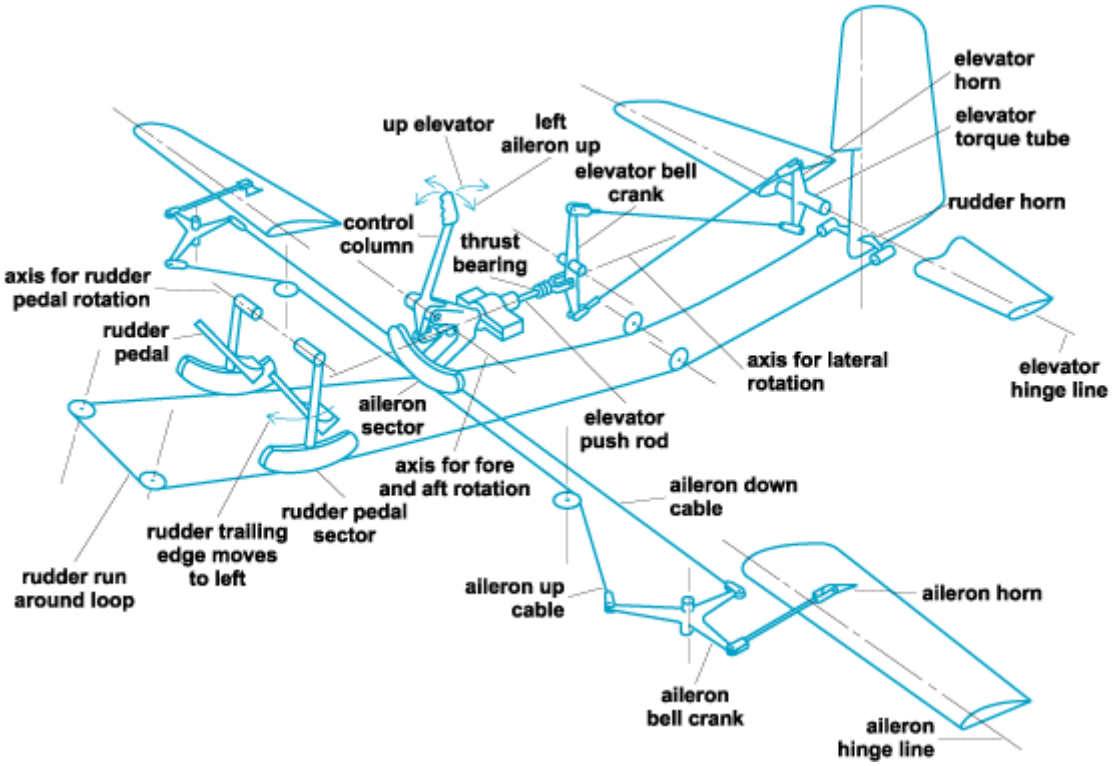

Figure 2. Classical flight control system [4]

Aircraft dimensions had continued to increase to carry more payloads such as passengers, weapons, and cargo. Mechanical linkages became insufficient to assist increased loads and after this point hydro-mechanical systems were introduced to help the pilot to deal with increased loads.

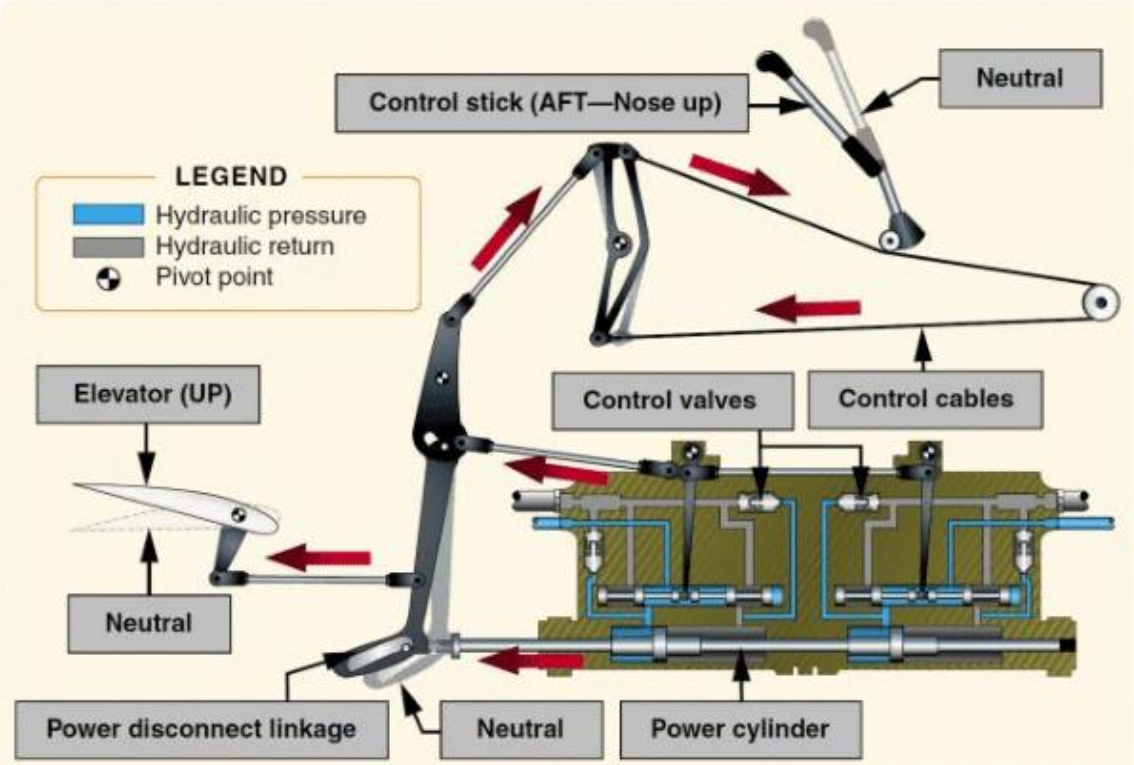

Figure 3. Hydromechanical flight control system [5]

Hydromechanical flight control systems worked well and proved themselves during the Second World War. Hydromechanical flight control systems were also used for the first and the second-generation jet civil transport aircrafts such as Boeing 720 (1960) , Douglas DC10 (1970), and Airbus A300 (1974) .

After the hydromechanical flight control systems, as parallel to improvements in electronics and computers, fully electronic fly by wire flight control systems were designed. In fly by wire flight control systems pilot stick and pedal inputs are transformed to electrical signals and then transmitted to related actuators. Introduction of fly by wire flight control systems also made enable to design automatic stability augmentation systems which use inertial rates to augment aircraft stability. Stability augmentation systems can handle with instability levels that pilot cannot augment by itself. More unstable aircrafts which are also more maneuverable had started to be designed and produced with the help of stability augmentation systems.

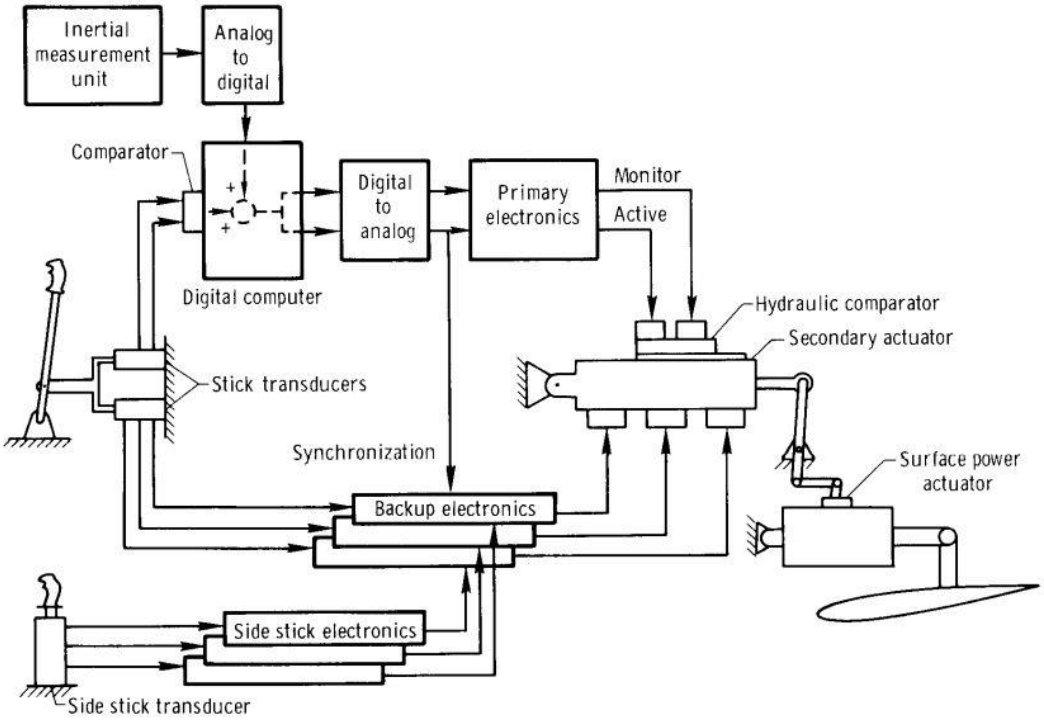

Figure 4. Fly by wire flight control system [6]

Fly by wire flight control systems are more effective and faster as compared to classical flight control systems. More sophisticated aircrafts are designed with help of fly by wire flight control systems. The main power of the fly by wire flight control systems come from capability of integrated operation with a series of systems which includes a flight control computer, a series of sensors, actuators, and sophisticated algorithms. This integrated structure also comes with some risks. Failure in one of these systems may cause catastrophic effects. Fault of each sub system should be taken into consideration during the design. Capability of fault tolerance plays an important role in fly by wire flight control system concept.

Fault tolerant control is an important topic especially for safety-critical systems. A jet trainer aircraft is a good example for a safety-critical system since jet trainers are used for the purpose of trainee pilot education, so; flight control algorithms in these aircrafts must be fault tolerant against possible failures.

There have been many different applications of fault tolerant flight control algorithm design.

There are passive and active fault tolerant control algorithms. In active algorithms status of the system is being monitored and any failure is being tried to be identified. After the classification process a predefined modification is being performed to control law designed for the nominal condition. Neural networks-based algorithms can be given as an example to active fault tolerant algorithms. They can be trained against possible failure conditions and then they can be used to provide corrective control action in case of failure. Usage of such neural networks with Nonlinear Dynamic Inversion technique is a very common application. [7]

The passive fault tolerant control algorithms, which will be applied in the scope of this proposed thesis, is not being modified in case of failure on the other hand. The key idea in passive fault tolerant algorithms is “robustness”. Algorithm is aimed to be robust in terms of stability and performance against possible failures. Different robust control techniques may be used for this purpose.

H_∞ norm minimization is a very common frequency domain robust control design technique. This methodology is based on minimization of H_∞ norm of interested transfer function or transfer functions, such as sensitivity or co sensitivity transfer functions. There are some experimental applications of this technique in aerospace.[8] H_∞ norm minimization technique is based on worst case scenario. Unstructured uncertainty can be modeled with multiplicative or additive ways. Solution of the H_∞ norm minimization problem is based on solution Riccati equation. Resulted controller’s order may be high and required to be reduced with a proper order reduction method.[9] Fixed order controller structure also can be tuned with various optimization algorithms such that resulted controller minimizes desired H_∞ norms. This technique is called as structured H_∞ synthesis.[10]

H_∞ loop shaping is also another effective method in terms of robust flight control algorithm design. This technique is so like classical loop shaping. The main idea is finding all stabilizing controllers via co prime factorization to reach shaped plant. (Shaped plant is one which has been given desired loop shape) An application of this method has been performed for a fly by wire helicopter.[11]

Robust Eigen structure assignment is another useful technique for multi-inputs multi-outputs systems. This technique guarantees decoupling between desired modes (in case of full rank solution). Structured uncertainty is introduced to state space models. Robustness is defined in Laplace's domain. The gains which guarantee the desired Eigen space and satisfy predefined decoupling in case of structured uncertainty is found via optimization. [12]

Parameter space approach is also very powerful method to design robust controllers. Robustness can be defined in both Laplace's domain and/or frequency domain. It is more useful especially for the controller structures which includes less than or equal to 3 variables. (In fourth and higher dimension visual tractability is being lost) [13] This technique deals with the uncertain controller parameters and find an acceptable "n" dimensional region which sustains predefined stability or Eigen value parameters (natural frequency or damping ratio)

Quantitative feedback theory (QFT) is the last method that will be explained in the scope of this literature survey. It is a frequency domain-based design technique. QFT deals all possible uncertain plants and defines the required loop shaping in terms of L(jw), S(jw) or T(jw) with respect to the predefined frequency domain stability and performance requirements. It is a very powerful method in terms of robust flight control algorithm design problem, there are many applications.[14] [15]

In the scope of the thesis a fault tolerant longitudinal flight control algorithm which is required to be robust in terms of stability and performance in case of CG_X position information fault is aimed. Stability is ensured via feedback stabilization with parameter space approach technique. Explicit model following is reached with disturbance rejection outer loop controller which is designed with structured H_∞ synthesis.

2. NONLINEAR AIRCRAFT MODEL

In the scope of the thesis six degree of freedom nonlinear model of a jet trainer aircraft is used. Jet trainers are used for education of trainee pilots, aerobatic demonstrations, and some light attack missions.

LTI models are generated around an equilibrium in other words trim point by small perturbation. Flight control algorithm design and flying-handling qualities assessment processes are performed with these LTI models. Anatomy of the nonlinear aircraft model and definition of subfunctions will be given in next sections.

2.1 Anatomy of the Nonlinear Aircraft Model

The nonlinear aircraft model directly reflects dynamics of the jet trainer aircraft. Model includes series of subfunctions to represent complete system; aerodynamics, atmosphere, equations of motion, engine, and mass – inertia dynamics. [16] Actuator and sensor dynamics are implemented in flight control algorithm design section, as LTI models.

Earth-Centered-Earth-Fixed frame is used in the nonlinear aircraft model. In ECEF the reference frame is Earth, considered as rigid body, and a geocentric local frame (North-East-Down), which is aligned to center of mass of Earth as fixed point, are defined. Orientation of aircraft body frame w.r.t NED is given with Euler angles. [17]

In addition to the body frame, stability and wind frames are also used for different purposes.[18] Orientation of the aircraft w.r.t NED is given in body frame. Aircraft equation of motions are constructed also in body frame. Flight control algorithm design and analysis processes are performed in stability frame. Detailed explanation of these frames will be given in next sections.

2.1.1 Coordinate Systems

2.1.1.1 Earth Frames

Since Earth is rotating, a reference frame which is aligned to Earth is required. ECEF is used as reference frame which is right-handed coordinate system. The origin of the ECEF is the center of mass of the Earth. X axis points 0 longitude. Y axis point 0 latitude and z axis points North Pole.

A local geocentric frame which is tangent to the surface of the Earth is defined with North-East-Down convention. Origin of the tangent local frame is fixed in ECEF frame. NED frame moves with aircraft and its orientation w.r.t the Earth centered frame is determined with aircraft's latitude and longitude. Orientation of the aircraft is transformed to NED with proper transformation matrices. NED frame is demonstrated in Figure 5.

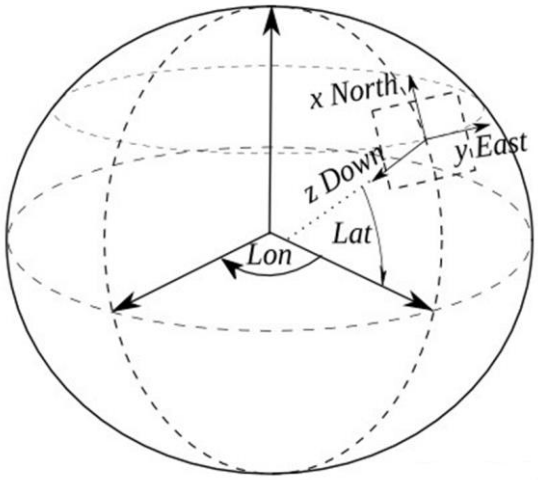

Figure 5. NED frame

2.1.1.2 Aircraft Frames

The body frame of the jet trainer aircraft is standard. The x axis is positive throughout the nose of the aircraft. The y axis is positive through right-wing w.r.t back view of aircraft. The z axis is perpendicular to x-y plane and positive through vertically downward as the aircraft flies in steady wing level condition. Body frame sign notation is given in Figure 6.

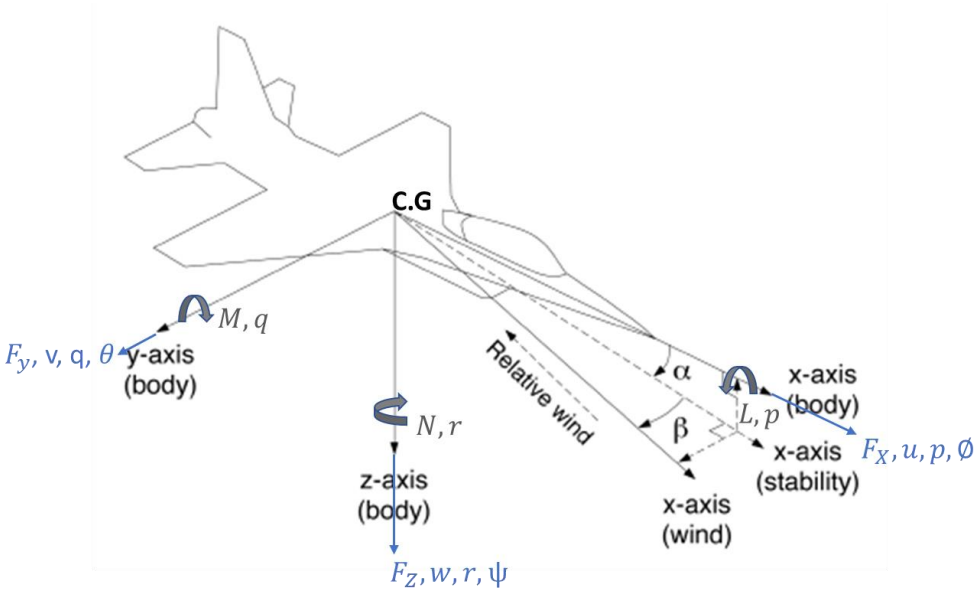

Figure 6. Aircraft body frame sign notation

The forces and moments which apply upon aircraft body frame are comply with the right-hand convention. Moments around x, y, and z axes are labelled as L, M, and N respectively. The body forces through body axes x, y, and z are indicated as F_X, F_y and F_z. The body rates (p, q, r) and Euler angles ($\emptyset$, θ and ψ) are measured w.r.t right hand rule sign convention. The body axes velocities are showed with lover cases (u, v, and w).

Body frame is convenient at most of the time to demonstrate forces and moments apply upon the aircraft. To investigate velocity of the aircraft relative to incoming air that aircraft fly trough, another axis systems are required, which are stability and wind frames. Forces and moments also can be demonstrated on stability and wind frames.

Demonstration of stability and wind frames are given in Figure 7.

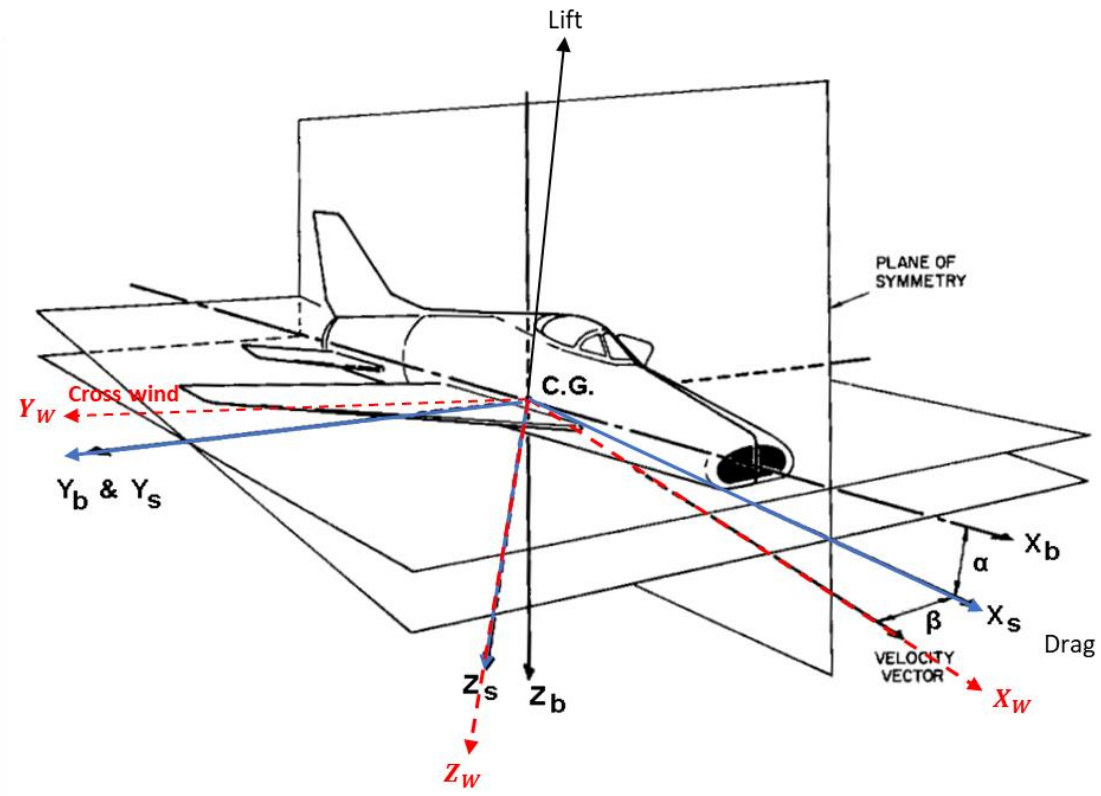

Figure 7. Aircraft stability and wind frames

Stability frame ($x_s, y_s, and\ z_s$) is modified body axis w.r.t angle of attack. Stability x axis is projection of aircraft velocity vector upon plane of symmetry. The angle between the aircraft body x axis and stability x axis is defined as angle of attack. In case of zero degree of angle of attack body axis and stability axis are aligned.

Lift is the force that holds the aircraft in the air. Majority of the lift force is generated by wing, and it is perpendicular to relative air.

Drag is the force that counteracts aircraft motion in air. Every part of the aircraft contributes to total drag of the aircraft. Drag force is parallel to relative air.

$$\alpha = \text{atan}\,(w, \text{u}) \tag{2.1}$$

Wind frame ($x_w, y_w, and\ z_w$) includes side slip angle in addition to angle of attack. Side slip is the angel between velocity vector and stability x axis. In wind axis system cross wind is aligned with y_w, in case of zero cross wind side slip angle

is zero, so; stability and wind axes are aligned to each other. Lift and drag are aerodynamic forces along z_w and x_w.

Side slip angle calculation is given in Eq. (2.2):

$$\beta = \text{asin}\,(\text{v}, v_T) \tag{2.2}$$

Transformation from wind axis to body axis can be performed in two steps. First step is transformation from wind axis to stability axis and second step is transformation from stability axis to body axis.

Transformation from wind axis to stability axis is given in Eq. (2.3):

$$\begin{bmatrix} x_s \\ y_s \\ z_s \end{bmatrix} = \begin{bmatrix} \cos\beta & \sin\beta & 0 \\ -\sin\beta & \cos\beta & 0 \\ 0 & 0 & 1 \end{bmatrix} \begin{bmatrix} x_w \\ y_w \\ z_w \end{bmatrix} \tag{2.3}$$

Transformation from stability axis to body axis is given in Eq.(2.4):

$$\begin{bmatrix} x_b \\ y_b \\ z_b \end{bmatrix} = \begin{bmatrix} \cos\alpha & 0 & \sin\alpha \\ 0 & 1 & 0 \\ -\sin\alpha & 0 & \cos\alpha \end{bmatrix} \begin{bmatrix} x_s \\ y_s \\ z_s \end{bmatrix} \tag{2.4}$$

Complete transformation from wind axis to body axis is given in Eq.(2.5):

$$\begin{bmatrix} x_b \\ y_b \\ z_b \end{bmatrix} = \begin{bmatrix} \cos\alpha & 0 & -\sin\alpha \\ 0 & 1 & 0 \\ \sin\alpha & 0 & \cos\alpha \end{bmatrix} \begin{bmatrix} \cos\beta & \sin\beta & 0 \\ -\sin\beta & \cos\beta & 0 \\ 0 & 0 & 1 \end{bmatrix} \begin{bmatrix} x_w \\ y_w \\ z_w \end{bmatrix} \tag{2.5}$$

Earth fixed reference frame is used for nonlinear aircraft model. Orientation of aircraft body axes w.r.t NED frame is given with Euler angles (∅, θ and ψ).

Demonstration of Euler angles is given in Figure 8.

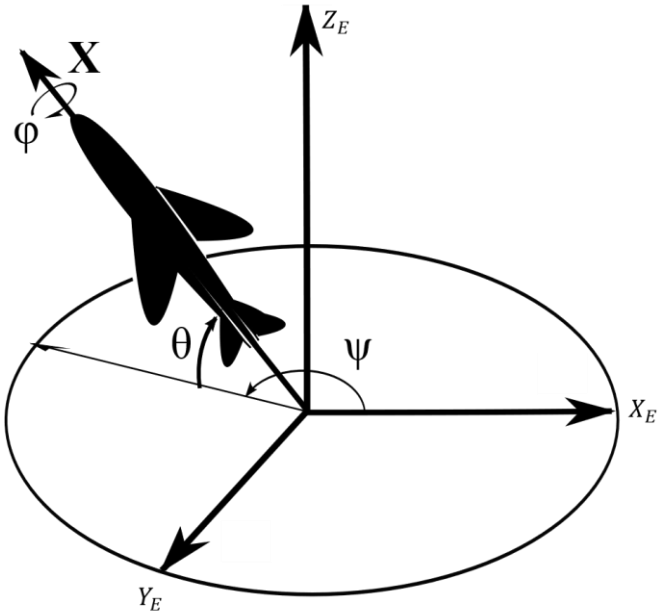

Figure 8. Euler angles

The transformation from earth fixed frame to aircraft body frame is given in Eq. (2.6) and (2.7):

$$\begin{bmatrix} x_b \\ y_b \\ z_b \end{bmatrix} = [T(\emptyset, \theta, \psi)] \begin{bmatrix} x_e \\ y_e \\ z_e \end{bmatrix} \tag{2.6}$$

$$[T(\emptyset, \theta, \psi)] = \begin{bmatrix} 1 & 0 & 0 \\ 0 & \cos\emptyset & \sin\emptyset \\ 0 & -\sin\emptyset & \cos\emptyset \end{bmatrix} \begin{bmatrix} \cos\theta & 0 & -\sin\theta \\ 0 & 1 & 0 \\ \sin\theta & 0 & \cos\theta \end{bmatrix} \begin{bmatrix} \cos\psi & \sin\psi & 0 \\ -\sin\psi & \cos\psi & 0 \\ 0 & 0 & 1 \end{bmatrix} \tag{2.7}$$

2.2 Plant Model

Plant model includes a series of sub blocks; atmosphere, aerodynamics, equation of motion, engine, and mass-inertia to represent aircraft dynamics. Actuator and sensor are elements of flight control system, so; they are considered in flight control system design section. Although actuator dynamics are not included, control surfaces must be defined to generate required moment and forces during trim and linearization. Limitation of control surfaces for each axis is given in Table 1.

Table 1. Control surfaces

Control Surface	Controlled Axis	Min Deflection	Max Deflection
Horizontal Tail	pitch	-25 [deg]	25 [deg]
Flaperon	Roll	-25 [deg]	25 [deg]
Rudder	Yaw -roll	-25 [deg]	25 [deg]
Leading Edge Flap	Pitch	-5 [deg]	20 [deg]
Trailing Edge Flap	Pitch	0 [deg]	15 [deg]

Horizontal tail, flaperon, and rudder are main control surfaces, they create moment and force to control proper axis. Leading edge flap and trailing edge flap are secondary control surfaces, they are used as external lift surfaces in terminal flight phases, such as take-off and landing. Positive sign notation of primary and secondary control surfaces is given in Figure 9.

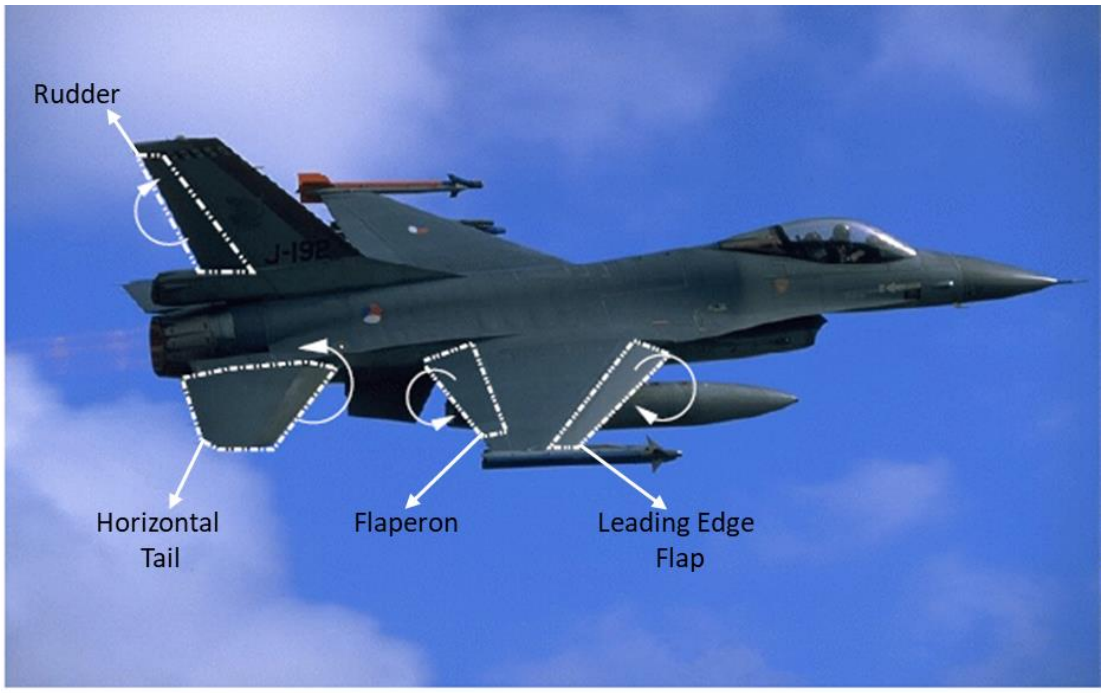

Figure 9. Control surfaces positive sign notation

There is only one surface that is used as both aileron and trailing edge flap with a proper control allocation algorithm.

Secondary control surfaces are extended when the LG or alternate flap switch is pulled down. Trailing edge flap is being driven with a 1 dimensional look up table w.r.t Mach number.

Leading edge is being driven w.r.t angle of attack and ratio of dynamic pressure to static pressure. Leading edge model is given in Figure 10.

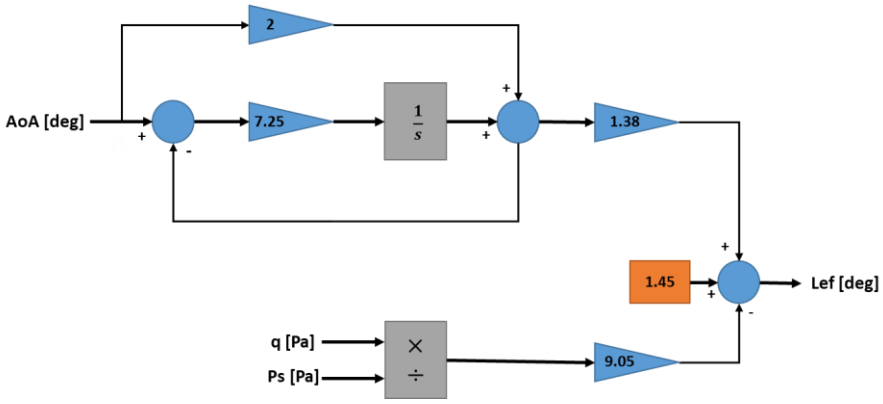

Figure 10. leading edge flap model

Deflection of LEF w.r.t varying ratio of dynamic pressure over static pressure for a fixed angle of attack, 5deg, is given in Figure 11.

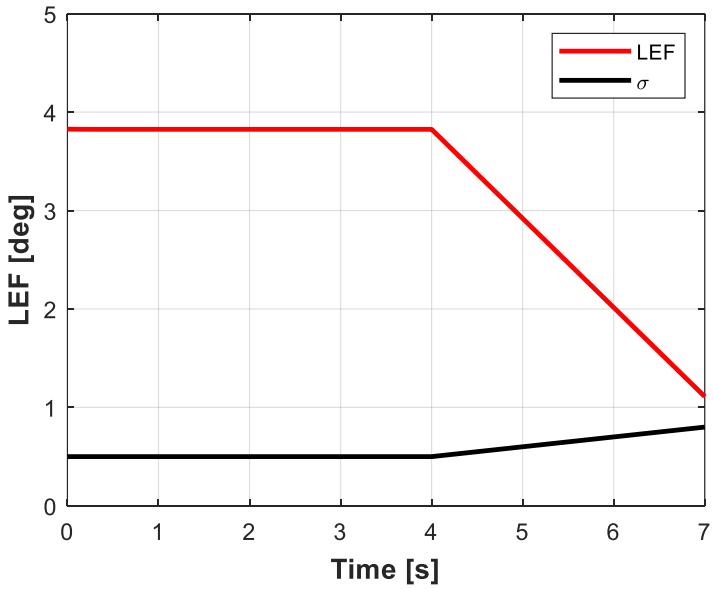

Figure 11. Leading edge flap response

According to the Figure 11 it is obvious that as the ratio of dynamic pressure to static pressure increases, LEF deflection decreases.

2.2.1 Atmosphere Block

Atmosphere block is responsible to calculate air data; Mach number, dynamic pressure ($\bar{q}$), and static pressure (Ps) with respect to the current true air speed and pressure altitude. Standard atmosphere model is used where delta ISA equals to zero.[16] [19]Simplified block diagram of air data block is given in Figure 12.

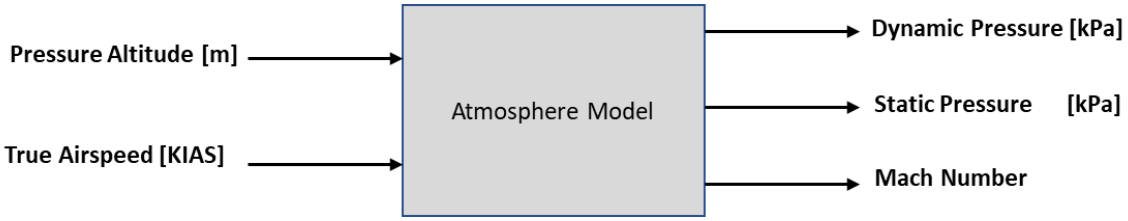

Figure 12. Atmosphere block

Atmosphere model flow chart is given in Figure 6.

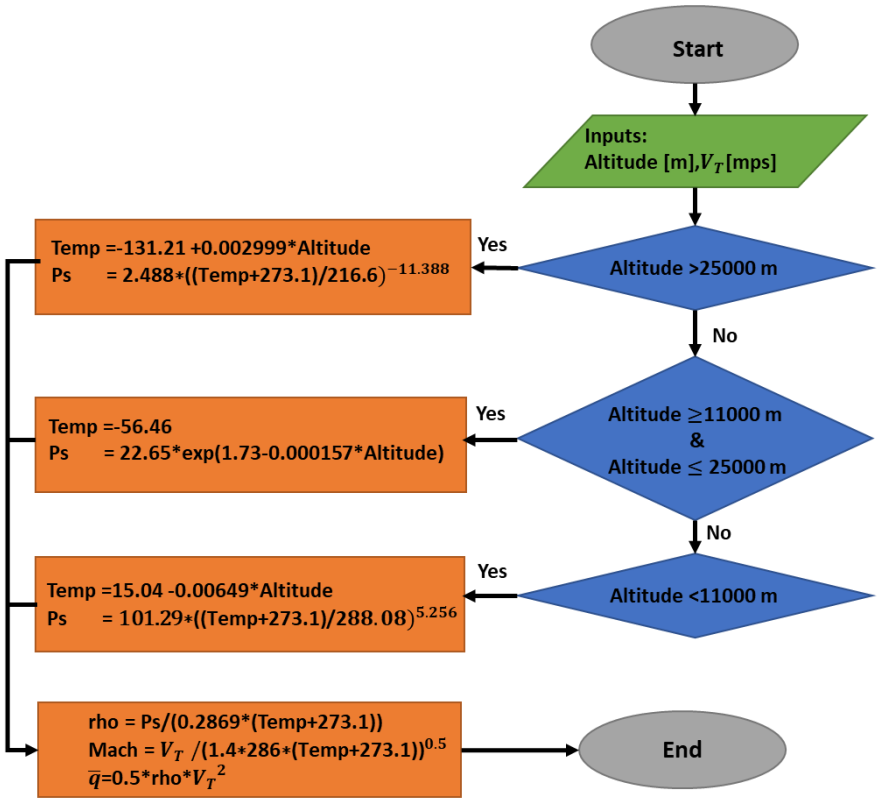

Figure 13. Atmosphere model

2.2.2 Aerodynamics Block

Aerodynamics block is responsible to construct aerodynamic forces and moments. Component of the aircraft that fly in air induces forces and moments upon aircraft body. These forces and moments can be represented in body or wind frame.

For an arbitrary geometry that moves in air, aerodynamic forces and moments are proportional to dynamic pressure, which is given in Eq. (2.8).

$$\bar{q} = \frac{1}{2}\rho {V_T}^2 \tag{2.8}$$

Dynamic pressure is considered as kinetic energy of the air in unit volume. Aerodynamic forces and moments can be nondimensionalized per unit span. These nondimensionalized aerodynamic coefficients are used to construct total aerodynamic forces and moments.

Aerodynamic coefficients depend on airfoil shape. An airfoil is a cross section of a body who is moving through air capable of generating lift due to this movement in air. A sample airfoil and aerodynamic forces in wind frame is given in Figure 14.

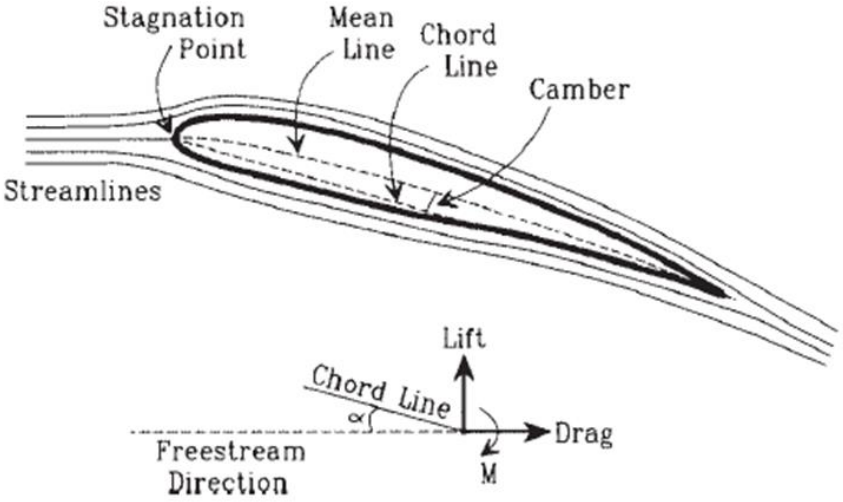

Figure 14. A sample airfoil

Rate of fluid's internal forces to external forces, in other words viscosity also affects aerodynamic coefficients.

Compressibility, the quantity of compressed air around airfoil, is the last parameter that aerodynamic coefficients depend.

These two parameters are called as similarity parameters. Two similar shapes in geometry but with different size can give exactly same aerodynamic coefficients if these two similarity parameters are equalized, this is how scaled models are tested in wind tunnels.[20]

Reynolds number which is related with viscosity of the fluid and Mach number which is related with compressibility are two conventional similarity parameters used in wind tunnels. Formulation of Mach number and Reynolds number are given in Eq. (2.9) and (2.10).

$$M = V_T / v_s \tag{2.9}$$

$$R_e = (\rho l_{chr} V_T)/\mu \tag{2.10}$$

Aerodynamic forces (lift & drag) and moment per unit effective length for given airfoil in Figure 6 are given below.

$$lift\ per\ unit\ span = \bar{q} c C_L(a, M, R_e) \tag{2.11}$$

$$drag\ per\ unit\ span = \bar{q} c C_D(a, M, R_e) \tag{2.12}$$

$$pitching\ moment\ per\ unit\ span = \bar{q} c^2 C_M(a, M, R_e) \tag{2.13}$$

The first aerodynamic coefficient, C_L, is lift coefficient and it is a measurement of how effectiveness airfoil to produce lift wr.t. current angle of attack, Mach number, and Reynolds number. The second aerodynamic coefficient, C_D ,is drag coefficient and third one, C_M, is pitching moment coefficient.[16]

Wing dimensions which are used to nondimensionalize aerodynamic forces and moment are given in Figure 15.

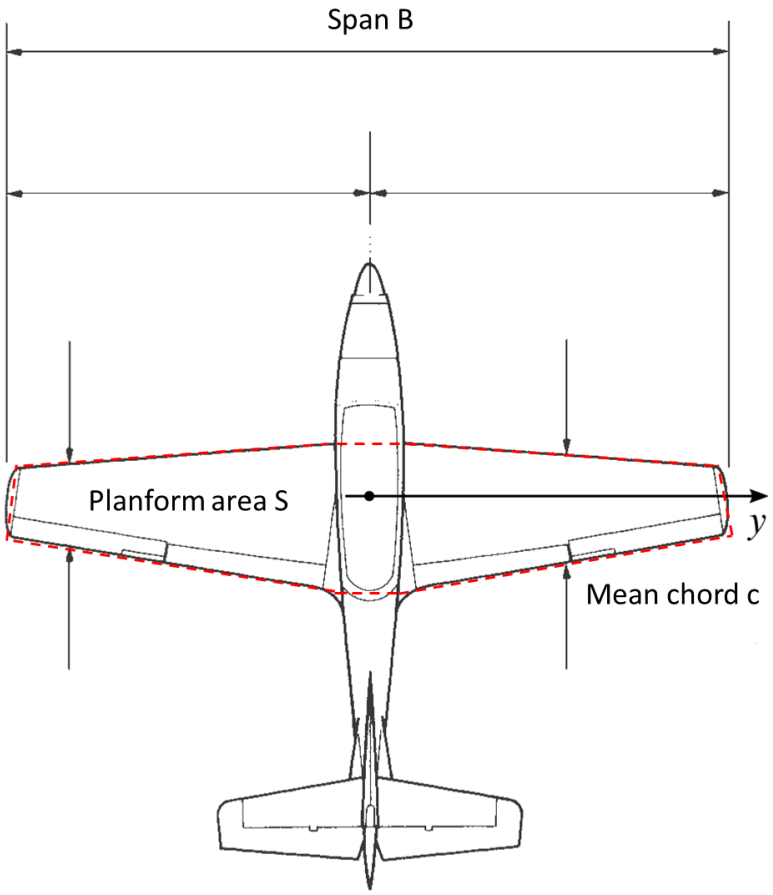

Figure 15. Wing dimensions

Aerodynamic forces are given in Table 2 w.r.t different frames.

Table 2. Forces apply on aircraft

Frame	**Forces**		
Body	F_{XA}	F_{YA}	F_{ZA}
Stability	*	F_{YA}	L
Wind	D	C	L

In nonlinear aircraft model, aerodynamic forces are constructed in body frame for the simplicity. Aerodynamic moments are given in Table 3 w.r.t different frames.

Table 3. Moments apply on aircraft

Frame	**Moments**		
Body	l	M	N
Stability	l_S	M	N_S
Wind	l_W	M_W	N_W

According to definition of the frames it is obvious that $N_W = N_S$. Rates and velocities are calculated in also body axis, but they can be written in stability and wind frames with proper transformation.

Aerodynamic forces and moments are finally calculated with aerodynamic coefficients which comes from wind tunnel tests and CFD solutions. Body frame force and moment coefficients are given in Table 4.

Table 4. Body frame force and moment coefficients

	X	**Y**	**Z**
Force coefficients	C_X	C_Y	C_Z
Moment coefficients	C_l	C_M	C_N

Wind frame force coefficients are given in Table 5.

Table 5. Wind frame force and moment coefficients

	X	Y	Z
Force coefficients	C_D	C_C	C_L
Moment coefficients	C_l	C_M	C_N

Same notation is used for moment coefficients in all frames. Different aerodynamic surfaces and body components contribute to aerodynamic coefficients and finally total coefficient of the aircraft is calculated for each force and moment that apply on aircraft. Calculation of total aerodynamic coefficients are given with Eq. (2.14) – (2.33). [21]

$* x_y$: *indicates partial derivative of* x *w.r.t* y

$$\frac{\partial X}{\partial Q} = \frac{C}{2V_T}(C_{X_Q} + C_{X_{Q_{LEF}}} LEF) \tag{2.14}$$

$$C_X = C_{X_0} + C_{X_{LEF}} LEF + \frac{\partial X}{\partial Q} Q \tag{2.15}$$

$$\frac{\partial Z}{\partial Q} = \frac{C}{2V_T}(C_{Z_Q} + C_{Z_{Q_{LEF}}} LEF) \tag{2.16}$$

$$C_Z = C_{Z_0} + C_{Z_{LEF}} LEF + \frac{\partial Z}{\partial Q} Q \tag{2.17}$$

$$\frac{\partial Y}{\partial R} = \frac{B}{2V_T}(C_{Y_R} + C_{Y_{R_{LEF}}} LEF) \tag{2.18}$$

$$\frac{\partial Y}{\partial P} = \frac{B}{2V_T}(C_{Y_P} + C_{Y_{P_{LEF}}} LEF \tag{2.19}$$

$$\frac{\partial Y}{\partial FLP} = C_{Y_{FLP}} + C_{Y_{FLP_{LEF}}} LEF \tag{2.20}$$

$$C_Y = C_{Y_0} + C_{Y_{LEF}} LEF + \frac{\partial Y}{\partial R} R + \frac{\partial Y}{\partial P} P + C_{Y_{RUD}} RUD + \frac{\partial Y}{\partial FLP} FLP \tag{2.21}$$

$$\frac{\partial M}{\partial Q} = \frac{C}{2V_T}(C_{M_Q} + C_{M_{Q_{LEF}}} LEF) \tag{2.22}$$

$$\Delta_{CG_{XM}} = (CG_{XR} - CG_X) \tag{2.23}$$

$$C_M = C_{M_\Delta} + C_M \eta_{HT} + C_Z \Delta_{CG_{XM}} + C_{M_{LEF}} LEF + \frac{\partial M}{\partial Q} Q \tag{2.24}$$

$$\frac{\partial N}{\partial R} = \frac{B}{2V_T}(C_{N_R} + C_{N_{R_{LEF}}} LEF) \tag{2.25}$$

$$\frac{\partial N}{\partial P} = \frac{B}{2V_T}(C_{N_P} + C_{N_{P_{LEF}}} LEF) \tag{2.26}$$

$$\frac{\partial N}{\partial FLP} = C_{N_{FLP}} + C_{N_{FLP_{LEF}}} LEF \tag{2.27}$$

$$\Delta_{CG_{XN}} = (CG_{XR} - CG_X)(\frac{C}{B}) \tag{2.28}$$

$$C_N = C_{N_0} + C_{N_{LEF}} LEF + \frac{\partial N}{\partial R} R + \frac{\partial N}{\partial P} P + C_{N_{RUD}} RUD + \frac{\partial N}{\partial FLP} FLP + C_{N_\beta} \beta - C_Y \Delta_{CG_{XN}} \tag{2.29}$$

$$\frac{\partial l}{\partial R} = \frac{B}{2V_T}(C_{l_R} + C_{l_{R_{LEF}}} LEF) \tag{2.30}$$

$$\frac{\partial l}{\partial P} = \frac{B}{2V_T}(C_{l_P} + C_{l_{P_{LEF}}} LEF \tag{2.31}$$

$$\frac{\partial l}{\partial FLP} = C_{l_{FLP}} + C_{l_{FLP_{LEF}}} LEF \tag{2.32}$$

$$C_l = C_{l_0} + C_{l_{LEF}} LEF + \frac{\partial l}{\partial R} R + \frac{\partial l}{\partial P} P + C_{l_{RUD}} RUD + \frac{\partial l}{\partial FLP} FLP + C_{l_\beta} \beta \tag{2.33}$$

Calculation of aerodynamic forces and moments are given in Eq. 2.34 – 2.39.

$$F_{XA} = \bar{q} S C_X \tag{2.34}$$

$$F_{YA} = \bar{q} S C_Y \tag{2.35}$$

$$F_{ZA} = \bar{q} S C_Z \tag{2.36}$$

$$\iota = \bar{q} S B C_l \tag{2.37}$$

$$M = \bar{q}ScC_M \tag{2.38}$$

$$N = \bar{q}SBC_M \tag{2.39}$$

2.2.3 Engine Block

Engine block is responsible to represent engine dynamics. Thrust is calculated w.r.t series of look up tables and modeled as first order lag. Block diagram of engine model is given in Figure 16.[16]

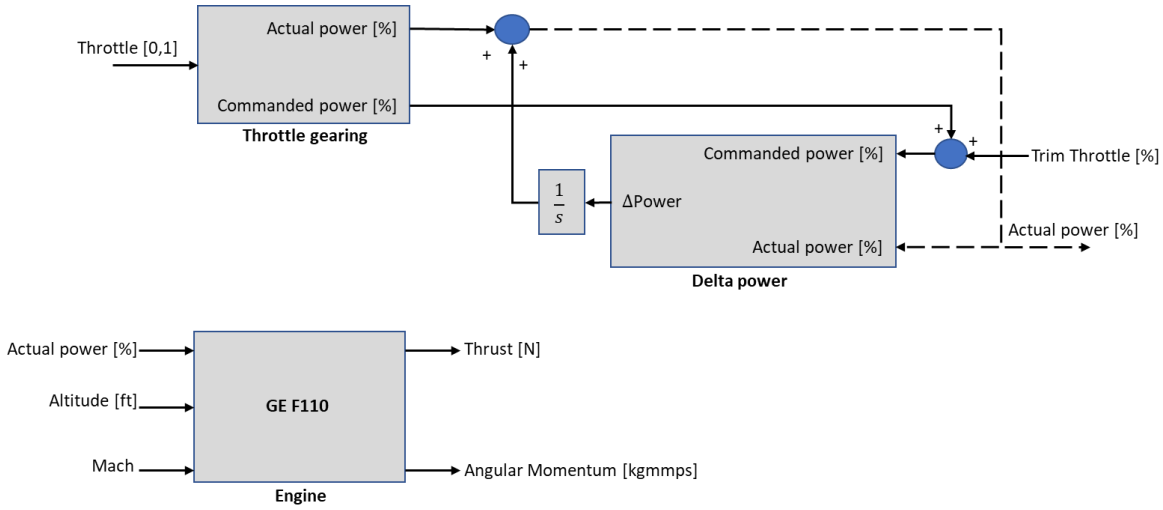

Figure 16. Engine model

Response of engine for 50% throttle command is given in Figure 9.

*Throttle level indicates the engine capacity and $0 \leq Throttle \leq 100$.

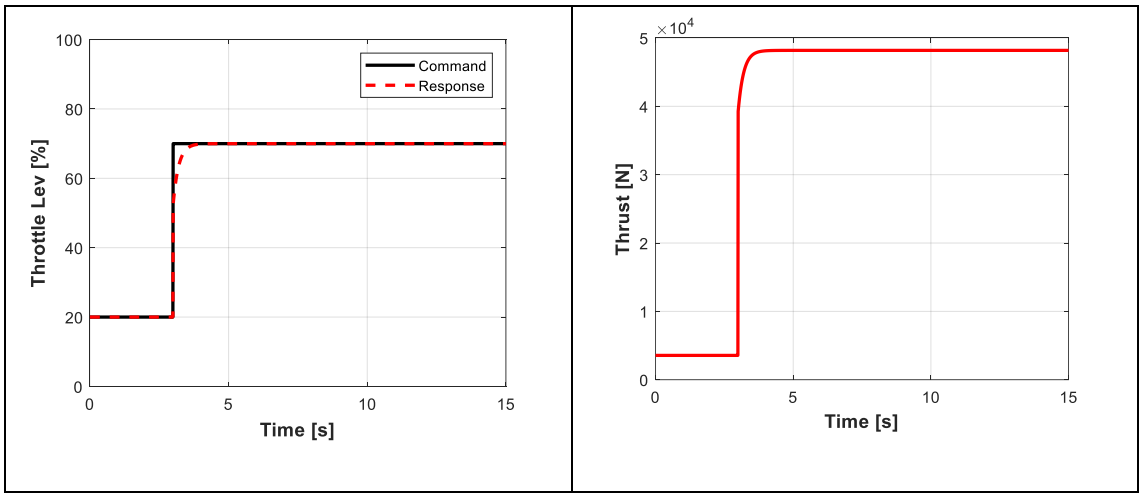

Figure 17. Engine response [0.5 Mach, 10kft]

According to the Figure 10 engine responds as first order system. The initial thrust value in Figure 17 indicates trim thrust value for 0.5 Mach 10 kft flight condition. Engine force and moment contribution to the aircraft is illustrated in Figure 18.

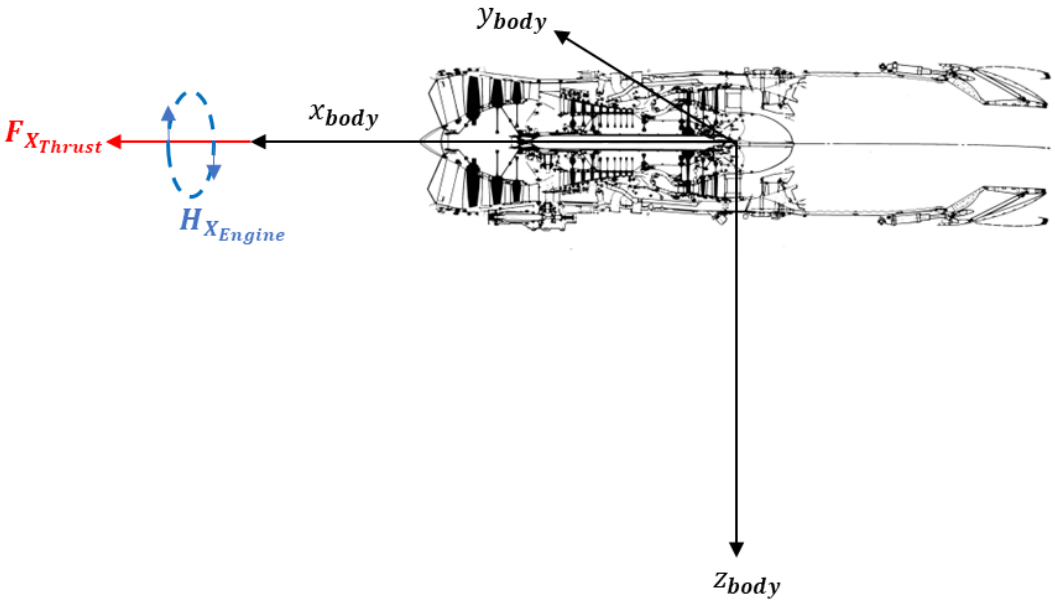

Figure 18. Engine force and moment contribution to aircraft

According to Figure 17 only contribution of the engine are thrust force along body x axis and angular momentum around body x axis.

2.2.4 Mass & Inertia Block

Mass and inertia block is responsible represent aircraft mass and inertia dynamics. Total mass, total inertia and CG position in body frame are calculated w.r.t fuel input, pilot weights and payload information.

Simplified block diagram of mass and inertia model is given in Figure 19.

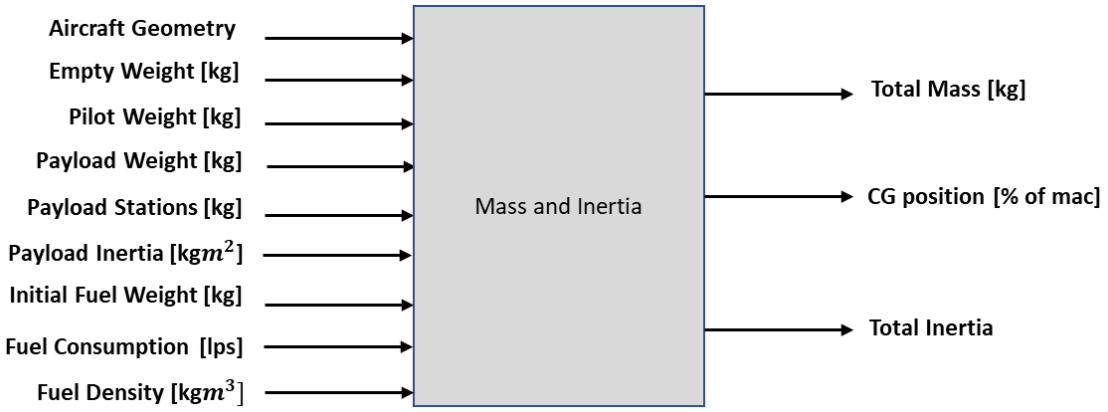

Figure 19. Mass and inertia model

2.2.5 Equations of Motion Block

Equation of motion block is responsible to combine aerodynamic forces – moments & engine forces – moments with vector equations of motion to represent aircraft dynamics. For the simplicity flat-Earth body equations are used, wind frame parameters are calculated with proper transformation.

Body frame translational accelerations are calculated with force equations which are given in Eq. (2.40), (2.41), and (2.42).[16]

$$\dot{U} = RV - QW - g_d \sin\theta + (X_A + X_T)/m \tag{2.40}$$

$$\dot{V} = -RU + PW + g_d \sin\emptyset \cos\theta + Y_A/m \tag{2.41}$$

$$\dot{W} = QU - PV + g_d \cos\emptyset \cos\theta + Z_A/m \tag{2.42}$$

Body frame rotational accelerations are calculated with moment equations which are given in Eq. (2.43) - (2.46).[16][21]

$$\tau\dot{P} = J_{XZ}\left[J_x - J_y + J_z\right]PQ - \left[J_z\left(J_z - J_y\right) + {J_{xz}}^2\right]QR + J_z l + J_{xz}\mathrm{N} + J_{xz}QH_{X_{Engine}} \tag{2.43}$$

$$J_y\dot{Q} = (J_Z - J_X)PR - J_{XZ}(P^2 - R^2) + \mathrm{M} - RH_{X_{Engine}} \tag{2.44}$$

$$\tau\dot{R} = \left[\left(J_x - J_y\right)J_x + {J_{xz}}^2\right]PQ - J_{XZ}\left[J_x - J_y + J_z\right]QR + J_{Xz}l + J_x\mathrm{N} + J_xQH_{X_{Engine}} \tag{2.45}$$

$$\tau = J_x J_z - {J_{xz}}^2 \tag{2.46}$$

Variation of Euler angles that relates the orientation of aircraft w.r.t body frame are calculated with kinematic equations given in Eq. (2.47), (2.48), and (2.49).[16]

$$\dot{\emptyset} = P + \tan\theta \ (Q \sin\emptyset + R \cos\emptyset) \tag{2.47}$$

$$\dot{\theta} = Q \cos\emptyset - R \sin\emptyset \tag{2.48}$$

$$\dot{\psi} = (Q \sin\emptyset + R \cos\emptyset)/\cos\theta \tag{2.49}$$

Change of orientation in geocentric frame, North-East-Down, is calculated with navigation equations which are given in Eq. (2.50), (2.51), and (2.52).[16]

$$\dot{P_N} = U\cos\theta\cos\psi + V(-\cos\emptyset\sin\psi + \sin\emptyset\sin\theta\cos\psi) + W(\sin\emptyset\sin\psi + \cos\emptyset\sin\theta\cos\psi) \tag{2.50}$$

$$\dot{P_E} = U\cos\theta\sin\psi + V(\cos\emptyset\cos\psi + \sin\emptyset\sin\theta\sin\psi) + W(-\sin\emptyset\cos\psi + \cos\emptyset\sin\theta\sin\psi) \tag{2.51}$$

$$\dot{h} = U\cos\theta - \mathrm{V}\sin\emptyset\cos\theta - W\cos\emptyset\cos\theta \tag{2.52}$$

First derivatives of aerodynamic angles can be found by differentiating Eq. (2.53) & Eq. (2.54).[16]

$$\dot{\alpha} = \frac{U\dot{W} + W\dot{U}}{U^2 + W^2} \tag{2.53}$$

$$\dot{\beta} = \frac{\dot{V}V_T - V\dot{V_T}}{V_T[U^2 + W^2]^{0.5}} \tag{2.54}$$

$$\dot{V_T} = \frac{U\dot{U} + V\dot{V} + W\dot{W}}{V_T} \tag{2.55}$$

Nonlinear aircraft state equations are solved via numerical methods such as Runga Kutta. For a given initial states X (t_0) and control input U(t) derivative of states can be written as:

$$\dot{X}(t) = f(X(t), U(t)) \tag{2.56}$$

EQM and numerical integration constructs a basis for time-history simulations. Change of state vector in n dimensional space are calculated via differential equations and by help of numerical integration trajectory of state vector is calculated. Process of time-history simulation is demonstrated with a simplified block diagram, which is given in Figure 20.

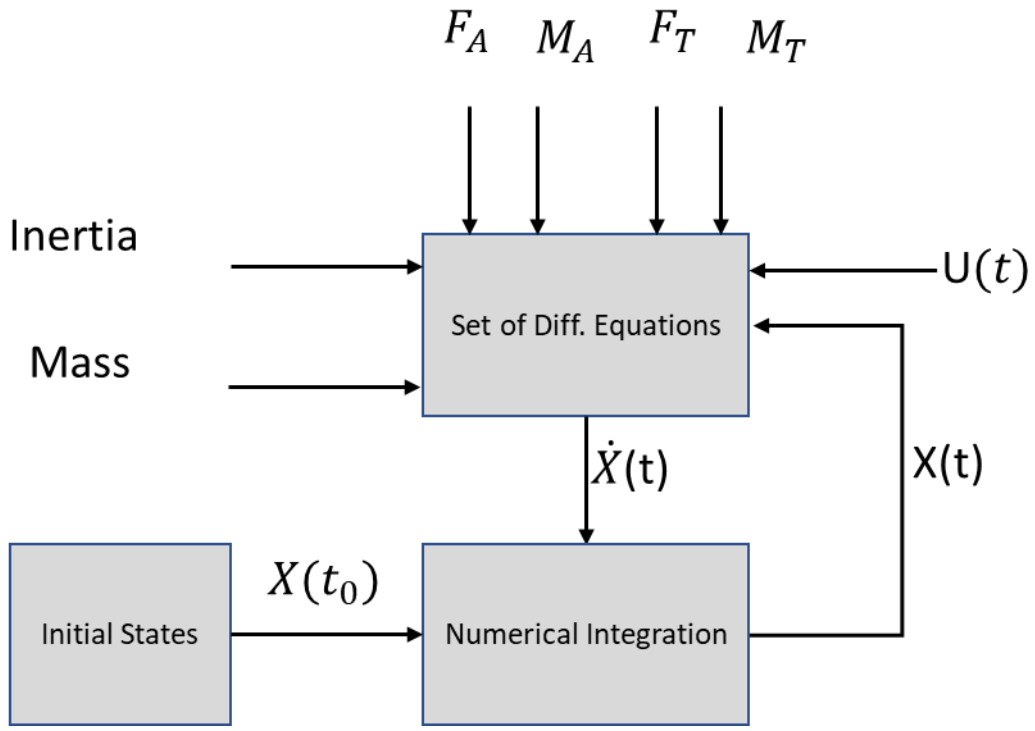

Figure 20. Time history simulation

2.3 Trim and Linearization

In real life flight starts on runaway; aircraft first taxi on the ground to its take off position and then pilot gives proper throttle input and release the brakes. Aircraft starts to accelerate and after a specific speed aircraft takes off.

In nonlinear simulation it is not necessary to initialize the simulation on ground, simulation can be started in any arbitrary point if the initial points are reachable. To calculate initial values; nonlinear aircraft model shall be trimmed w.r.t desired flight condition.

Trim point is an equilibrium point for nonlinear aircraft model, where different constraints are satisfied w.r.t trim type. In the scope of the thesis steady wings

level trim condition is used. In steady wings level trim condition state derivatives shall be zero.

The constraints that describe the steady wings level trim are given below.

$$\{\dot{U}, \dot{V}, \dot{W}\} = 0 \tag{2.57}$$

$$\{\dot{P}, \dot{Q}, \dot{R}\} = 0$$

$$\{\emptyset, \gamma\} = 0 \tag{2.58}$$

A trim algorithm such that finds a proper state and input vector such that satisfies Eq. (2.57) and (2.58) is required.

There are different approaches to solve nonlinear aircraft equations and find proper state and input vectors which make state derivatives zero. A cost function can be constructed with the derivative of the states. A search algorithm can be used and then, to find appropriate input and state vectors that minimizes the cost.[16]

Another approach is that suitable input and state vector can be found by solving the nonlinear state equations directly via different numerical methods. The second approach has some advantages upon the first one, such as speed.

For this reason, the second approach is followed. Nonlinear state equations are solved via Newton Raphson method and finally the input and state vectors which satisfy Eq. (2.57) and (2.58) are found.

Newton Raphson method is an iterative approach to find the roots of the nonlinear equations; approach is given below.

$$X_{i+1} = X_i - \frac{f(X_i)}{\dot{f}(X_i)}$$

$$X_{i+2} = X_{i+1} - \frac{f(X_{i+1})}{\dot{f}(X_{i+1})} \tag{2.59}$$

…

$$X_n = X_{n-1} - \frac{f(X_{n-1})}{\dot{f}(X_{n-1})}$$

Iteration is repeated until absolute error between X_n and X_{n+1} reaches predefined threshold value. Graphical illustration is given in Figure 21.

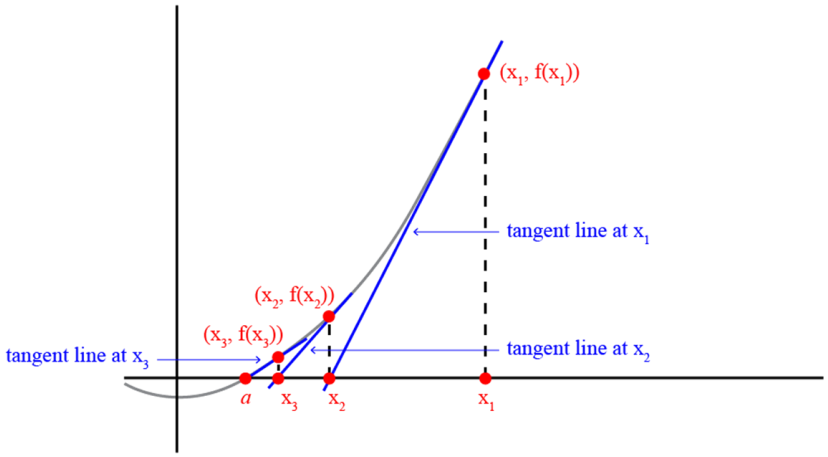

Figure 21. Newton Raphson method graphical illustration

Trim algorithm flow chart is given blow.[16]

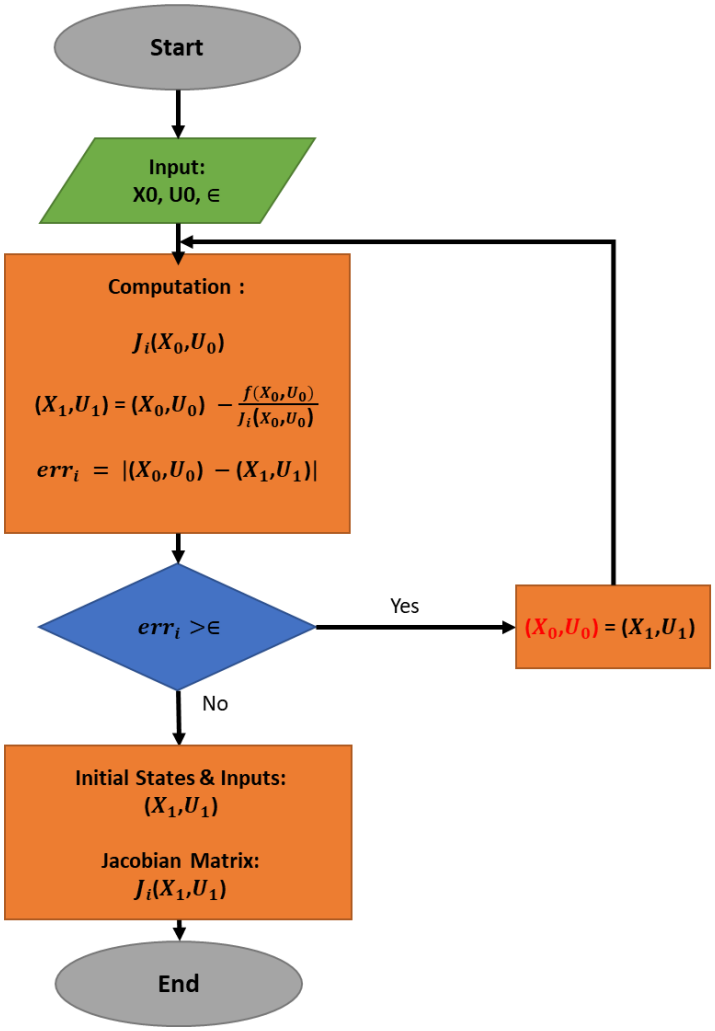

Figure 22. Trim algorithm

Jacobian matrices are calculated via central difference method, which is given below.

$$perturbation = \Delta x_i = 0.01 x_i \tag{2.60}$$

$$x_f | \, x_{f_i} = x_i + \Delta x_i \tag{2.61}$$

$$x_b | \, x_{b_i} = x_i - \Delta x_i \tag{2.62}$$

$$\frac{\partial f(x,u)}{\partial x_i} = \frac{f(x_f,u) - f(x_b,u)}{2\Delta x_i} \in R^{1Xn} \tag{2.63}$$

Linear A and B matrices are the Jacobians, wr.t states and inputs respectively, where $err \leq \in$.

$$A = A_i{}^{nxn} = \begin{bmatrix} \frac{\partial fy_1}{\partial x_1} & \cdots & \frac{\partial fy_1}{\partial x_n} \\ \vdots & \ddots & \vdots \\ \frac{\partial fy_n}{\partial x_1} & \cdots & \frac{\partial fy_n}{\partial x_n} \end{bmatrix} | \, err_i \leq \in \tag{2.64}$$

$$B = B_i{}^{nx1} = \begin{bmatrix} \frac{\partial fy_1}{\partial u_1} \\ \vdots \\ \frac{\partial fy_n}{\partial u_1} \end{bmatrix} | \, err_i \leq \in \tag{2.65}$$

3. FLIGHT CONTROL ALGORITHM DESIGN REQUIREMENTS

In the scope of the thesis a fault tolerant longitudinal flight control algorithm is designed. This algorithm is required to satisfy performance and stability robustness in case of CG_X information fault.

Stability robustness is defined with respect to the classical stability margins requirements. Performance robustness is defined in terms of reference model tracking capability, handling qualities requirements and PIO requirements.

Fault definition and detection method, stability, and performance requirements will be explained in this section.

3.1 Fault Definition and Detection

Position of CG w.r.t body axes (CG_x, CG_y, CG_z) plays an important role upon aircraft dynamics. Especially the position of CG_x is more critical since the equipment layout is not symmetric w.r.t body y axis and this situation creates heterogeneous mass distribution along body x axis. For this reason, position of CG_x is considered in beginning of airframe design process.

Desired CG_x is not reachable always as result of other constraints that must be considered during the design process.

In this case, CG_x position can be controlled by relocating a mass actively. Fuel management system can be used for this purpose. It controls the fuel pumps and relocate the fuel such that CG_x position is in desired range.

Another way to handle with wide range of CG_x position is monitoring it in real time and adapting flight control algorithm parameters w.r.t current CG_x position. Second approach is simpler as compared the first one.

In jet trainer aircraft there is a wide range of CG_x position, which is almost 6% of mac. The second approach is being followed; control algorithm parameters are scheduled w.r.t bounded CG_x position information. According to the CG_x position input comes from configuration management computer; flight control algorithm parameters are changed.

There are some risks in this approach. In case of any failure or erroneous operation of configuration management computer, CG_x position information is fixed to mid position which is assumed to be most robust one. The problem is that aircraft cannot reach level 1 handling qualities and desired stability without controller parameters scheduling w.r.t CG_x position information.

An alternative longitudinal flight control algorithm which guarantees predefined stability and performance robustness without any adaptation mechanism w.r.t CG_x position is aimed in the scope of the thesis.

Fault detection algorithm is given in Figure 23.

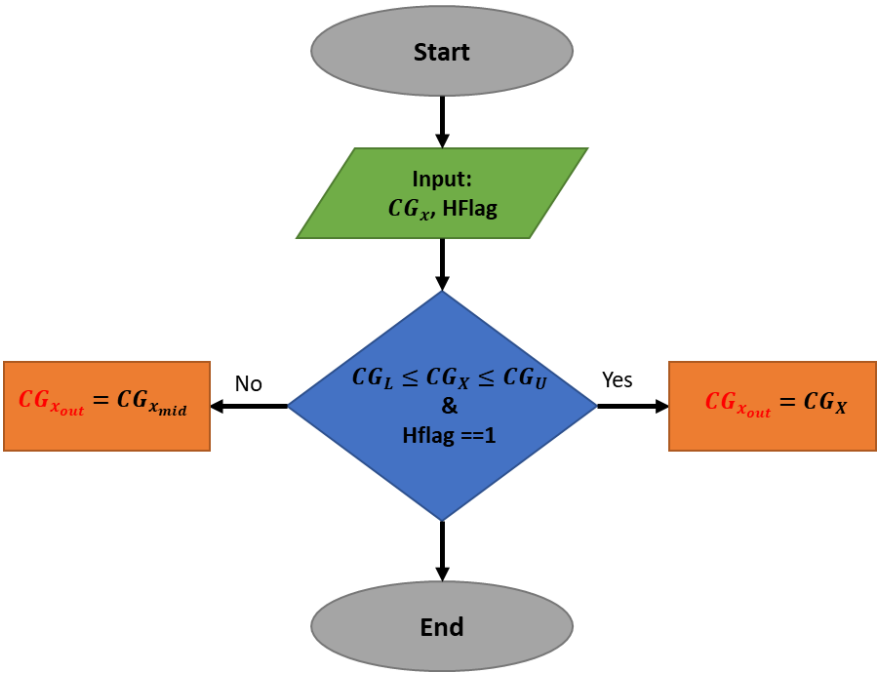

Figure 23. Fault detection algorithm

Fault detection algorithm parameters are given in Table 6.

Table 6. Fault detection algorithm parameters

Parameter	Definition	Value
HFlag	Conf. Management computer health status 1: Healthy 0: Failed	{0,1}
CG_L	CG_x position lower limit (% of mac)	28.45
CG_U	CG_x position upper limit (% of mac)	34.02

According to the Figure 23 if the configuration computer is healthy (HFlag =1) and calculated CG_x position is between the boundaries ($CG_L \leq CG_X \leq CG_U$) algorithm

outputs the calculated CG_x position and then flight control algorithm adapts parameters w.r.t this information.

If one of the statements given above is not satisfied, fault detection algorithm outputs mid CG_x position and flight control algorithm starts to use mid CG_x configuration parameters.

3.2 Stability Requirements

Stability robustness is defined with respect to the classical stability margins requirements which are given in Table 7.[22]

Table 7. Stability requirements

*C_{params}: $Controlle\ rparameters$

Stability Requirements	Constraints
Hurwitz stability in Nyquist	{C_{params}| re(Roots(num(1+L(jw, C_{params})))< 0}
Stability Margin	≥ 0.5
Gain Margin	≥ 6 [dB]
Phase Margin	≥ 45 [deg]
Nichols exclusion zone	Frequency locus shall not violate exclusion zone

GM and PM are relative stability margins. SM which is the closest distance of Loop gain to critical point is absolute stability margin.

Demonstration of absolute and relative stability on Nichols chart is given in Figure 24.

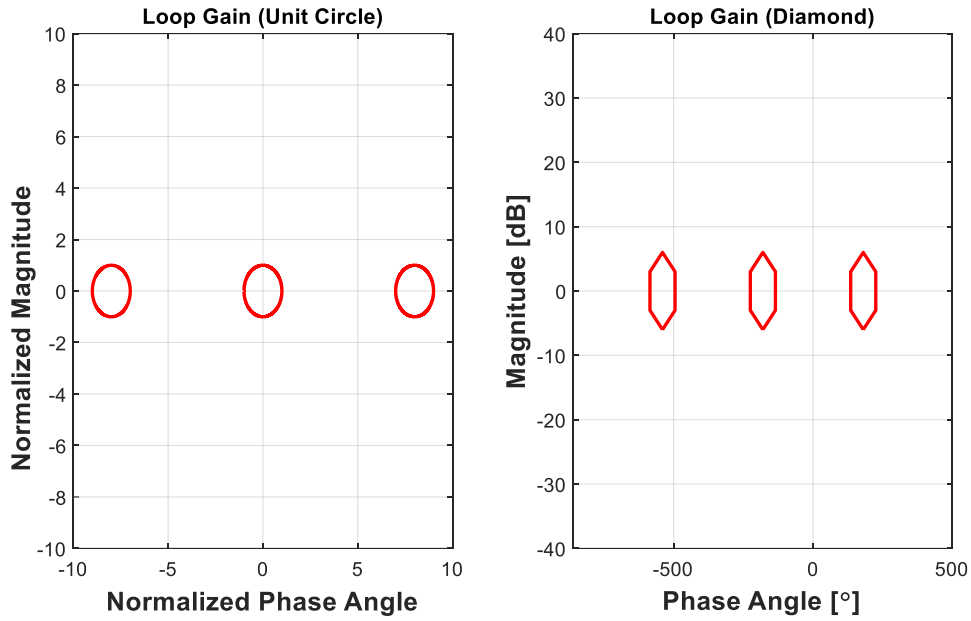

Figure 24. Demonstration of relative and absolute stability margins on Nichols chart

3.3 Performance Requirements

Performance requirements; reference model tracking capability, handling qualities requirements, and PIO requirements are given in this chapter.

3.3.1 Reference Model Tracking Capability

Proposed flight control algorithm is required to track reference model at design and off-design points w.r.t predefined constraint. Reference model is pitch rate to stick transfer function which directly represents desired pitch rate characteristics.

Tracking constraint is defined as:

$$|G_d(jw) - G(jw)| \leq \left|\frac{2.5(jw)+10}{(jw)+100}\right| \; for \; 0.1[rps] \leq \omega \leq 40[rps] \tag{3.1}$$

3.3.2 Handling Qualities

Handling qualities can be described as the “characteristics of the aircraft that govern the ease and precision with a pilot can perform the task required in support of an aircraft role”, according to [23] .

Handling qualities requirements vary w.r.t flight phase and aircraft class. Definition flight phases and aircraft classes will be given in the rest of the section. Finally selected handling qualities requirements will be explained.

3.3.2.1 Flight Phase Categories

It is important to classify each mission segments w.r.t handling quality tasks to assign appropriate handling criteria. Flight phase categories are given in Table 8. [24]

Table 8. Flight Phase categories

Category	Definiton
A	Tasks that are precise and aggressive.
B	Tasks that are non-precise and non-aggressive.
C	Tasks that are precise and non-aggressive.
D	Tasks that are non-precise and aggressive.

Boundaries of handling qualities criteria may change w.r.t flight phase category. Detailed boundaries for each criterion will be given for related handling qualities criteria.

Some example missions w.r.t flight phase categorization is given in Table 9.

Table 9. Missions w.r.t flight phase categorization

Category	Mission
A	Tracking maneuvering target
B	Inflight refueling – tanker (RT)
C	Inflight refueling – receiver (RR)
D	Gross acquisition using loaded roll

3.3.2.2 Classification of Aircraft

Aircrafts can be classified w.r.t their size and maneuverability. Boundaries of handling qualities criteria may vary wr.t. aircraft classes. Classification of aircrafts are given in Table 10. [25]

Table 10. Classification of aircrafts

Class	Definition
I	Small, light airplanes, such as light utility aircrafts
II	Medium – weight, low-to-medium maneuverability airplanes, such as heavy utility/search and rescue aircrafts
III	Large, heavy, low-to-medium maneuverability airplanes, such as heavy transport aircrafts
IV	High-maneuverability airplanes, such as fighter/interceptor aircrafts

The jet trainer aircraft, being studied in the scope of the thesis, is classified as class IV.

3.3.2.3 Cooper Harper Handling Qualities Scale

The Cooper-Harper Handling Qualities Rating Scale (HQRS) is pilot metric. The pilots use it to evaluate handling qualities of aircraft during the task. Cooper-Harper scale is ranging between 1 and 10. [24] Cooper - Harper Handling Qualities Rating scale is given in Figure 25.[26]

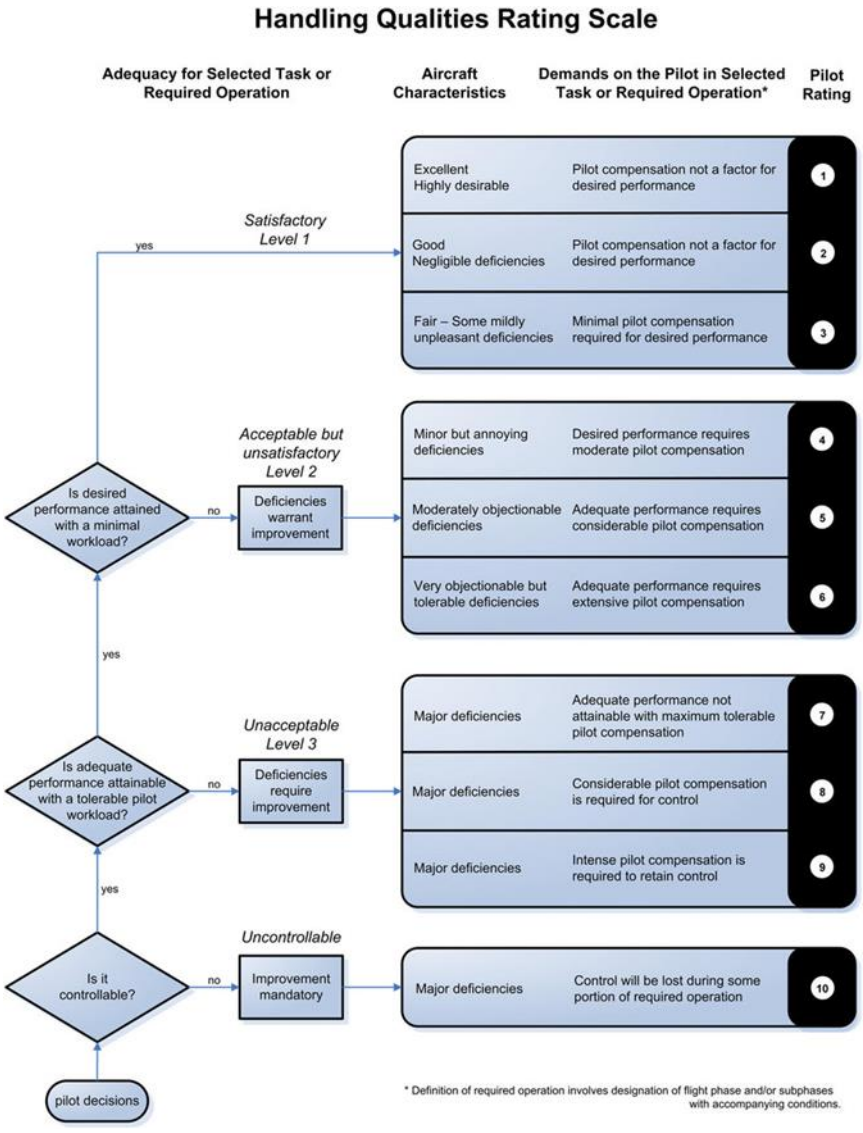

Figure 25. Cooper – Harper Handling Qualities Rating Scale

According to the Figure 25 handling qualities are evaluated in three levels. Each level also includes three sub levels which define aircraft characteristics w.r.t current task. These levels are evaluated w.r.t pilot commands. Since the piloted tests are not considered in the scope of the thesis, only the handling qualities levels are considered as a success criterion.

3.3.2.4 Handling Qualities Requirements

A Set of handling qualities requirements are constructed in the scope of flight control algorithm design performance requirements. Handling qualities requirements guide the designer about desired aircraft characteristics. Selected handling qualities requirements and their domains are given in Table 11.

Table 11. Selected Handling Qualities Requirements

Handling Qualities Requirements	**Domain**
Pitch attitude bandwidth & Phase Delay	Frequency
Transient Peak Ratio	Time
Drop Back	Time

3.3.2.4.1 Pitch Attitude Bandwidth and Phase Delay

According to the [24] pitch attitude bandwidth is defined as the highest frequency where there is at least 45 degree of phase margin and 6 dB of gain margin. Illustration of pitch attitude bandwidth is given in Figure 26. [27]

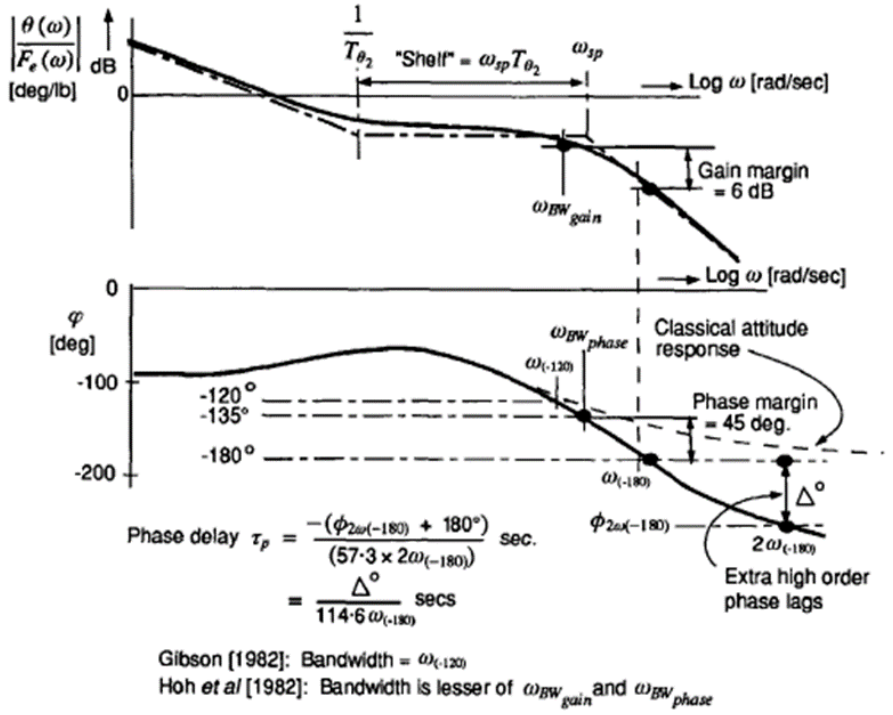

Figure 26. Pitch attitude bandwidth

Phase delay calculation is given in Eq. (3.2).

$$\tau_p = \frac{\Delta\Phi 2w_{-180}}{57.3(2w_{-180})} \tag{3.2}$$

According to the [24] pitch attitude and phase delay values must satisfy the regions indicated for related success level in Figure 27.

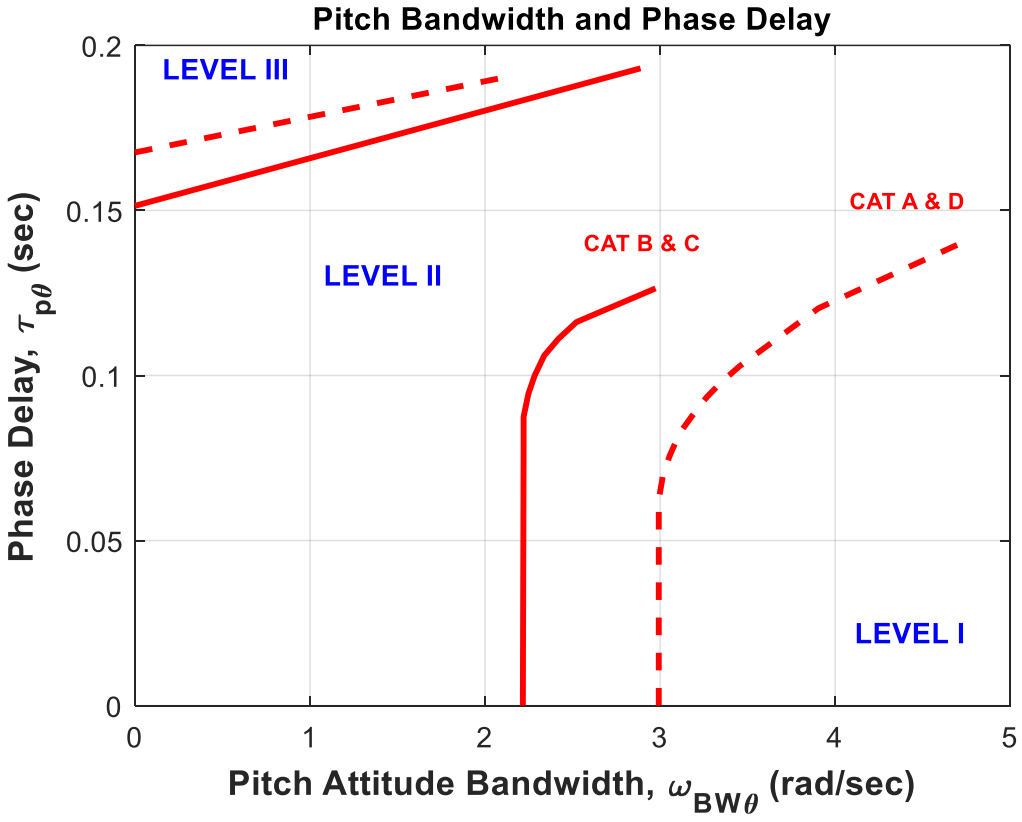

Figure 27. Pitch attitude bandwidth criterion regions

According to the Figure 24 it is obvious that for flight phases B & C level 1 region starts with lower bandwidth value as compared to flight phases A & D since flight phase B & C are categorized as nonaggressive. On the other hand, flight phases A & D are categorized as aggressive and requires higher bandwidth values for level 1 . (Aggressiveness and bandwidth are proportional to each other)

3.3.2.4.2 Transient Peak Ratio

Transient peak ratio criterion includes the parameters; effective time delay, effective rise time, and transient peak ratio which gives the name of the criterion. These three parameters shape a time response of pitch rate to longitudinal stick input.

Illustration of transient peak ratio criterion is given Figure 28.[24]

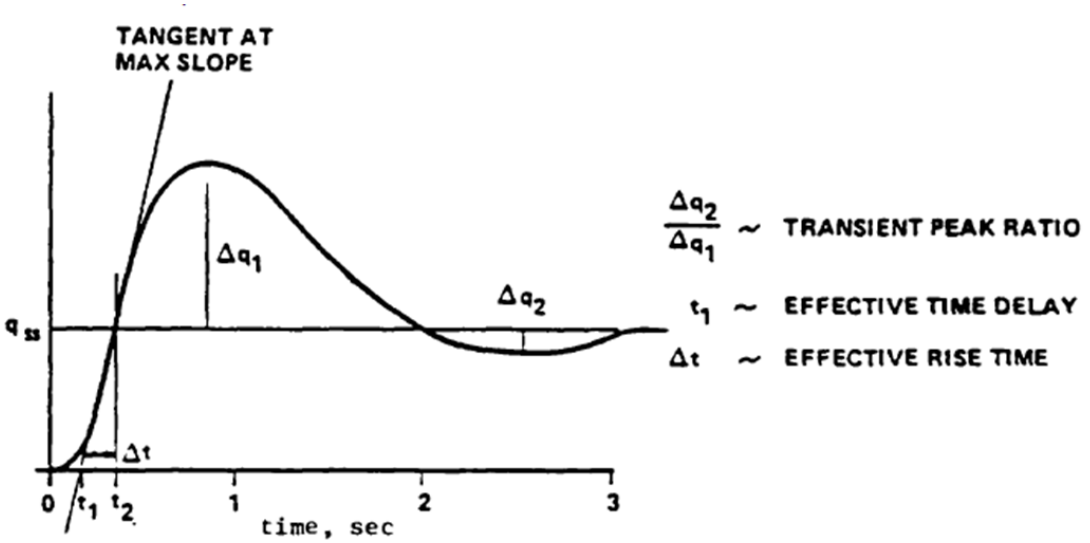

Figure 28. Transient peak ratio

Time delay is inactive time between pilot stick input and beginning of aircraft response. There are different time delay sources. If the system exactly follow the input after a specific time interval, this specific time is called as pure or transport time delay. It is introduced by the digital implementation of control laws.

Another type of time delay is effective time delay, which is caused because of flight control algorithm dynamics such as cascade filters. Transient peak ratio requirement boundaries are given in Table 12.

Table 12. TPR requirement boundaries

Parameter	**Level I**	**Level II**	**Level III**
t_1	0.10 s	0.20 s	0.25 s
Δt	$[\frac{9}{V_T}, \frac{500}{V_T}]$ flight phase A & D $[\frac{9}{V_T}, \frac{200}{V_T}]$ flight phase B & C	$[\frac{3.2}{V_T}, \frac{1600}{V_T}]$ flight phase A & D $[\frac{3.2}{V_T}, \frac{645}{V_T}]$ flight phase B & C	NA
$\frac{\Delta_{q1}}{\Delta_{q2}}$	0.30	0.60	0.85

TPR and effective time delay requirement regions w.r.t success levels are given in Figure 29.

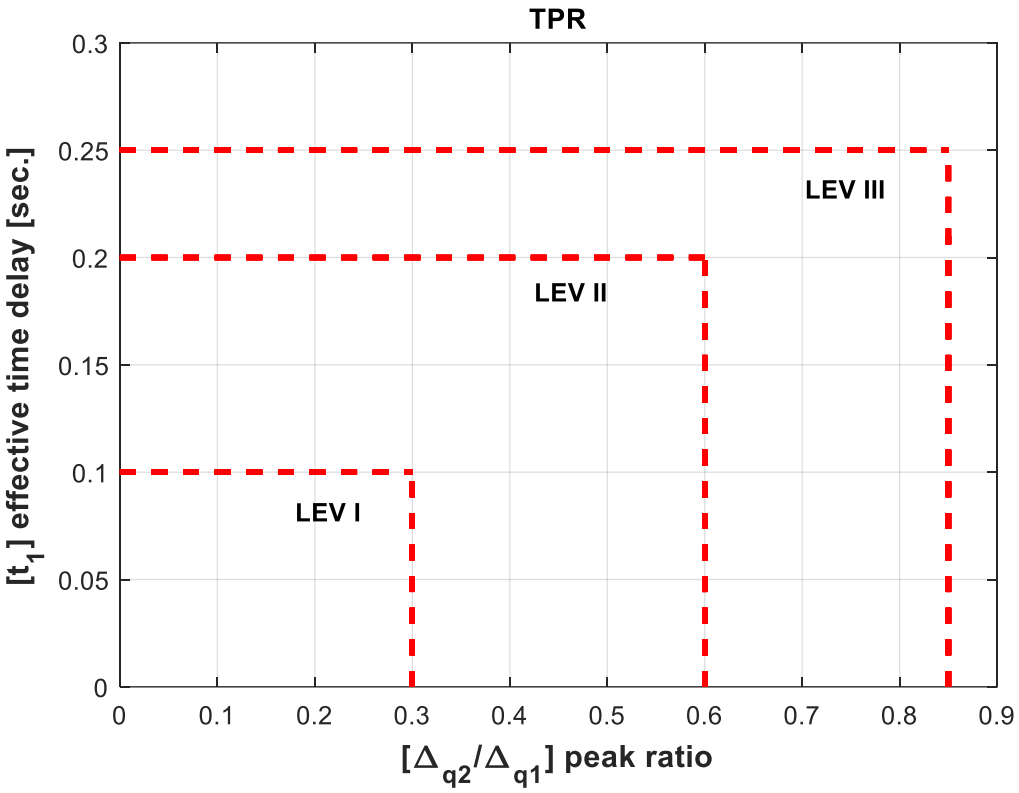

Figure 29. Transient peak ratio and effective time delay criterion regions

3.3.2.4.3 Drop back

During the flight, in longitudinal axis, pilot controls pitch attitude with pitch rate demand by giving proper stick inputs. Besides pitch attitude, angle of attack and flight path also change because of stick input. Pitch rate and angle of attack are short term responses, but flight path is long term response. Relation between pitch attitude and flight path characteristics play a key role upon handling qualities w.r.t different mission types.

Drop back is difference between pitch attitude when pilot releases stick and steady state pitch attitude value after pilot has relaxed stick. According to the sign of the drop back, relation between pitch attitude and flight path characteristics are understood.

Change of θ, $\dot{\theta}$,α, and γ w.r.t longitudinal stick input and drop back definition are illustrated in Figure 30.[27]

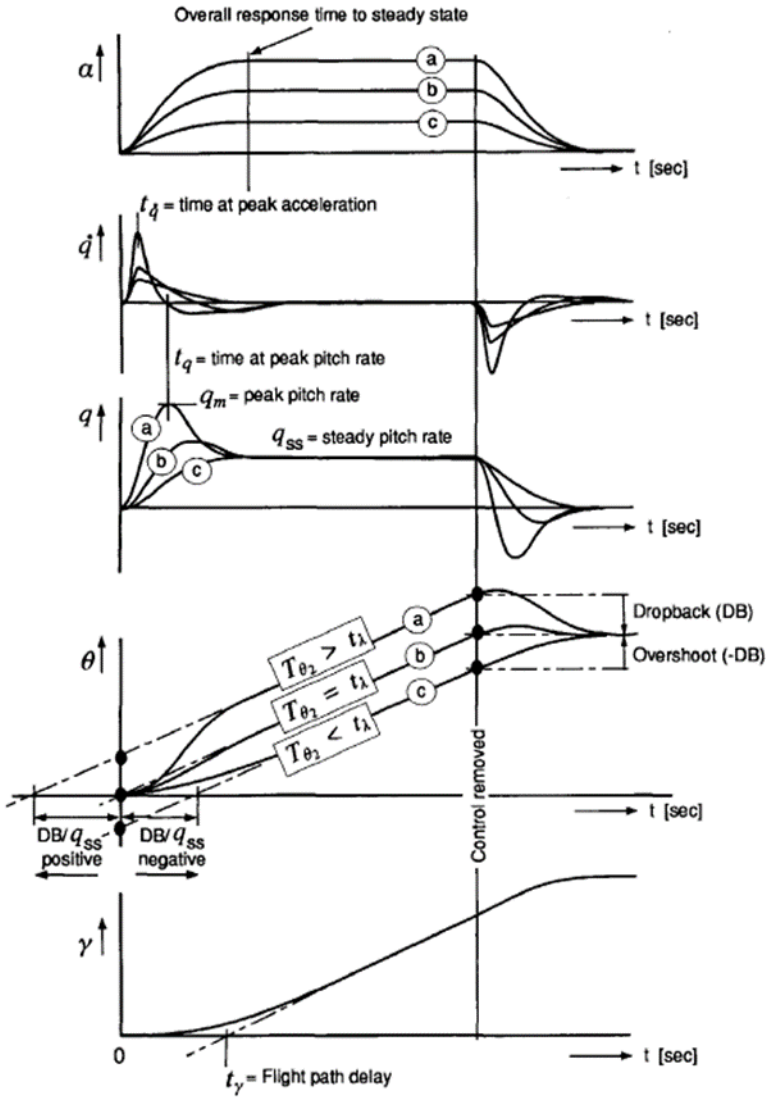

Figure 30. Drop back

According to the Figure 30 drop back is calculated in Eq. (3.3) and Eq. (3.4).

$$t_\gamma = \frac{2\zeta_{sp}}{\omega_{sp}} \tag{3.3}$$

$$\frac{DB}{q_{ss}} = T_{\theta_2} - t_\gamma \tag{3.4}$$

Drop back criterion success level is determined w.r.t $\frac{DB}{q_{ss}}$ and $\frac{q_{max}}{q_{ss}}$. Drop back criterion regions in terms of $\frac{DB}{q_{ss}}$ and $\frac{q_{max}}{q_{ss}}$, w.r.t success levels are given in Figure 31.

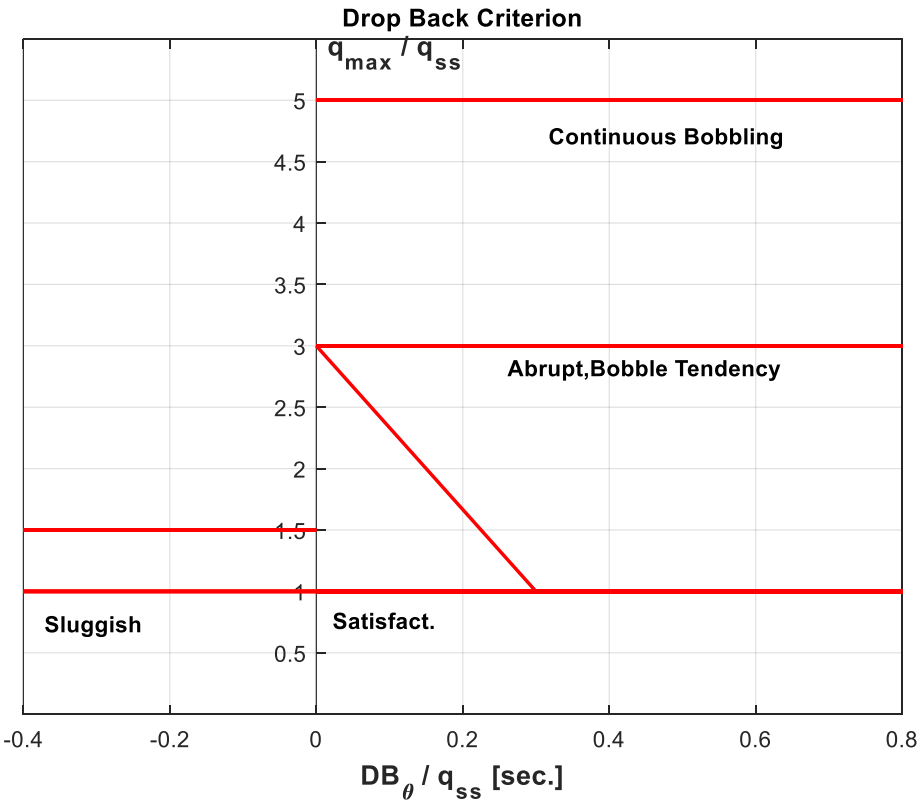

Figure 31. Drop back criterion regions

According to the mission type different drop back values are desired for satisfactory handling qualities. For instance, precision task requires small drop back values, almost super augmented type pitch rate response is preferred. On the other hand, for air to air refueling faster flight path control is required, so; high drop back is preferred.

3.3.3 Pilot Induced Oscillation

PIO is a dangerous phenomenon for aircrafts especially fly by wire ones. For this reason, in the scope of the thesis proposed flight control algorithm is required to be PIO free.

PIO definition and categorization , PIO scaling, and prediction of PIO methods are given in this section.

3.3.3.1 Definition and Categorization of PIO

Pilot induced oscillation is defined as " sustained or uncontrollable oscillations resulting from efforts of pilot to control aircraft" according to [24]. It doesn't mean any kind of oscillation can be considered as PIO. Sometimes these oscillations may be part of standard pilot compensation, such as typical ballooning that generally student pilots encounter during the landing training is a part of standard pilot compensation. [24]

Pilot induced oscillation can be categorized into three groups: type I, type II, and type III.

Type Ⅰ PIO is generally linear pilot- vehicle coupled oscillations which is a result of high frequency lag in the control augmentation system. Type Ⅱ PIO are described as quasi – linear pilot – vehicle coupled oscillations. The main result in this type of PIO are generally control surface rate or position limiters. Although type Ⅰ and type Ⅱ PIO are classified as linear and quasi linear, type Ⅲ PIO is classified as nonlinear. Generally abrupt shifts in augmented dynamics or pilot inputs causes this type of PIO.[28]

3.3.3.2 PIO Scaling

A scaling to assess the susceptibility of aircraft to PIO is designed. This scale is being used by test pilots and test engineers. This scale is similar to Cooper-Harper Handling Qualities Scaling.

PIO scale is given in Figure 32.[24]

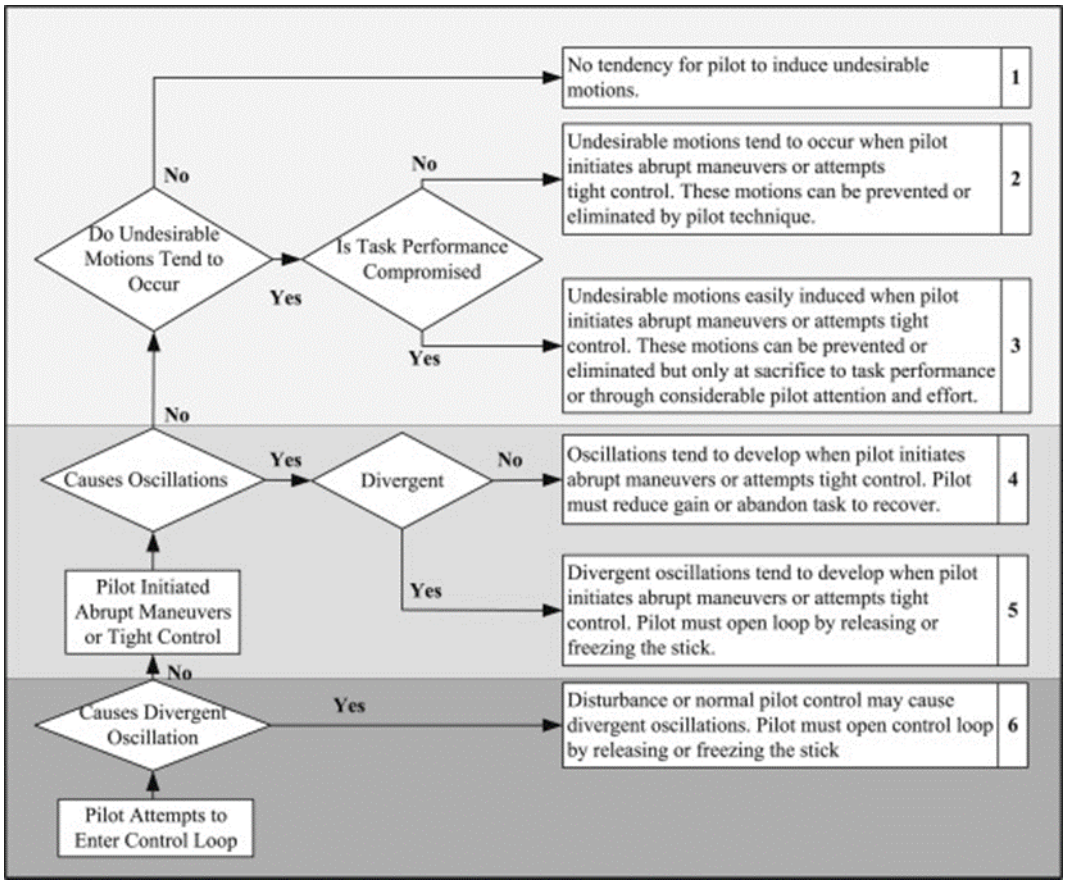

Figure 32. PIO scaling

3.3.3.3 PIO Prediction Methods

Several prediction criteria have been developed for type Ⅰ and type Ⅱ PIO, with the help of PIO scaling. A set of type Ⅰ PIO prediction criteria are selected as design requirement in the scope of the thesis. According to these requirements type Ⅰ PIO free longitudinal flight control algorithm design is aimed. Detailed explanation of each criterion will be given in rest of this section.

Selected type I PIO prediction methods are given in Table 13.

Table 13. Selected type I PIO prediction methods

Requirement	Domain
Pitch attitude bandwidth – pitch rate overshoot	Frequency
Gibson average phase rate	Frequency
Gibson gain-phase template	Frequency

3.3.3.3.1 Pitch Attitude Bandwidth – Pitch Rate Overshoot

This criterion is based on pitch attitude bandwidth, phase delay and pitch rate overshoot. Definition of pitch attitude bandwidth and phase delay were already given in section 3.3.6.1. Definition pitch rate overshoot is given in Figure 33.

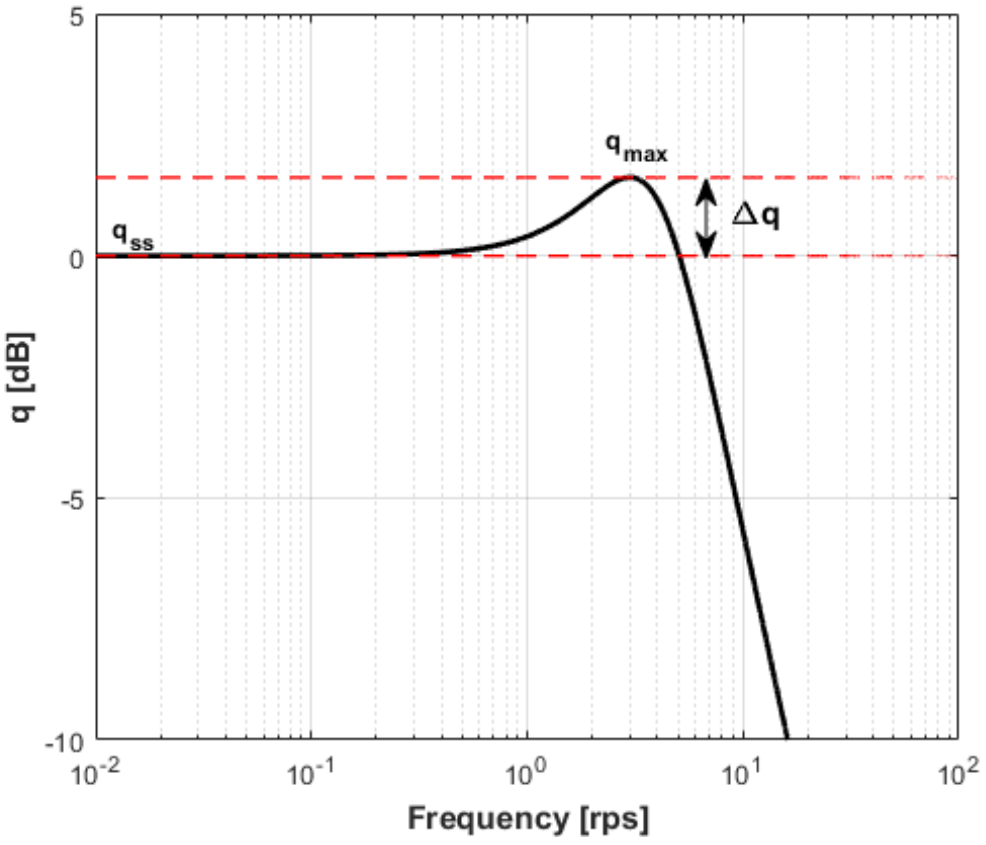

Figure 33. Pitch rate overshoot

Pitch rate overshoot is given in Eq. (3.5).

$$\Delta q = q_{max} - q_{ss} \tag{3.5}$$

Boundaries of pitch attitude bandwidth – pitch rate overshoot criterion is given in Figure 34.

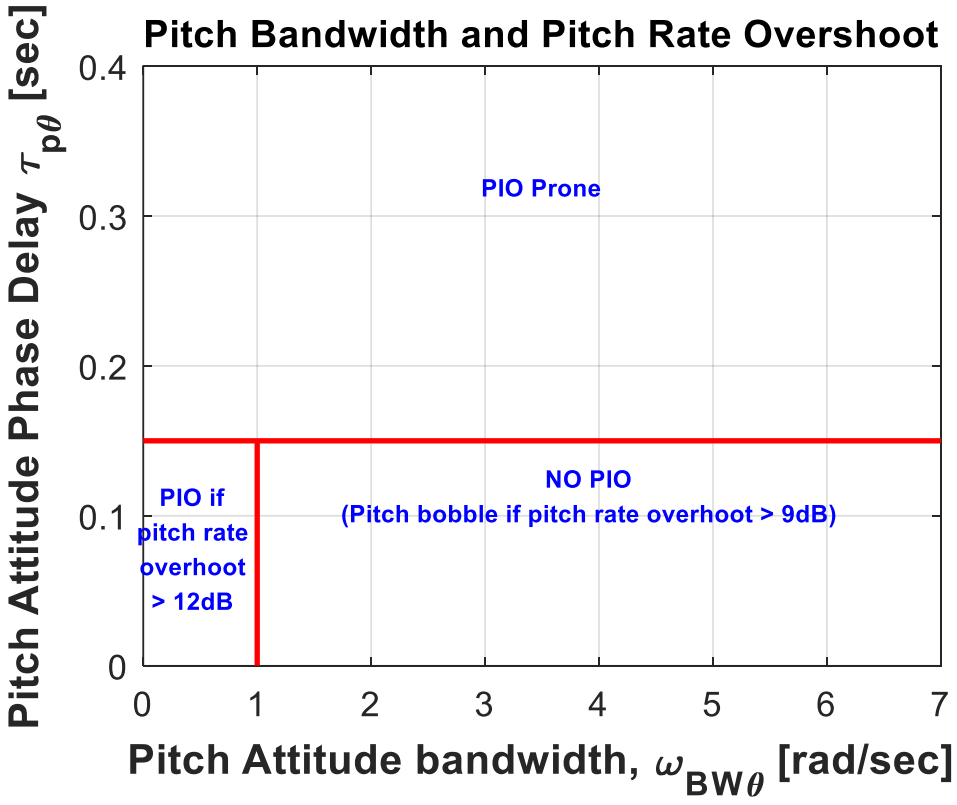

Figure 34. Pitch attitude bandwidth – pitch rate overshoot criterion regions

3.3.3.3.2 Gibson Average Phase Rate and gain-Phase Template

Average phase rate criterion focuses on around -180 degree attitude phase to investigate effect of the higher order dynamics in augmentation system. The frequency (ω_{-180}) where the attitude transfer function phase reaches -180 degree is called as PIO frequency because landing PIO is being triggered around this frequency. Average phase rate is a ratio of phase lag that introduced between ω_{-180} and $2\omega_{-180}$ to PIO frequency , in other words it is a local slope around ω_{-180}.

Average phase rate is given in Eq. (3.6).

$$\varphi_{2\omega_{-180}}: Phase\ at\ \omega = 2\omega_{-180}$$

$$Average\ phase\ rate = \frac{-(\varphi_{2\omega_{-180}} + 180)}{\omega_{-180}}\ \ deg/Hz \tag{3.6}$$

Illustration of average phase rate is given in Figure 35. [27]

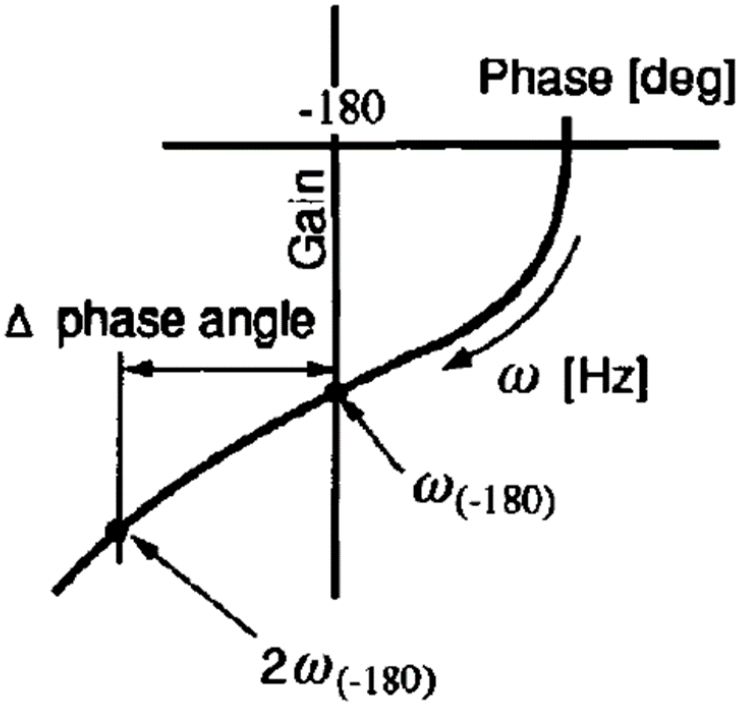

Figure 35. Average phase rate

The philosophy of average phase rate criterion is that PIO occurs around the ω_{-180} and local slope of pitch attitude phase response must be inside the defined region w.r.t frequency.

There is another criterion which has been introduced by Gibson is gain - phase template. It is a region defined in Nichols chart in terms of pitch attitude gain and phase responses. This template bounds the pitch attitude gain w.r.t pitch attitude phase angle.

Illustration of gain – phase template and PIO susceptibility is given in Figure 36.[27]

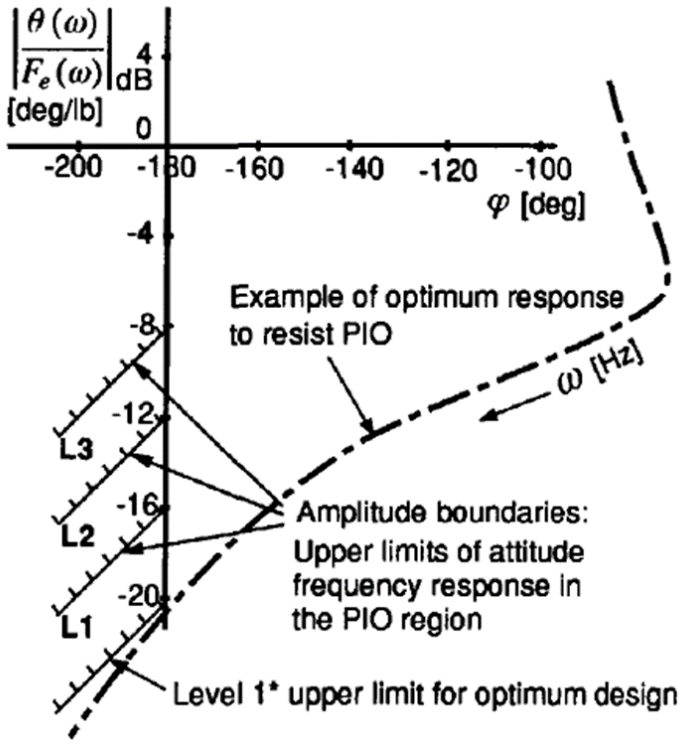

Figure 36. Gain phase template and PIO susceptibility

Gibson average phase rate & gain - phase template regions w.r.t success levels are given in Figure 37.

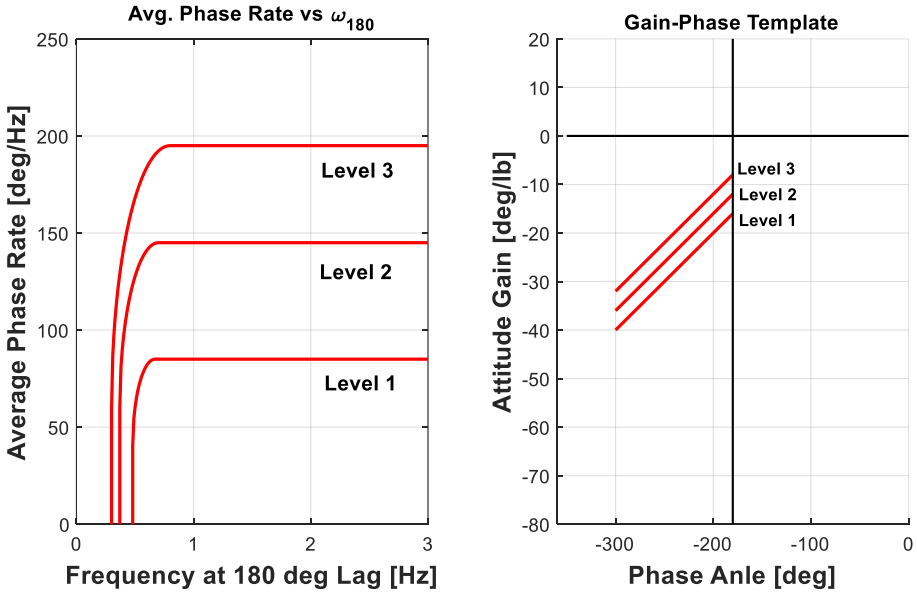

Figure 37. Average phase rate & gain phase template criteria regions

4. LONGITUDINAL FLIGHT CONTROL ALGORITHM

In this section architecture and design of base longitudinal flight control algorithm and two alternate proposed fault tolerant longitudinal flight control algorithms will be explained and applied for 10000 ft 0.7 Mach and CG_X =[28.45 31.34 34.02] (% of mac) which corresponds to most forward, nominal, and most aft CG_X positions respectively.

4.1 Controller Architecture

In the scope of the thesis three controller architectures are studied. The first one is base controller which is PI with feedforward dynamics. The second controller architecture is same with the first one but designed with different methodology. The last one is explicit model following with disturbance rejection controller. Detailed information about each controller architecture will be given in the rest of this section.

4.1.1 Base Controller

Base controller is PI with feedforward dynamics. Stability augmentation is performed with pitch rate and angle of attack feedbacks with addition of pitch rate integrator. Control augmentation is performed with pitch rate integrator and feedforward dynamics which are feedforward gain and feedforward filter respectively. Illustration of architecture is given in Figure 38.

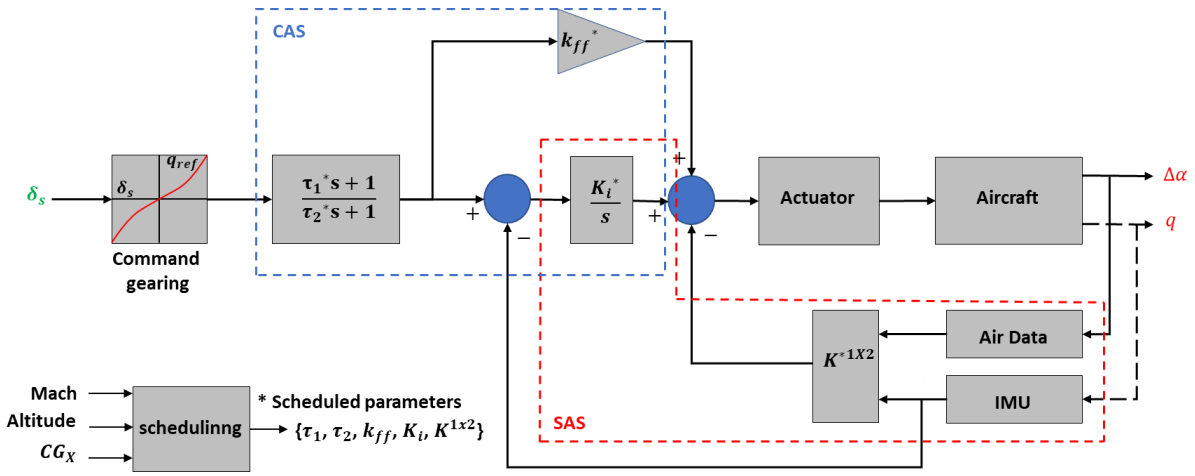

Figure 38. Base controller architecture

4.1.2 Alternative Controller No1

First alternative controller architecture is based on PI with feedforward dynamics, same as base controller. Controller is designed via structured H_∞ synthesis-based design methodology. Illustration of architecture is given in Figure 39.

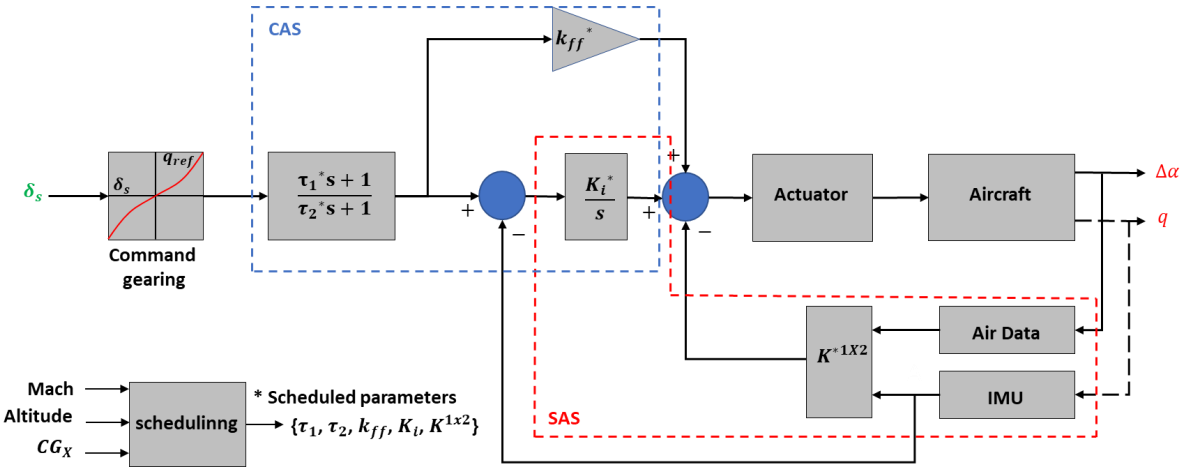

Figure 39. First alternative controller architecture

4.1.3 Alternative Controller No2

Explicit model following with disturbance rejection architecture is illustrated in Figure 40.

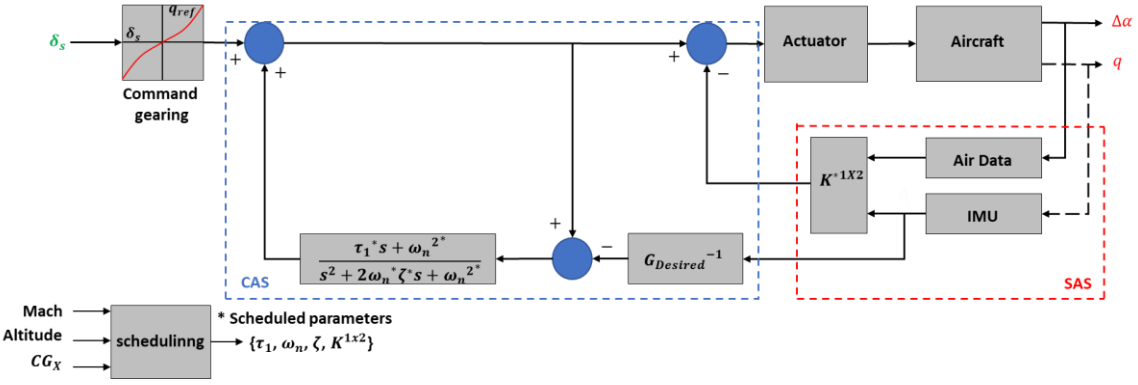

Figure 40. Second alternative controller architecture

Second alternative controller is based on model following with disturbance rejection architecture. Explicit model following is reached with disturbance rejection compensator which is tuned via structured H_∞ synthesis-based design methodology.

4.2 Explanation of Design Methodology and Application

Design methodology for base and two alternative longitudinal flight control algorithms will be explained in this section.

4.2.1 Generation of LTI Models

Base and alternative controllers are designed with linear time invariant models which are generated around a trim point. Detailed information about trim and linearization was given in section 2.3.

In stability augmentation system design 4by4 longitudinal state space model is used. Control augmentation system is designed with 2by2 short period approximation state space model on the other hand. The reason of this difference is that full longitudinal dynamics are considered for stability check. Performance requirements consider only short period dynamics on the other hand because of that flight control algorithm augments short period dynamics.

After generation of open loop aircraft longitudinal LTI models, flight control system elements which are actuator, imu, and air data are implemented as LTI models. Computational time delays are also considered to increase fidelity.

4.2.1.1 Full State Longitudinal LTI Model

Stability augmentation system is designed with open loop aircraft longitudinal 4by4 state space model which is constructed in aircraft body axis and given in Eq.(4.1) – Eq. (4.3).

$$X_{long} = [u\ w\ q\ \Delta\theta]', Y_{long} = [w\ q]', U = de \tag{4.1}$$

$$\dot{X}_{long} = A_{long}X_{long} + B_{long}U \tag{4.2}$$

$$Y_{long} = C_{long}X_{long} + D_{long}U \tag{4.3}$$

Longitudinal flight control algorithm augments aircraft short period dynamics (q, a), so; it is more convenient to construct open loop state space model in stability axis.

Proper transformation from aircraft body frame to stability frame is given in Eq. (4.4) – (4.10).

$$X_1 = [q\ \Delta\alpha\ v_T\ \Delta\theta]', Y_1 = [q\ \Delta a]', U = de \tag{4.4}$$

$$T_1 = \begin{bmatrix} \cos\alpha_n & 0 & 0 & -V_n \sin a_n \\ \sin a_n & 0 & 0 & V_{n\cos\alpha_n} \\ 0 & 0 & 1 & 0 \\ 0 & 1 & 0 & 1 \end{bmatrix} \tag{4.5}$$

$$T_2 = \begin{bmatrix} 0 & 0 & 1 & 0 \\ 0 & 0 & 0 & 1 \\ 1 & 0 & 0 & 0 \\ 0 & 1 & 0 & 1 \end{bmatrix} \tag{4.6}$$

$$A_1 = {T_2}^{-1}{T_1}^{-1}A_{long}T_1T_2 \tag{4.7}$$

$$B_1 = {T_2}^{-1}{T_1}^{-1}B_{long} \tag{4.8}$$

$$C_1 = C_{long} \tag{4.9}$$

$$D_1 = D_{long} \tag{4.10}$$

Jet trainer aircraft longitudinal state space matrices for 10 kft 0.7 Mach are given for most forward, nominal, and most aft CG_X positions.

$$CG_X = 28.45\%\ of\ mac\ (mfwd) \tag{4.11}$$

$$A_1 = \begin{bmatrix} -1.3421 & -0.4983 & -0.0001 & 0.0000 \\ 0.9628 & -1.2815 & -0.0004 & 0.0000 \\ -0.1353 & -10.9829 & -0.0170 & -9.8060 \\ 0.0322 & 1.2815 & 0.0004 & 0.0000 \end{bmatrix}, B_1 = \begin{bmatrix} -28.1356 \\ -0.1503 \\ -0.6270 \\ 0.1503 \end{bmatrix}$$

$$CG_X = 31.34\%\ of\ mac\ (nominal) \tag{4.12}$$

$$A_1 = \begin{bmatrix} -1.2947 & 3.1054 & -0.0001 & 0.0000 \\ 0.9628 & -1.4360 & -0.0004 & 0.0000 \\ -0.1321 & -8.1879 & -0.0190 & -9.8060 \\ 0.0372 & 1.4360 & 0.0004 & 0.0000 \end{bmatrix}, B_1 = \begin{bmatrix} -28.8330 \\ -0.1710 \\ -0.4372 \\ 0.1710 \end{bmatrix}$$

$$CG_X = 34.02\%\ of\ mac\ (maft) \tag{4.13}$$

$$A_1 = \begin{bmatrix} -1.2376 & 6.9977 & -0.0001 & 0.0000 \\ 0.9632 & -1.4229 & -0.0004 & 0.0000 \\ -0.1301 & -8.2979 & -0.0188 & -9.8060 \\ 0.0368 & 1.4229 & 0.0004 & 0.0000 \end{bmatrix}, B_1 = \begin{bmatrix} -29.2109 \\ -0.1688 \\ -0.4275 \\ 0.1688 \end{bmatrix}$$

In the scope of the controllability and observability; state and output controllability and observability analyses are performed for three CG_X positions. State controllability matrix is given as:

* $Q_{i=1,2,3}$ indicates state controllability matrices for different CG_X position configurations; 1.mfwd, 2.nominal, 3maft.

$$Q_{i=1,2,3} = [B \vdots AB \vdots A^2B \vdots A^3B] \tag{4.14}$$

$$\text{Rank } (Q_{i=1,2,3}) = 4 \tag{4.15}$$

According to Eq. (4.15) open loop systems, with three different CG_X positions, are state controllable. Output controllability matrix is given as:

* $R_{i=1,2,3}$ indicates output controllability matrices for different CG_X position configurations; 1.mfwd, 2.nominal, 3maft.

$$R_{i=1,2,3} = [CB \vdots CAB \vdots CA^2B \vdots CA^3B] \tag{4.16}$$

$$\text{Rank } (R_{i=1,2,3}) = 4 \tag{4.17}$$

According to Eq. (4.17) open loop systems, with three different CG_X positions, are output controllable. Observability matrix is given as:

* $J_{i=1,2,3}$ indicates observability matrices for different CG_X position configurations; 1.mfwd, 2.nominal, 3maft.

$$J_{i=1,2,3} = [C' \vdots A'C' \vdots A'^2C' \vdots A'^3C'] \tag{4.18}$$

$$\text{Rank } (J_{i=1,2,3}) = 4 \tag{4.19}$$

*C'indicates transpose of C.

According to Eq. (4.19) open loop systems, with three different CG_X positions, are observable.

4.2.1.2 Short Period Longitudinal LTI Model

Aircraft longitudinal dynamics can be separated into two modes: short period mode and long period mode in other words Phugoid mode. This categorization is performed w.r.t period of dynamics. Pitch rate and angle of attack represent short period dynamics. Long period dynamics include theta and true speed on the other hand.

In short period approximation it is assumed that change in theta and true air speed are small, and they can be negligible (definition in stability axis). Short period state space matrices which are constructed with aerodynamic derivatives in stability axis are given in Eq. (4.20) – Eq.(4.26).

$$X_{SP} = [\, q\ \Delta a]', Y_{sp} = [q\ \Delta a]',\ U = de \tag{4.20}$$

$$A_{sp} = \begin{bmatrix} M_q & M_a \\ 1 - \frac{L_q}{V_n} & \frac{L_a}{V_n} \end{bmatrix} \tag{4.21}$$

$$B_{sp} = \begin{bmatrix} M_{de} \\ \frac{-L_{de}}{V_n} \end{bmatrix} \tag{4.22}$$

$$C_{sp} = \begin{bmatrix} 1 & 0 \\ 0 & 1 \end{bmatrix} \tag{4.23}$$

$$D_{sp} = \begin{bmatrix} 0 \\ 0 \end{bmatrix} \tag{4.24}$$

$$\dot{X}_{sp} = A_{sp}X_{sp} + B_{sp}U \tag{4.25}$$

$$Y_{sp} = C_{sp}X_{sp} + D_{sp}U \tag{4.26}$$

Jet trainer aircraft short period state space matrices for 10 kft 0.7 Mach are given in Eq.(4.27) - (4.29) for most forward, nominal, and most aft CG_X positions.

$$CG_X = 28.45\%\ of\ mac\ (mfwd), A_{sp} = \begin{bmatrix} -1.34 & -0.50 \\ 0.97 & -1.28 \end{bmatrix}, B_{sp} = \begin{bmatrix} -28.14 \\ -0.15 \end{bmatrix} \tag{4.27}$$

$$CG_X = 31.34\%\ of\ mac\ (nominal), A_{sp} = \begin{bmatrix} -1.30 & 3.10 \\ 0.96 & -1.44 \end{bmatrix}, B_{sp} = \begin{bmatrix} -28.83 \\ -0.17 \end{bmatrix} \tag{4.28}$$

$$CG_X = 34.02\%\ of\ mac\ (maft), A_{sp} = \begin{bmatrix} -1.24 & 7.00 \\ 0.96 & -1.42 \end{bmatrix}, B_{sp} = \begin{bmatrix} -29.21 \\ -0.17 \end{bmatrix} \quad (4.29)$$

Normalized time response comparison of pitch rate to stick transfer functions for three CG_X positions is given in Figure 41.

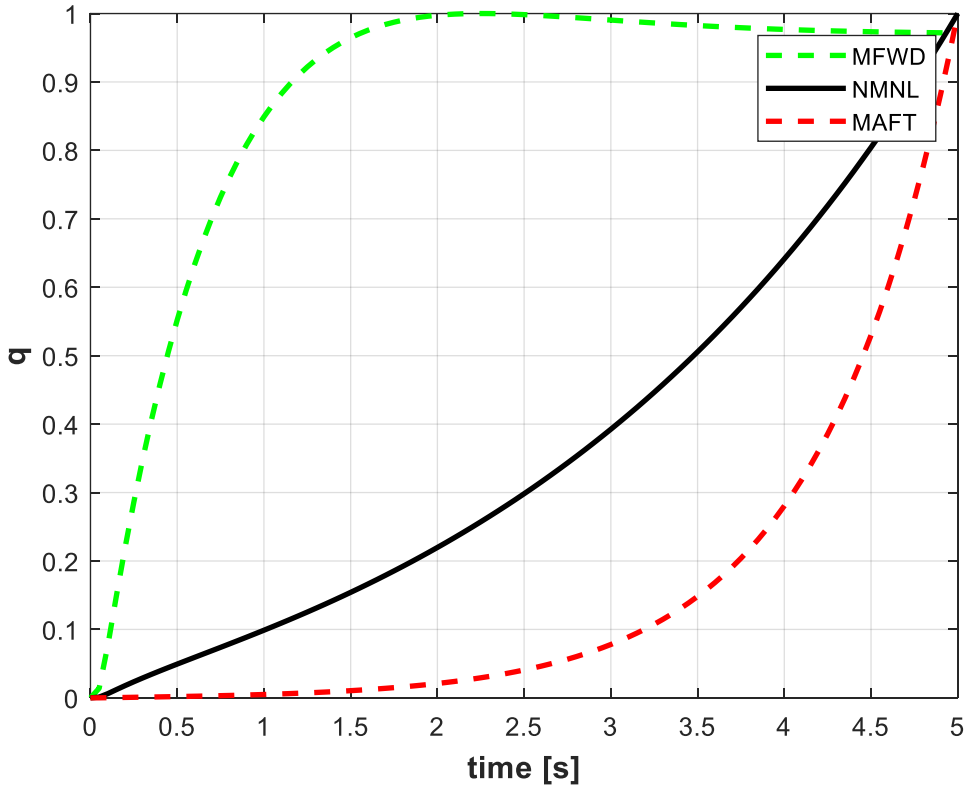

Figure 41. Normalized time response comparison of pitch rate to stick transfer functions for three CG_X positions

Frequency response comparison of pitch rate to stick transfer functions for three CG_X positions is given in Figure 42.

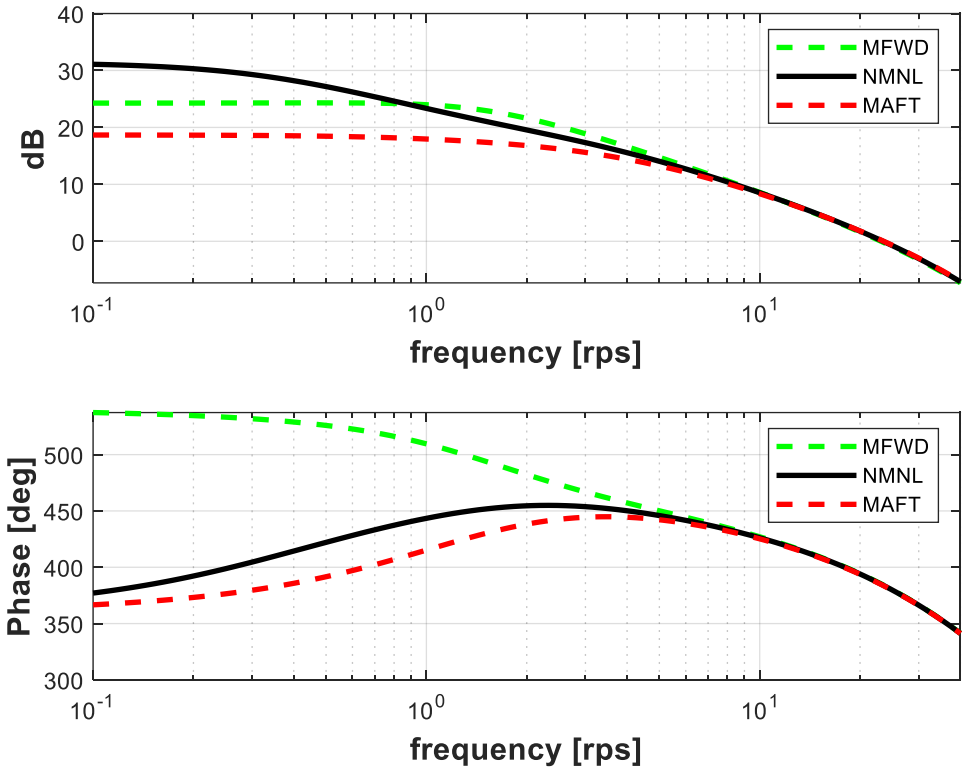

Figure 42. Frequency response comparison of pitch rate to stick transfer functions for three CG_X positions

4.2.1.3 Flight Control System LTI Models

Flight control systems: command gearing, actuator, IMU, and air data are modeled as LTI systems.

Command gearing is map which transforms pilot stick deflection to reference demand signal which is reference pitch rate. For the convenience, one-to-one command gearing ($\delta_s = q_{ref}$) is used in the scope of thesis.

Block diagram of 5th order actuator LTI model with nonlinear elements is given in Figure 43 .

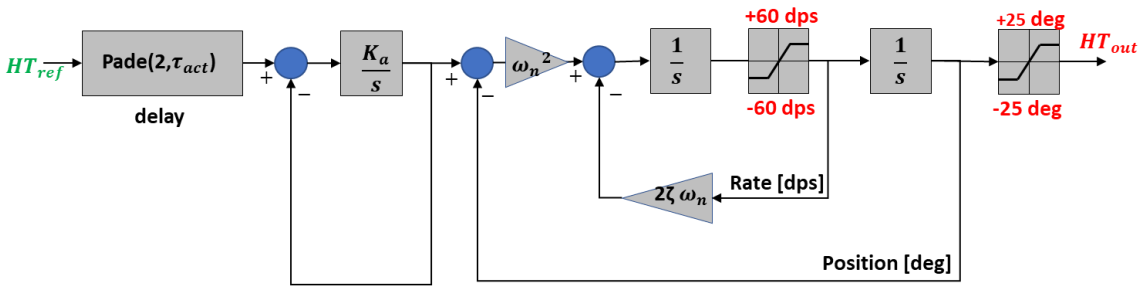

Figure 43. Actuator model

Actuator model parameters are given in Table 14.

Table 14. Actuator parameters

Parameter	Value
ω_n	71.4 [rps]
ζ	0.736
K_a	35
τ_{act}	0.005 [s]

Actuator transfer function model is given in Eq. in (4.30) and Eq. (4.31).

2nd order pade approximant of 5 ms delay (4.30)

$$delay\ (s) = \frac{s^2 - 1200s + 480000}{s^2 + 1200s + 480000}$$

$$Act(s) = delay(s) \times \frac{1.784e + 05}{s^3 + 140.1s^2 + 8776s + 1.784e + 05} \quad (4.31)$$

Actuator state space model is given in Eq. (4.32) – Eq. (4.34).

* $Spade1$ & $Spade2$ indicates states of time delay pade approximant.

$$X_{act} = [de\ dedot\ de2dot\ Spade1\ Spade2]', Y_{act} = [de]', U = de\_comm \tag{4.32}$$

$$\dot{X}_{act} = A_{act}X_{act} + B_{act}U \tag{4.33}$$

$$Y_{act} = C_{act}X + D_{act}U \tag{4.34}$$

IMU and air data sensor are modeled as 4th order system with same natural frequency and damping ratio. The model used for both IMU and air data sensor is given in Figure 44.

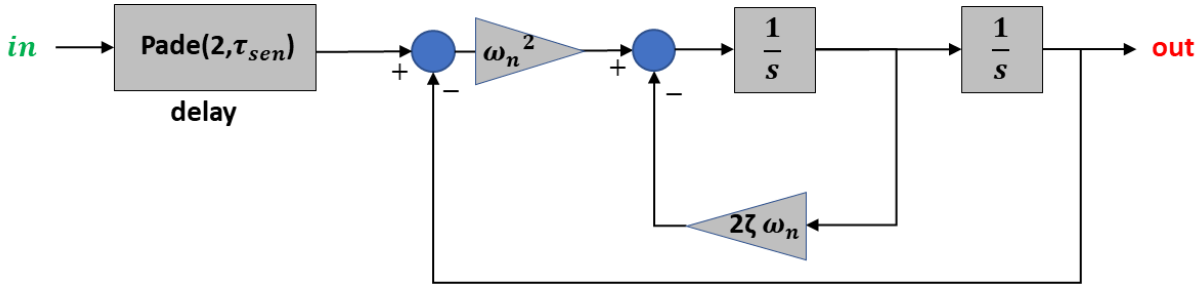

Figure 44. IMU and air data model

IMU and air data sensor model parameters are given in Table 15.

Table 15. IMU and air data sensor parameters

Parameter	Value
ω_n	200 [rps]
ζ	0.890
τ_{sen}	0.005 [s]

IMU and air data sensor transfer function models are given in Eq. (4.35).

$$IMU(s) = AirD(s) = delay(s) \times \frac{40000}{s^2 + 356s + 40000} \tag{4.35}$$

IMU and air data sensor state space models are given in Eq. (4.36) – Eq. (4.41).

$$X_{imu} = [Simu\ Simudot\ Spade1\ Spade2\ ]', Y_{imu} = [Simu]', U_{imu} = q \tag{4.36}$$

$$\dot{X}_{imu} = A_{imu}X_{imu} + B_{imu}U_{imu} \tag{4.37}$$

$$Y_{imu} = C_{imu}X_{imu} + D_{imu}U_{imu} \tag{4.38}$$

$$X_{aird} = [Saird\ Sairddot\ Spade1\ Spade2\ ]', Y_{imu} = [Saird]', U_{imu} = \Delta a \tag{4.39}$$

$$\dot{X}_{aird} = A_{aird}X_{aird} + B_{aird}U_{aird} \tag{4.40}$$

$$Y_{aird} = C_{aird}X_{aird} + D_{aird}U_{aird} \tag{4.41}$$

For convenience IMU and air data sensor state space models are merged and called as sensor. Sensor state space model is given in Eq. (4.42) – Eq. (4.46).

$$X_{sen} = [Simu\ Simudot\ Saird\ Sairddot\ Spade1\ Spade2\ Spade1\ Spade2\ ]' \tag{4.42}$$

$$Y_{sen} = [Simu; Saird]', U_{sen} = [q; \Delta a]$$

$$A_{sen} = \begin{bmatrix} A_{imu} & zeros(4,4) \\ zeros(4,4) & A_{aird} \end{bmatrix} \tag{4.43}$$

$$B_{sen} = \begin{bmatrix} B_{imu} & zeros(4,1) \\ zeros(4,1) & B_{aird} \end{bmatrix} \tag{4.44}$$

$$C_{sen} = \begin{bmatrix} C_{imu} & zeros(1,4) \\ zeros(1,4) & C_{aird} \end{bmatrix} \tag{4.45}$$

$$B_{sen} = \begin{bmatrix} D_{imu} & 0 \\ 0 & D_{aird} \end{bmatrix} \tag{4.46}$$

4.2.2 Controller Design

Longitudinal stability is enhanced with feedback augmentation for the three controller architectures. Feedback gains are calculated with people placement methodology for base controller. Parameter space approach methodology is followed to calculate feedback gains for two alternative controllers.

Control augmentation is performed with PI feedback controller and feedforward dynamics in base controller. Control augmentation system is designed with pole - zero assignment methodology.

The first alternative controller uses same architecture with base controller, for control augmentation. Parameters of PI feedback controller are tuned with structured H_∞ synthesis-based design methodology. Feedforward dynamics are designed via pole - zero assignment methodology, like performed in base controller.

The second alternative controller is based on completely different architecture; explicit model following with disturbance rejection. Control augmentation is performed a series for compensators. Control augmentation system parameters are calculated via structured H_∞ synthesis-based design methodology, like performed in first alternative controller.

4.2.2.1 Base Controller

In base controller architecture, stability augmentation is performed with output feedbacks which are pitch rate and angle of attack. Base controller SAS loop is illustrated in Figure 45.

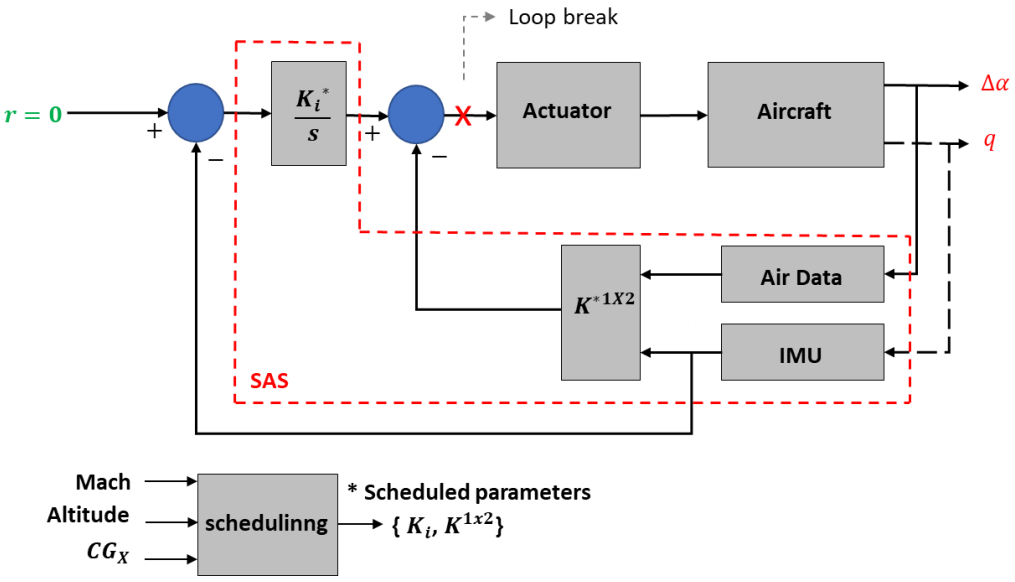

Figure 45. Base controller SAS loop

According to the Figure 45 loop gain L(ss) is given in Eq. (4.47).

*Actuator, Aircraft, IMU, and Air Data are given in state space (ss) format. I(ss) represents state space model of integrator.

$$L(ss) = [K_{(1,1)} \quad K_{(1,2)} \quad K_i] \begin{bmatrix} Actuator * Aricraft(1,1) * \boldsymbol{IMU} \\ Actuator * Aricraft(2,1) * \boldsymbol{AirData} \\ -Actuator * Aricraft(1,1) * \boldsymbol{IMU} * \boldsymbol{I}(ss) \end{bmatrix} \tag{4.47}$$

To prevent rank deficiency; IMU and air data sensors are only considered in analysis section. Loop gain state space representation, without integrator, for design processes is modified in Eq. (4.48) – Eq. (4.53). Implementation of integrator will be explained in detail and finally total loop gain state space representation will be given.

$$L(ss) = [K_{(1,1)} \quad K_{(1,2)}] \begin{bmatrix} Actuator * Aricraft(1,1) \\ Actuator * Aricraft(2,1) \end{bmatrix} \tag{4.48}$$

$$X_2 = [X_1 \; X_{act}]', Y = [q \; \Delta a]', U = d_e \tag{4.49}$$

$$A_2 = \begin{bmatrix} A_1 & B_1 C_{act} \\ zeros(4,4) & A_{act} \end{bmatrix} \tag{4.50}$$

$$B_2 = \begin{bmatrix} zeros(4,1) \\ B_{act} \end{bmatrix} \tag{4.51}$$

$$C_2 = [eye(2) \quad zeros(2,2) \quad zeros(2,5)] \tag{4.52}$$

$$D_2 = \begin{bmatrix} 0 \\ 0 \end{bmatrix} \tag{4.53}$$

Loop gain state space representation for analysis processes is modified in Eq. (4.54) – Eq. (4.58). (sensor model is added)

$$X_3 = [X_{sen} \; X_2]', Y = [q \; \Delta a]', U = d_e \tag{4.54}$$

$$A_3 = \begin{bmatrix} A_{sen} & B_{sen} C_2 \\ zeros(9,8) & A_2 \end{bmatrix} \tag{4.55}$$

$$B_3 = \begin{bmatrix} zeros(8,1) \\ B_2 \end{bmatrix} \tag{4.56}$$

$$C_3 = [c_{sen} \quad zeros(2,9)] \tag{4.57}$$

$$D_3 = \begin{bmatrix} 0 \\ 0 \end{bmatrix} \tag{4.58}$$

The purpose of stability augmentation system is to augment longitudinal dynamics by assigning desired Eigen space parameters which are natural frequency (ω_{sp}) and damping ratio (ζ_{sp}). Desired Eigen space parameters are selected w.r.t military standards.[24]

Short period approximation pitch rate to stick transfer function is given in Eq. (4.59).

$$\frac{q}{\delta_{stick}}(s) = \frac{K_q(1 + T_{\theta 2}s)}{s^2 + 2\omega_n\zeta s + \ {\omega_n}^2} \tag{4.59}$$

In Eq. 4.59 $T_{\theta 2}$ time constant of airframe “zero” which is related with lift characteristics of the aircraft. Position of airframe zero can be changed via lift devices such as trailing edge flap. In the scope of the thesis trailing edge flap or other any lift devices are not used as primary control surface, so; the position of the airframe zero is assumed as fixed.

Desired Eigen space parameters can be selected wr.t $\frac{n}{a}$ which is normal acceleration per angle of attack. This property is unique to aircraft. Derivation of $\frac{n}{a}$ is given in Eq. (4.60).

$$\frac{n}{a} = \frac{V_T}{gT_{\theta 2}} \tag{4.60}$$

A diagram which relates Eigen space parameters (ω_{sp}, ζ_{sp}) with $\frac{n}{a}$ is given in Figure 46 & Figure 47.[27][29]

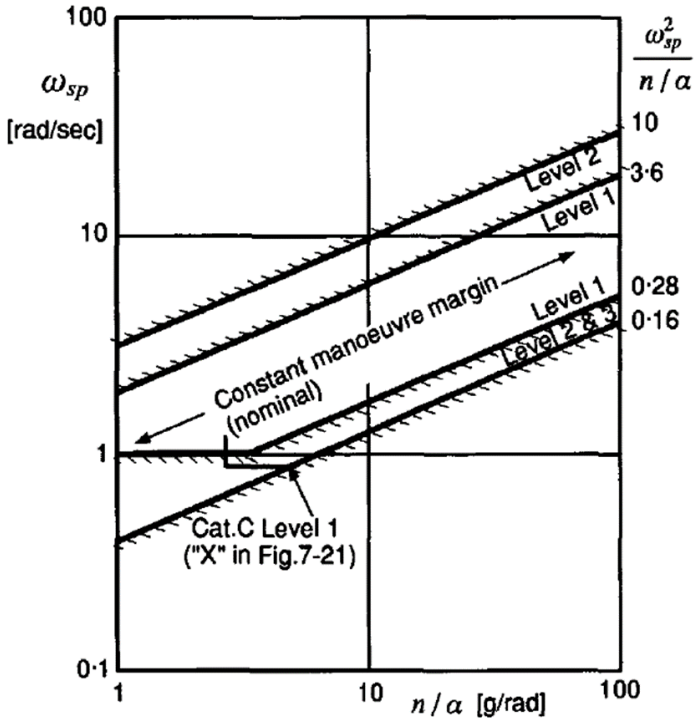

Figure 46. Allowable short period natural frequency vs n/a

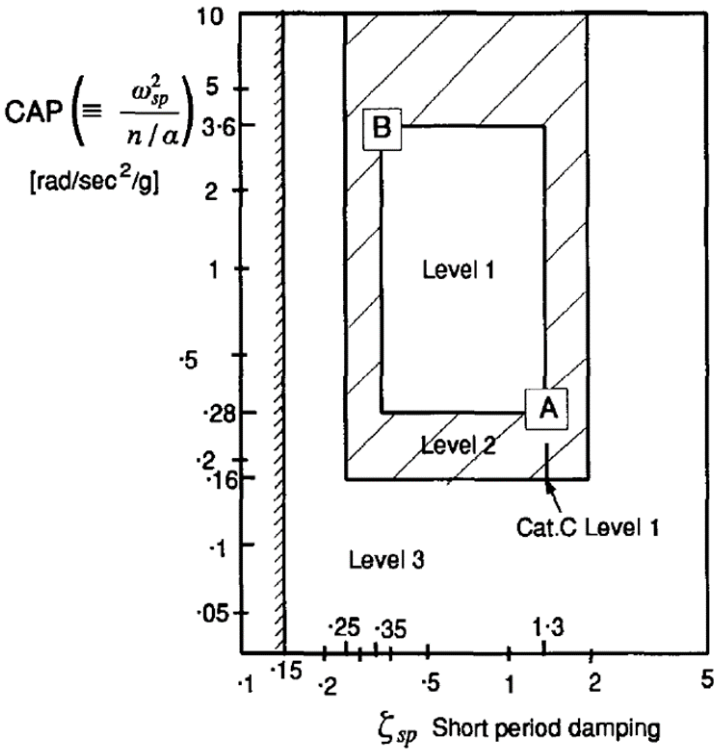

Figure 47. Allowable short period damping ratio vs n/a

According to the Figure 46 & Figure 47 minimum and maximum allowable ω_n and ζ are given in Eq. (4.61) & Eq. (4.62).

$$(0.28n/a)^{0.5} \leq \omega_{sp} \leq (3.6n/a)^{0.5} \tag{4.61}$$

$$0.35 \leq \zeta_{sp} \leq 1.3 \tag{4.62}$$

Selected Eigen space parameters for the jet trainer aircraft which satisfies Eq. (4.61) & Eq. (4.62) for three CG_X positions are given in Table 16.

Table 16. Selected Eigen space parameters

Selected Eigen Space Parameter	**Value**
ω_{sp}	4.3140 [rps]
ζ_{sp}	0.8250

Desired Eigen space parameters are assigned via Eigen value assignment with output feedback algorithm. Evaluation of the algorithm is given in Eq. (4.63) - (4.68).

$$\lambda_{1,2} = -\zeta_{sp}\omega_{sp} \pm i\omega_{sp}\sqrt{1-{\zeta_{sp}}^2} \tag{4.63}$$

$$(A + BKC)v_i = \lambda_i v_i \tag{4.64}$$

$$[\lambda_i I - A \quad \vdots \quad B]\begin{bmatrix} v_i \\ -KCv_i \end{bmatrix} = 0 \tag{4.65}$$

$$\begin{bmatrix} v_i \\ -KCv_i \end{bmatrix} = \begin{bmatrix} v_i \\ w_i \end{bmatrix} \tag{4.66}$$

$$\begin{bmatrix} v_i \\ w_i \end{bmatrix} \; is\; orthogonal\; null\; space\; of\; [\lambda_i I - A \quad \vdots \quad B]$$

$$w_i = -K_i C v_i \tag{4.67}$$

$$K_i = -w_i(Cv_i)^{-1} \tag{4.68}$$

Calculation of the feedback gains is performed after integration of PI controller. It is not possible to separate PI controller from SAS loop but for the convenience and modular design approach PI controller is assumed as a part of CAS which is responsible for disturbance rejection and command shaping.

Separated CAS structure is given in Figure 48.

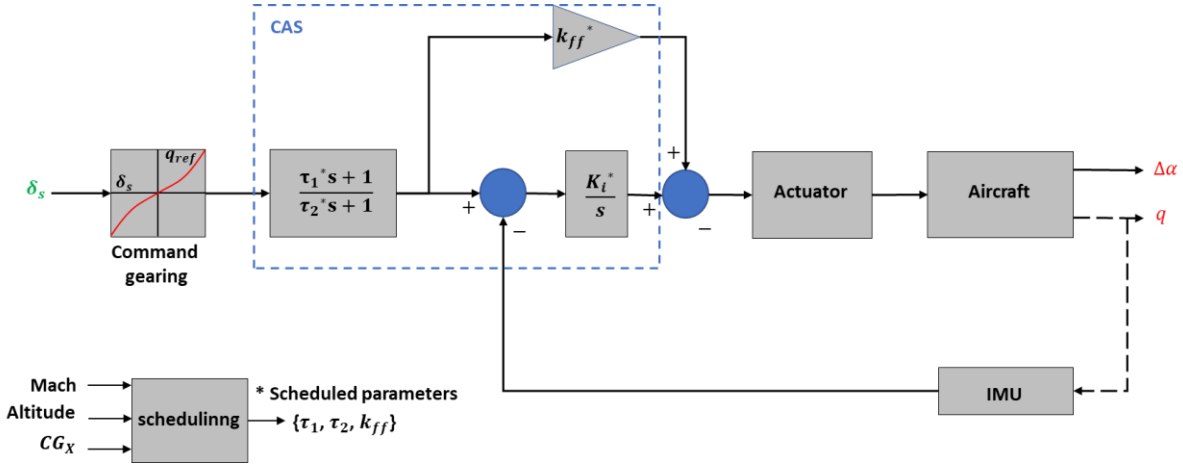

Figure 48. Base controller CAS loop

The main purpose of integrator is disturbance rejection. Addition of integrator mode violates classical aircraft longitudinal dynamics. To get classical aircraft longitudinal dynamics response a feedforward gain is added which cancels integrator mode when pilot gives input. By this structure pilot reaches classical aircraft response. Feedforward filter is used to assign transfer zero and cancel out air frame zero to improve handling qualities in terms of drop - back criterion. Complete controller structure assigns desired dynamics with feedback and feedforward elements.

Integrator mode is selected in Eq. (4.69).

$$\lambda_I = -\min\left(0.7{T_{\theta 2}}^{-1}, 0.5\right) \tag{4.69}$$

Feedforward gain is calculated in Eq. (4.70).

$$k_{ff} = -\frac{K_i}{\lambda_I} \tag{4.70}$$

Feedforward filter time constants w.r.t desired drop – back criterion is given in Eq. (4.71) – Eq. (4.74). Desired drop back is selected w.r.t drop back criterion satisfactory region, given in Figure 31.

$$desired\ drop\ back = \frac{DB}{q_{ss}} = 0.10 \tag{4.71}$$

$$T_{\theta 2_{des}} = \frac{DB}{q_{ss}} + \frac{2\zeta_{sp}}{\omega_{sp}} \tag{4.72}$$

$$\tau_1 = T_{\theta 2_{des}} \tag{4.73}$$

$$\tau_2 = T_{\theta 2_{airframe}} \tag{4.74}$$

Illustration of pole - zero assignment is given in Figure 49.

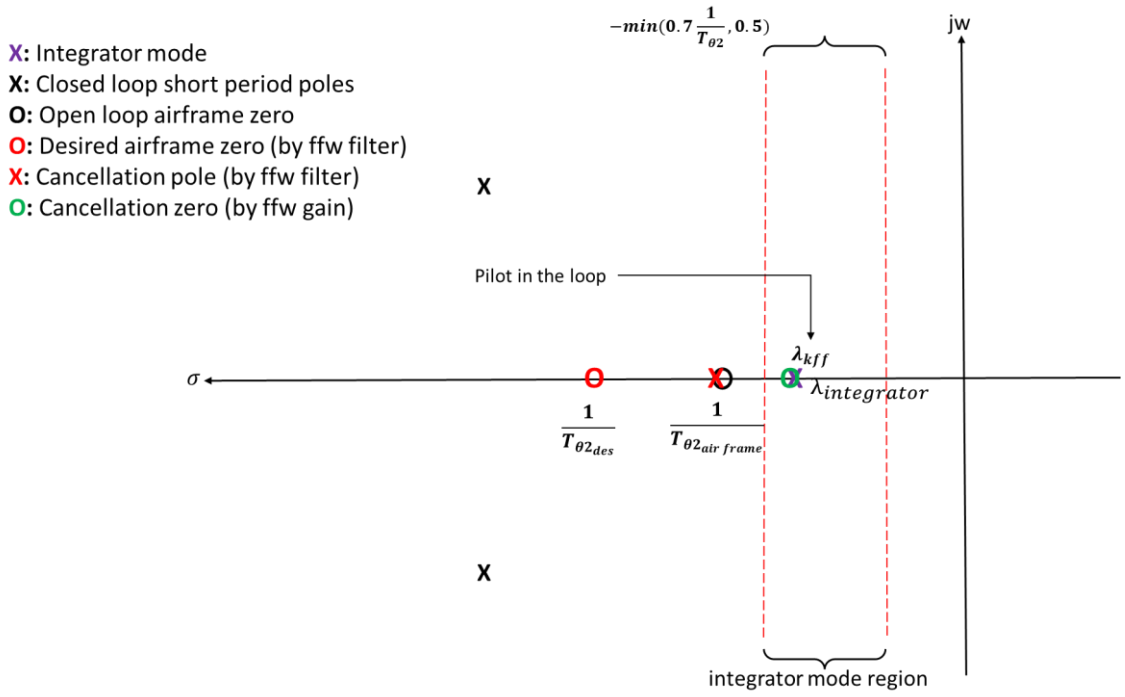

Figure 49. Assignment of desired Eigen space parameters

Complete loop gain design matrix after implementation of pitch rate error integrator is given in Eq. (4.75) – Eq. (4.79).

$$X_4 = [X_1\ X_{act} X_{err}]', Y = [q\ \Delta a]', U = d_e \tag{4.75}$$

$$A_4 = \begin{bmatrix} A_2 & zeros(9,1) \\ -C_2(1,:) & 0 \end{bmatrix} \tag{4.76}$$

$$B_4 = \begin{bmatrix} B_2 \\ 0 \end{bmatrix} \tag{4.77}$$

$$C_4 = \begin{bmatrix} C_2 & zeros(2,1) \\ zeros(1,9) & 1 \end{bmatrix} \tag{4.78}$$

$$D_4 = \begin{bmatrix} D_2 \\ 0 \end{bmatrix} \tag{4.79}$$

Feedback gains are calculated w.r.t Eq. (4.80) and by following the procedure given in Eq. (4.63) – Eq. (4.68).

$$[\lambda_i I - A_4 \quad \vdots \quad B_4] \begin{bmatrix} v_i \\ -K_i{}^{1X3} C_4 v_i \end{bmatrix} = 0 \tag{4.80}$$

Controller parameters are given in Table 17 for three CG_X positions.

Table 17. Controller parameters

Configuration	k_q	k_a	K_i	K_{ff}	τ_1	τ_2
$CG_{X\ MFW}$	-0.1432	-0.1545	0.1934	-0.3868	0.4825	0.7820
$CG_{X\ NMNL}$	-0.1421	-0.2664	0.1663	-0.3327	0.4825	0.6876
$CG_{X\ AFT}$	-0.1472	-0.3840	0.1617	-0.3233	0.4825	0.6834

Controller parameters are scheduled w.r.t Mach number, altitude [ft] and CG_X position (% of mac).

4.2.2.2 Alternative Controller No1

In first alternative controller the same architecture with base controller is tried to be tuned such that stability and performance robustness are enhanced without any adaption w.r.t CG_X position information. The purpose is to design longitudinal flight control algorithm that successes stability and performance robustness in case of CG_X position information fault, which is explained in section 3.1.

Controller architecture with design structure (desired model, weights) is given in Figure 50.

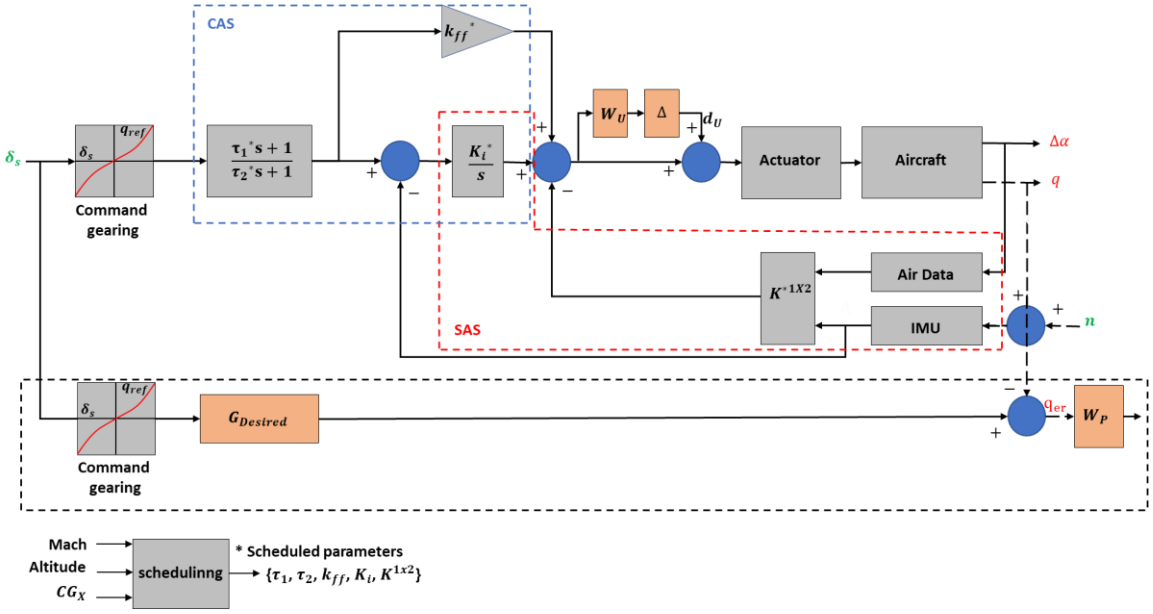

Figure 50. First alternative controller architecture with design structure

In base controller the feedback gains were calculated via Eigen value assignment methodology. Exact CG_X position is required to find feedback gains such that desired Eigen values are reached. In the first alternative controller instead of Eigen value assignment, “Eigen space” assignment methodology where the stability robustness is guaranteed for three CG_X positions is followed.

For the convenience, problem statement base is transformed form Eigen Space to feedback gains. The new statement is given as; a two dimensional (k_q, k_a) feedback gain basis which satisfies predefined stability robustness requirements is calculated via parameter space approach methodology.[13] An appropriate subspace from this basis is selected w.r.t time domain handling qualities for nominal CG_X position configuration. At the end of the processes, selected feedback gains guarantee relative and absolute stability margin for three different CG_X position configurations and satisfies handling qualities for nominal CG_X position configuration. Parameter space approach is a frequency domain-based methodology, so; it is convenient to represent relative and absolute stability in frequency domain.

According to [30] “Stability requirements can be represented on Nyquist diagram with region (γ) and its counterpart ($\bar{\gamma}$). This region consists of n boundaries ($\partial\gamma_{i=1,2..n}$) which are generated in terms of mathematical curve equations ($F_{\partial\gamma_{i=1,2..n}}(\sigma, w) = 0$).” Nyquist diagram with defined stability region (γ) and its counterpart ($\bar{\gamma}$) is given in Figure 51. [30]

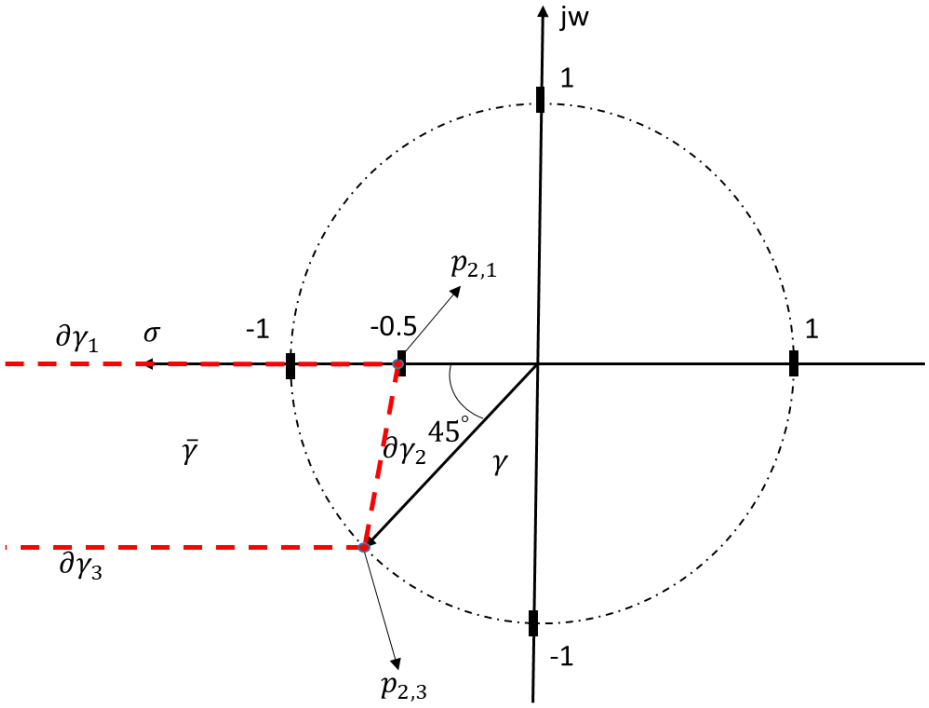

Figure 51. Demonstration of stability requirements on Nyquist diagram

Each mathematical curve equations ($F_{\partial\gamma_{i=1,2..n}}(\sigma, w) = 0$) that defines the boundaries ($\partial\gamma_{i=1,2..n}$) are given in Eq. (4.81) – Eq. (4.83). [30]

$$\partial\gamma_1 \quad F_{\partial\gamma_1}(\sigma, w) = w = 0 \qquad \{\sigma + wj |\ \sigma \leq -0.5\} \tag{4.81}$$

$$\partial\gamma_2 \quad F_{\partial\gamma_2}(\sigma, w) = 2\sigma + \left(\sqrt{2} - 2\right)w + 1 = 0 \qquad \{\sigma + wj | -0.7071 \leq \sigma \leq -0.5\} \tag{4.82}$$

$$\partial\gamma_3 \quad F_{\partial\gamma_3}(\sigma, w) = w = -0.7071 \qquad \{\sigma + wj |\ \sigma \leq -0.7071\} \tag{4.83}$$

Stability robustness can be defined for a set of loop transfer functions with feedback gains $\{k_q, k_a\} \in K^{1x2}$, which is given in Eq. (4.84).

$$K_\gamma = \left\{ \{k_q, k_a\} | L\left(jw, \{k_q, k_a\}\right)_{i=1,2..m} \subset \gamma, \forall w \in [0.1,40] rad/s \right\} \tag{4.84}$$

As indicated in Figure 51 region (γ) is formed with basic convex equations for the simplicity. The equations which describe the point condition in Nyquist diagram is given in Eq. (4.85) – Eq. (4.88). [30]

$$L(jw,\{k_q,k_a\}) = x_1 + jy_1 \tag{4.85}$$

$$L(jw,\{k_q,k_a\}) = \frac{N_L(jw,\{k_q,k_a\})}{D_L(jw)} = x_1 + jy_1 \tag{4.86}$$

$$\frac{N_L(jw,\{k_q,k_q\})}{D_L(jw)} = \frac{N_{L_R}(w,\{k_q,k_a\}) + jN_{L_I}(w,\{k_q,k_a\})}{D_{L_R}(w) + jD_{L_I}(w)} = x_1 + jy_1 \tag{4.87}$$

$$L(jw,\{k_q,k_a\}) = L_R(w,\{k_q,k_a\}) + jL_I(w,\{k_q,k_a\}) = x_1 + jy_1 \tag{4.88}$$

Imaginary and real parts of loop gain transfer function $L(jw,\{k_q,k_a\})$ are given in Eq. (4.89) – Eq. (4.92).

$$L_R(w,\{k_q,k_a\}) = \frac{(N_{L_R}(w,\{k_q,k_a\})D_{L_R}(w) + N_{L_I}(w,\{k_q,k_a\})D_{L_I}(w))}{D_{L_R}(w)^2 + D_{L_I}(w)^2} = x_1 \tag{4.89}$$

$$L_I(w,\{k_q,k_a\}) = \frac{(N_{L_I}(w,\{k_q,k_a\})D_{L_R}(w) - N_{L_R}(w,\{k_q,k_a\})D_{L_I}(w))}{D_{L_R}(w)^2 + D_{L_I}(w)^2} = y_1 \tag{4.90}$$

$$(N_{L_R}(w,\{k_q,k_a\})D_{L_R}(w) + N_{L_I}(w,\{k_q,k_a\})D_{L_I}(w)) \tag{4.91}$$

$$-(D_{L_R}(w)^2 + D_{L_I}(w)^2) * x_1 = 0$$

$$(N_{L_I}(w,\{k_q,k_a\})D_{L_R}(w) - N_{L_R}(w,\{k_q,k_a\})D_{L_I}(w)) \tag{4.92}$$

$$-(D_{L_R}(w)^2 + D_{L_I}(w)^2) * y_1 = 0$$

Feedback gains $\{k_q,k_a\}$ such that satisfies Eq. (4.89) & Eq. (4.90) can be found by solving the resultant of Eq. (4.89) & Eq. (4.90) for one of the feedback gains for each frequency. Second feedback gain can be found easily by substituting the first feedback gain and related frequency to Eq. (4.89) or Eq. (4.90) and solving the equation for the second feedback gain.

Tangent condition indicates that frequency locus $L(jw, \{k_q, k_a\})$ is tangent to the boundary ($\partial\gamma_2$) at $\varphi = x_2 + jy_2$.The equations that describe the tangent condition are given in Eq. (4.93) & Eq. (4.94).

$$L_R(w, \{k_q, k_a\}) = x_2 \tag{4.93}$$

$$L_I(w, \{k_q, k_a\}) = y_2 \tag{4.94}$$

If the frequency locus $L(jw, \{k_q, k_a\})$ is tangent to ($\partial\gamma_2$), they must share common point of contact, which is expressed in Eq. (4.95).

$$F_{\partial\gamma_2}(L_R(w, \{k_q, k_a\}), L_I(w, \{k_q, k_a\})) = 0 \tag{4.95}$$

Second condition indicates that slope of the frequency locus $L(jw, \{k_q, k_a\})$ must be equal to slope of ($\partial\gamma_2$) at the point of contact, which is expressed in Eq. (4.96).

$$\frac{F_{\partial\gamma_2}(L_R(w, \{k_q, k_a\}), L_I(w, \{k_q, k_q\}))}{\partial w} = 0 \tag{4.96}$$

Finally, feedback gains $\{k_q, k_a\}$ such that satisfies Eq. (4.95) & Eq. (4.96) can be found by solving the resultant of Eq. (4.95) & Eq. (4.96) for one of the feedback gains for each frequency. Second feedback gain can be found easily by substituting the first feedback gain and related frequency to Eq. (4.95) or Eq. (4.96) and solving the equation for the second feedback gain.

This solution procedure is repeated for three CG_X position configurations and final 2D feedback gain basis is generated.

The feedback gains subspace which is generated w.r.t allowable short period natural frequency and damping ratio is indicated in the stability guaranteed basis. Desired Eigen value which satisfies allowable natural frequency and damping ratio region for nominal CG_X position configuration and guarantees relative and absolute stability for three CG_X position configurations can be easily selected.

Stability guaranteed 2D feedback gains basis is given with time domain design subspace in Figure 52.

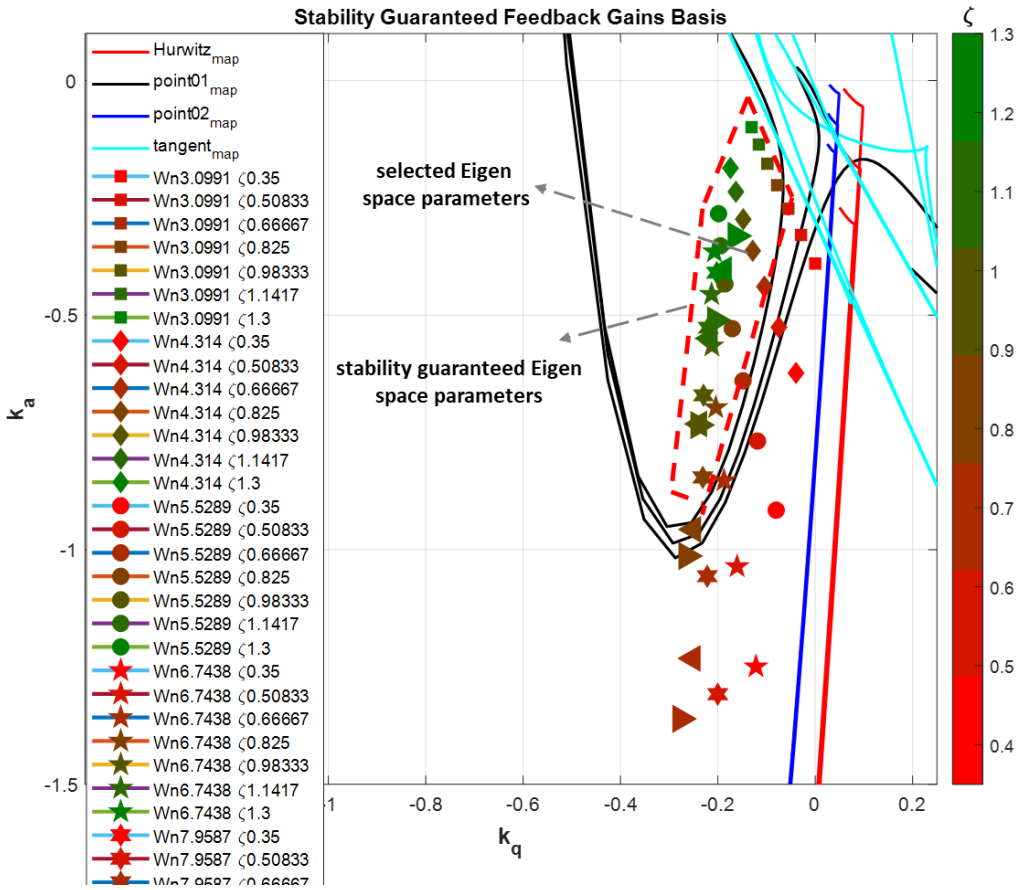

Figure 52. Stability guaranteed feedback gains basis

In Figure 52 each line indicates a condition defined in Eq. (4.81) – Eq. (4.83). This figure is a transformation of stability requirements in Nyquist diagram to 2D controller parameters space. It also maps desired Eigen space parameters, w.r.t Eq. (4.61) and Eq. (4.62), to controller parameters space.

Each marker indicates different natural frequency. The color bar which is located to right hand side indicates short period damping ratio.

Same Eigen space parameters (ω_{sp}, ζ_{sp}) with basis controller are selected which are 4.314 rps and 0.825 respectively.

Control augmentation system parameters which minimize the H_∞ norm of the error between desired model and current pitch rate response are searched via optimization.

A desired pitch rate handling qualities model is generated with selected Eigen space parameters. Desired pitch rate handling quality model is given:

$$G_d(s) = \frac{q}{\delta_{stick}}(s) = \frac{K_{q_{des}}(1 + T_{\theta 2_{des}} s)}{s^2 + 2\omega_{des}\zeta_{des} s + \omega_n{}^2} \tag{4.97}$$

Denominator parameters of the desired pitch rate handling quality model are selected Eigen space parameters. Desired system zero is calculated with same methodology as performed in base controller design. Pitch rate gain of desired handling quality model ($K_{q_{des}}$) is calculated such that DC gain of the desired pitch rate handling quality model equals to 1. Desired pitch rate handling quality model parameters are given in Table 18.

Table 18. Desired pitch rate handling quality model parameters

Parameter	**Value**
ω_{des}	4.314 [rps]
ζ_{des}	0.825
$K_{q_{des}}$	8.9792
$T_{\theta 2_{des}}$	0.4825 [s]

Desired pitch rate handling quality model time and frequency responses are given in Figure 53 & Figure 54.

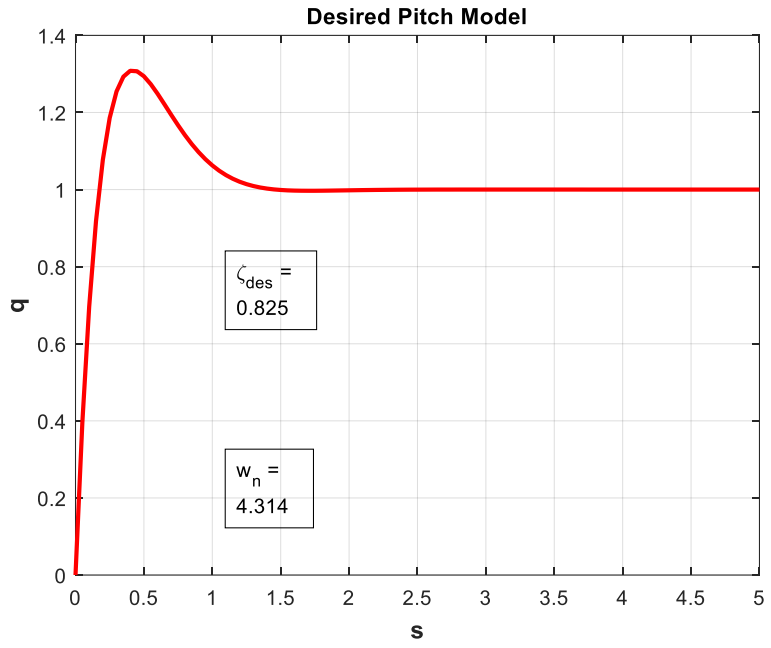

Figure 53. Desired pitch rate handling quality model time response

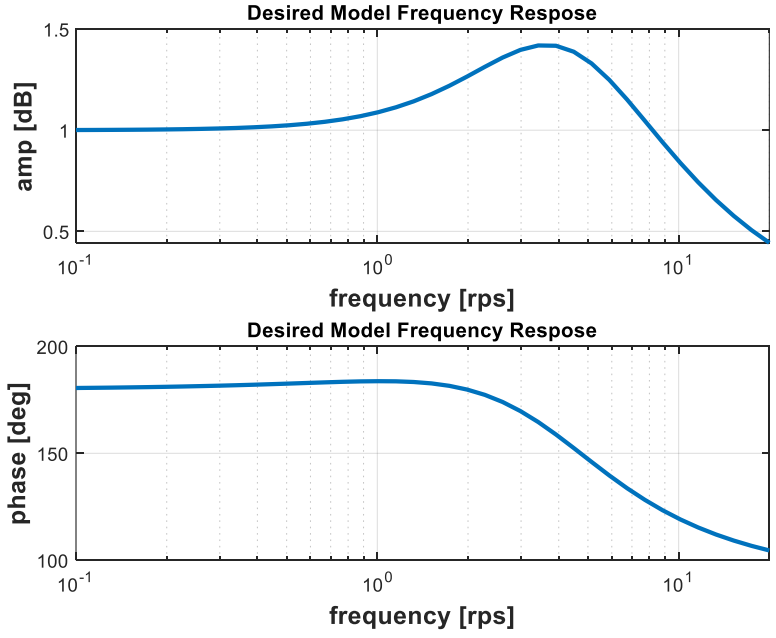

Figure 54. Desired pitch rate handling quality model frequency response

Variation of CG_X position from nominal to forward and aft position is modeled as multiplicative uncertainty on nominal CG_X position configuration. Uncertainty weight is designed in Eq. (4.98) – Eq. (4.103).

*$\frac{q}{\delta_{stick}}$ represents stability augmented pitch rate to stick transfer function

$$\Delta_{CG1_i} = \left| \frac{q}{\delta_{stick}}(jw_i)_{NMNL} - \frac{q}{\delta_{stick}}(jw_i)_{MFW} \right| \tag{4.98}$$

$$\Delta_{CG2_i} = \left| \frac{q}{\delta_{stick}}(jw_i)_{NMNL} - \frac{q}{\delta_{stick}}(jw_i)_{MAFT} \right| \tag{4.99}$$

$$W_{Uamp_{i=1,2..n}} = \max\left(\Delta_{CG1_i}, \Delta_{CG2_i}\right) \text{ for } \omega_{i=1,2..n} \tag{4.100}$$

$$W_U(jw) = fit(4^{th}\ order\ system, W_{U_{amp}}, w) \tag{4.101}$$

$$|\Delta|_\infty \leq 1 \tag{4.102}$$

$$\frac{q}{\delta_{stick}}(jw)_{CG_X} = \frac{q}{\delta_{stick}}(jw)_{NMNL}(1 + W_U\Delta) \tag{4.103}$$

Uncertainty weight is given in Figure 55.

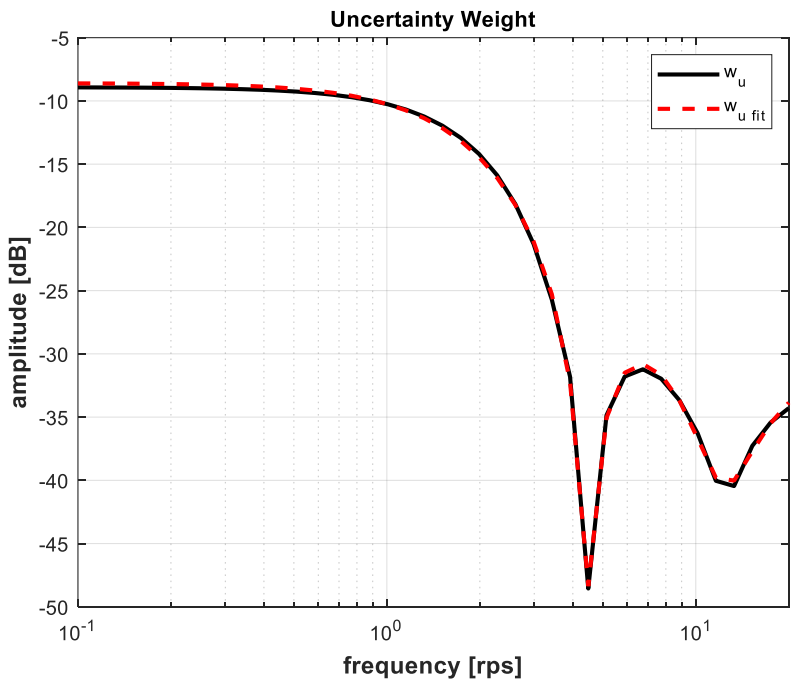

Figure 55. Uncertainty weight

Inverse of the weight which has been given in Eq. (3.1) to define reference model following capability is used as performance weight, and it is given in Eq. (4.104).

$$W_P(s) = \frac{s + 100}{2.5s + 10} \tag{4.104}$$

Frequency response of inverse of performance weight is given in Figure 56.

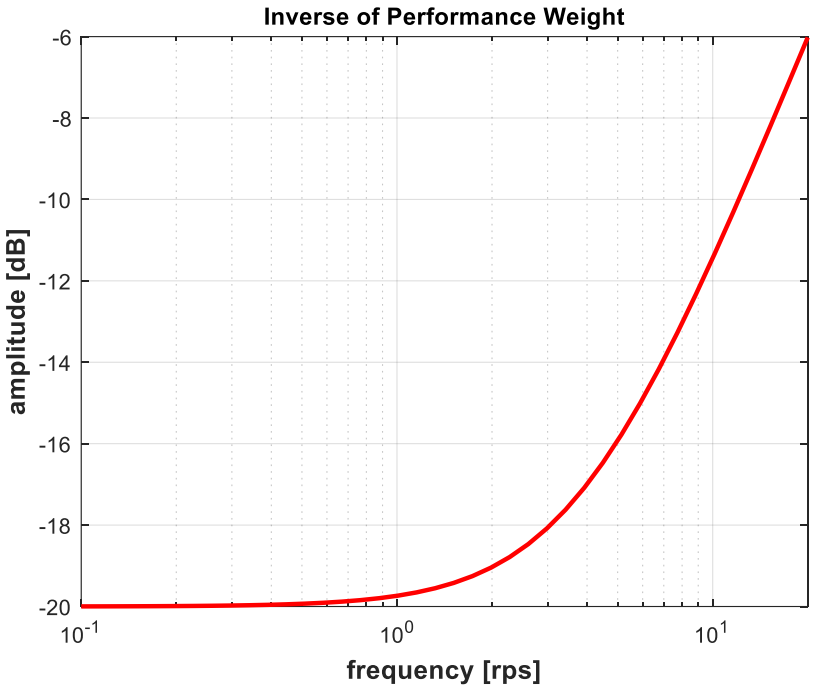

Figure 56. Inverse of performance weight

Control augmentation parameters; K_i , k_{ff} , τ_1 , and τ_2 are searched via optimization algorithm w.r.t constraints given in Eq. (4.105) – Eq. (4.108).

$$E(jw) = G_d(jw) - G(jw) \tag{4.105}$$

$$T(jw) = \frac{-q}{n}(jw) \tag{4.106}$$

$$\left\| W_U T(K, K_i, k_{ff}, \tau_1, \tau_2) \right\|_\infty \leq 1 \tag{4.107}$$

$$\left\| W_P E\left(K, K_i, k_{ff}, \tau_1, \tau_2\right) \right\|_\infty \leq 1 \tag{4.108}$$

Controller parameters are found as a solution of structured H_∞ synthesis problem. Controller parameters are given in Table 19 for nominal CG_X position.

Table 19. Controller parameters

Configuration	k_q	k_a	K_i	K_{ff}	τ_1	τ_2
$CG_{X\ NMNL}$	-0.1243	-0.3623	-0.5	-0.1332	1.9120	1.5130

Solver constraints are given in Table 20.

Table 20. Solver constraints for structured H_∞ synthesis problem

Configuration	K_i	K_{ff}	τ_1	τ_2
min	-2.5	-2.5	0.2*$T_{\theta 2_{des}}$	0.2*$T_{\theta 2_{airframe}}$
max	-0.5	0.001	5*$T_{\theta 2_{des}}$	5*$T_{\theta 2_{airframe}}$

4.2.2.3 Alternative Controller No2

The second alternative controller is based on explicit model following with disturbance rejection structure. Controller architecture with design elements (desired model and weights) is given in.

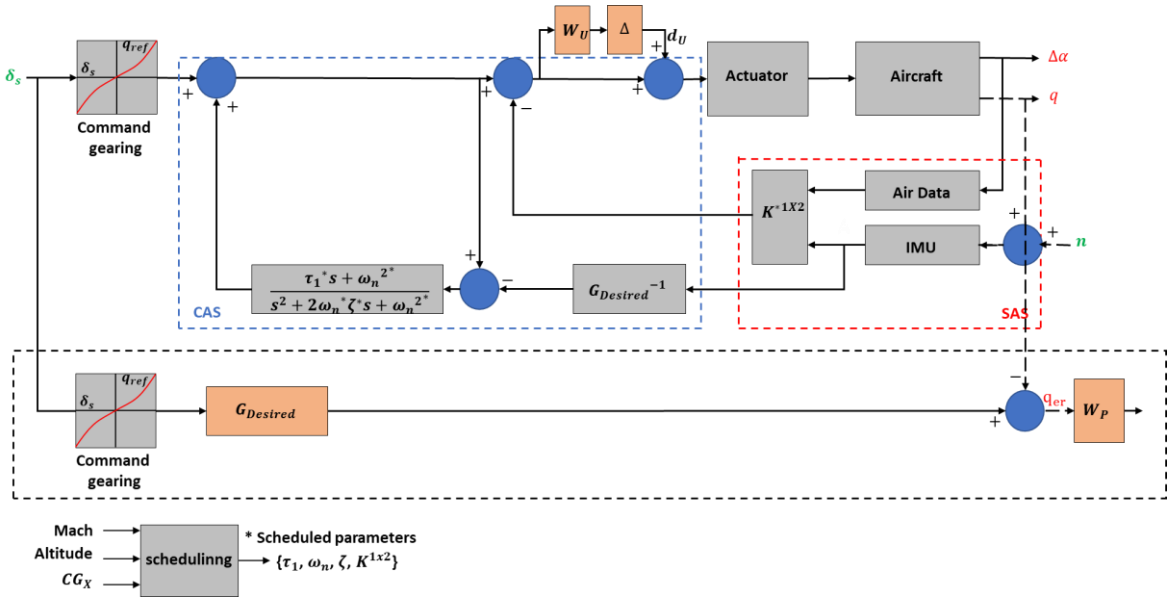

Figure 57. Disturbance rejection controller with design structure

Explicit model following with disturbance rejection controller architecture provides insensitivity to disturbances and model uncertainty. It makes enable desired closed loop dynamics to be defined explicitly.

Stability is enhanced with output feedback augmentation as same as with base controller and first alternative controller. Feedback gains are calculated with parameter space approach which has been applied in the first alternative controller. The same Eigen space parameters are selected with base controller and first alternative controller.

Control augmentation is performed with explicit model following with disturbance rejection controller which is combination of disturbance rejection compensator and inverse of desired pitch rate handling quality model.

Loop gain (L), disturbance rejection (S), noise rejection (T), and model regulation (H) transfer functions for disturbance rejection controller are given in Eq. (4.109) – Eq. (4.115).

$$G(jw) = \frac{q}{\delta_{stick}}(jw) \tag{4.109}$$

$$G_1(jw) = Actuator(jw)G(jw)IMU(jw) \tag{4.110}$$

$$G_2(jw) = Actuator(jw)G(jw) \tag{4.111}$$

$$L(jw) = \frac{Q(jw)}{(1 - Q(jw))}\frac{G_1(jw)}{G_d(jw)} \tag{4.112}$$

$$H(jw) = \frac{q}{\delta_s}(jw) = \frac{G_d(jw)G_2(jw)}{G_d(jw)(1 - Q) + G_1(jw)Q(jw)} \tag{4.113}$$

$$S(jw) = \frac{q}{d}(jw) = \frac{1}{1 + L(jw)} = \frac{G_d(jw)(1 - Q(jw))}{G_d(jw)(1 - Q) + G_1(jw)Q(jw)}) \tag{4.114}$$

$$T(jw) = \frac{-q}{n}(jw) = \frac{L(jw)}{1 + L(jw)} = \frac{G_2(jw)Q(jw)}{G_d(jw)(1 - Q) + G_1(jw)Q(jw)}) \tag{4.115}$$

According to the Eq. (4.112) the design philosophy is based on selection of $Q(jw)$ such a low pass filter with a unity gain, which results in $\frac{q}{\delta_s}(jw) = G_d(jw)$ and $\frac{q}{d}(jw) = 0$ at low frequencies, where gain of $Q(jw)$ reaches to 1, and $\frac{q}{n}(jw) = 0$ at high frequencies, where gain of $Q(jw)$ reaches to 0.[13] Disturbances up to bandwidth of $Q(jw)$ are rejected successfully.

$$H(jw)|_{Q(jw)=1} = \frac{q}{\delta_s}(jw) = G_d(jw) \tag{4.116}$$

$$S(jw)|_{Q(jw)=1} = \frac{q}{d}(jw) = \frac{1}{1 + L(jw)} = 0 \tag{4.117}$$

$$T(jw)|_{Q(jw)=0} = \frac{-q}{n}(jw) = \frac{L(jw)}{1 + L(jw)} = 0 \tag{4.118}$$

Disturbance rejection compensator is given Eq. (4.119).

$$Q(s) = \frac{\tau_c s + {\omega_c}^2}{s^2 + 2\zeta_c \omega_c s + {\omega_c}^2} \tag{4.119}$$

Relative degree of $Q(s)$ must equal to relative degree of desired pitch rate handling quality model $G_d(s)$, which is 1. Equality of relative degrees is important for implementation, such as $\frac{Q(s)}{G_d(s)}$ must be proper.

Disturbance rejection compensator bandwidth must be smaller than actuator's bandwidth. Sensor noise also must be considered when setting bandwidth of $Q(jw)$.

Disturbance rejection compensator damping ratio is another parameter that must be taken into the consideration. A proper minimum damping ratio limit must be set for un oscillatory responses.

Disturbance rejection compensator parameters; $\{\tau_c, \omega_c, \zeta_c\}$ are searched via optimization algorithm w.r.t constraints given in Eq. (4.120) & Eq. (4.121).

$$\left\| W_U T(K, K_i, k_{ff}, \tau_1, \tau_2) \right\|_\infty \leq 1 \tag{4.120}$$

$$\left\| W_P E\left(K, K_i, k_{ff}, \tau_1, \tau_2\right) \right\|_\infty \leq 1 \tag{4.121}$$

Controller parameters are found as a solution of structured H_∞ synthesis problem w.r.t Eq. (4.120) & Eq. (4.121). Controller parameters are given in Table 21 for nominal CG_X position.

Table 21. Controller parameters

Configuration	$\boldsymbol{\omega_c}$	$\boldsymbol{\zeta_c}$	$\boldsymbol{\tau_c}$
$CG_{X\ NMNL}$	27.3590 [rps]	0.7000	39.9905

Solver constraints are given in Table 22.

Table 22. Solver constraints for structured H_∞ synthesis problem

Parameter	ω_c	ζ_c
min	2*ω_{des}	0.7
max	0.4*$\omega_{BW_{Actuator}}$	1

5. RESULTS

In this section stability and performance assessment of base controller and two alternative controllers will be performed in case of CG_X position fault where base controller architecture uses the nominal CG_X position configuration parameters. Alternative controllers don't require CG_X position information on the other hand.

Flight condition parameters where stability and performance assessments are performed are given in Table 23.

Table 23. Stability and performance assessment flight condition parameters

Parameter	**Value**
Mach	0.7
Altitude	10 kft

Frequency domain analyses frequency of interest is given in Eq. (5.1).

$$\omega_{interest} = logspace(\log_{10} 0.1\,, \log_{10} 20\,, 40) \tag{5.1}$$

Loop break for stability analysis is given in Figure 58.

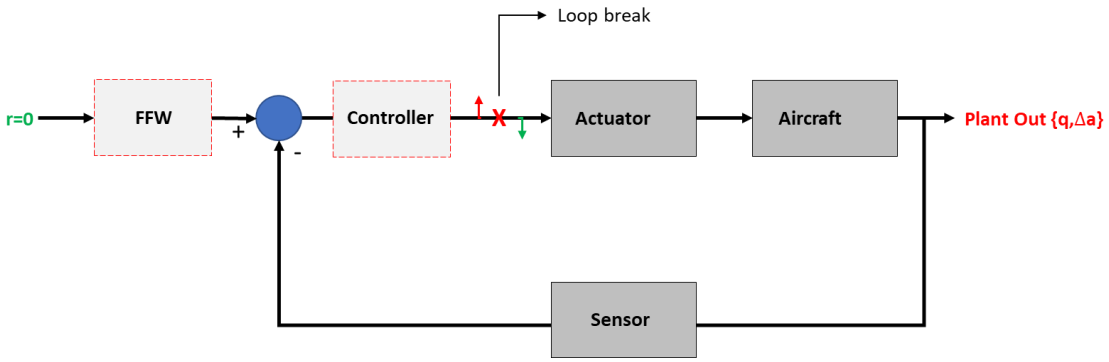

Figure 58. Loop break for stability analyses

In the scope of the relative and absolute stability analyses; it is assumed that pilot reference input is zero. Relative and absolute stability margins are calculated w.r.t Figure 58.

5.1 Base Controller

5.1.1 Performance Assessment

In the scope of the of the performance assessment; reference model tracking capability analysis, handling qualities and PIO requirements checks are performed.

5.1.1.1 Reference Model Tracking Capability

In the scope of the reference model tracking capability analysis; time and frequency responses are compared with reference model. Model mismatch is illustrated via comparison between inverse of performance weight and error between current pitch rate response and desired pitch rate handling quality model.

Time response comparison of the base controller with nominal CG_X position configuration parameters for three different CG_X position is given in Figure 59.

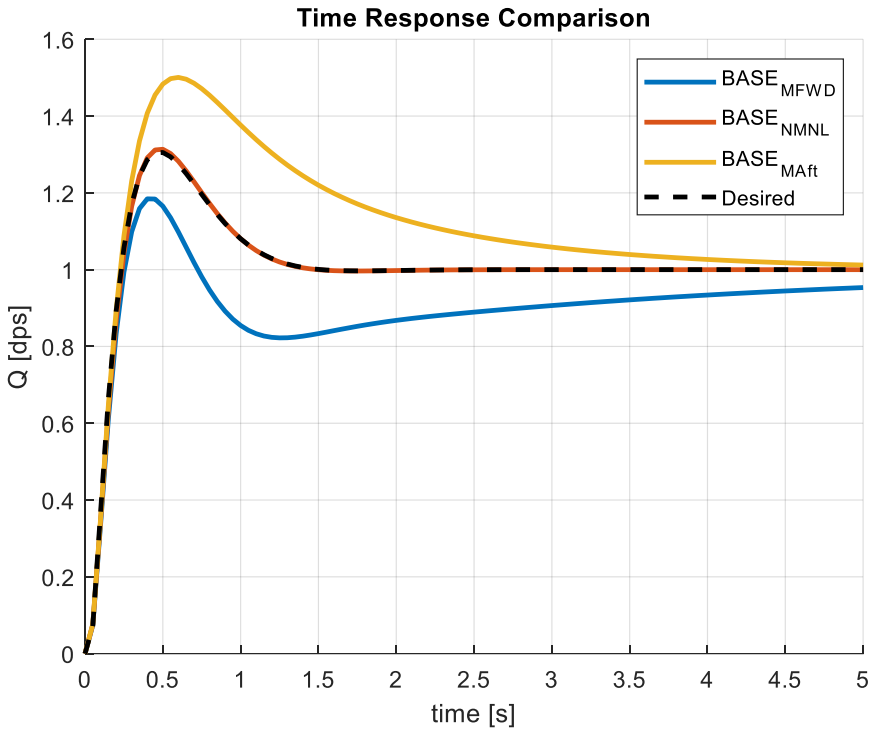

Figure 59. Base controller time response comparison

According to Figure 59 it is obvious that base controller cannot track desired pitch rate handling quality model except for the design point. In most forward CG_X position configuration time response characteristics is sluggish, as expected. As CG_X moves forward, inertia around y axis increases; so, required HT deflection per unit pitch rate increases. Time response for most aft CG_X position demonstrates overshoot higher than desired one. As CG_X moves backward inertia around y axis decreases; so, required HT deflection per unit pitch rate decreases.

Aircraft inertia around y axis for three CG_X positions are given in Table. 24.

Table. 24 Jet trainer CG_X vs I_{YY}

Configuration	I_{yy} [kgmm]	CG_X [% of mac]
$MFW\ CG_X$	5.9042e+04	28.45
$NMNL\ CG_X$	5.6860e+04	31.34
$MAFT\ CG_X$	5.5292e+04	34.02

Frequency response comparison for base controller is given in Figure 60.

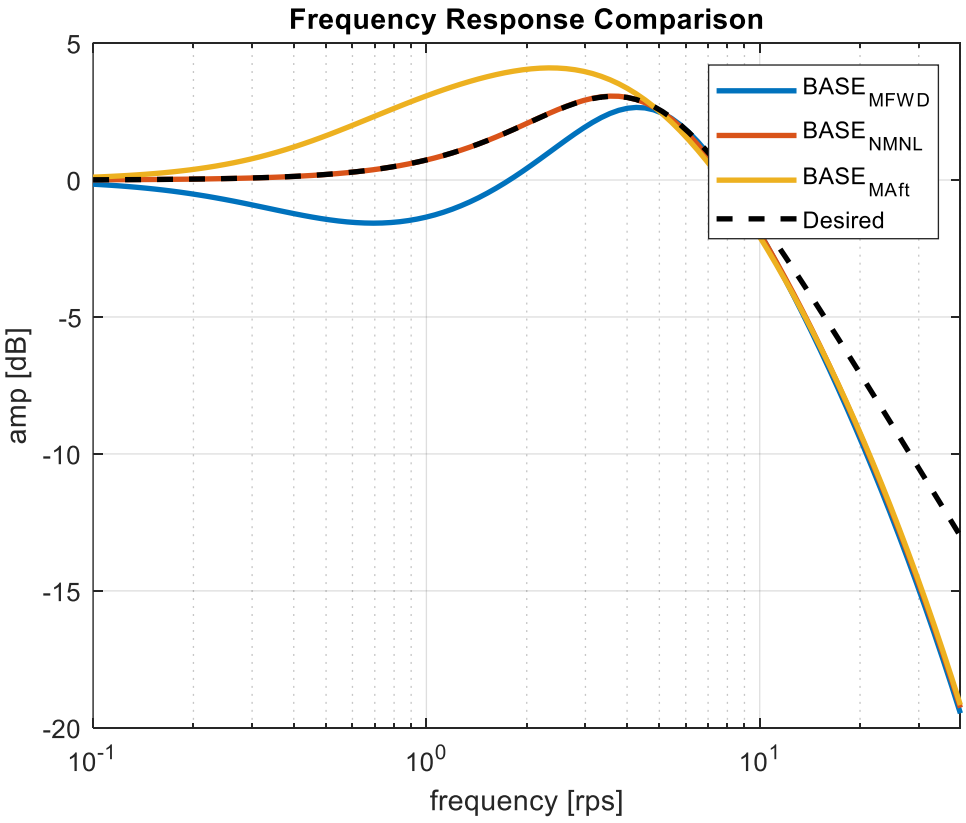

Figure 60. Base controller frequency response comparison

Frequency responses also supports that base controller is not capable of tracking desired response in case of CG_X position information fault.

Inverse of performance weight is also given to demonstrate mismatch. Adequate reference model tracking was stated w.r.t Eq. (5.2).

$$\left|E\left(jw, K, K_i, k_{ff}, \tau_1, \tau_2\right)\right| \leq \left|W_P(jw)^{-1}\right| \text{ for } 0.1 \leq \omega \leq 40\ [rps] \tag{5.2}$$

Inverse of performance weight and error between closed loop response and desired pitch rate handling quality model is given in Figure 61.

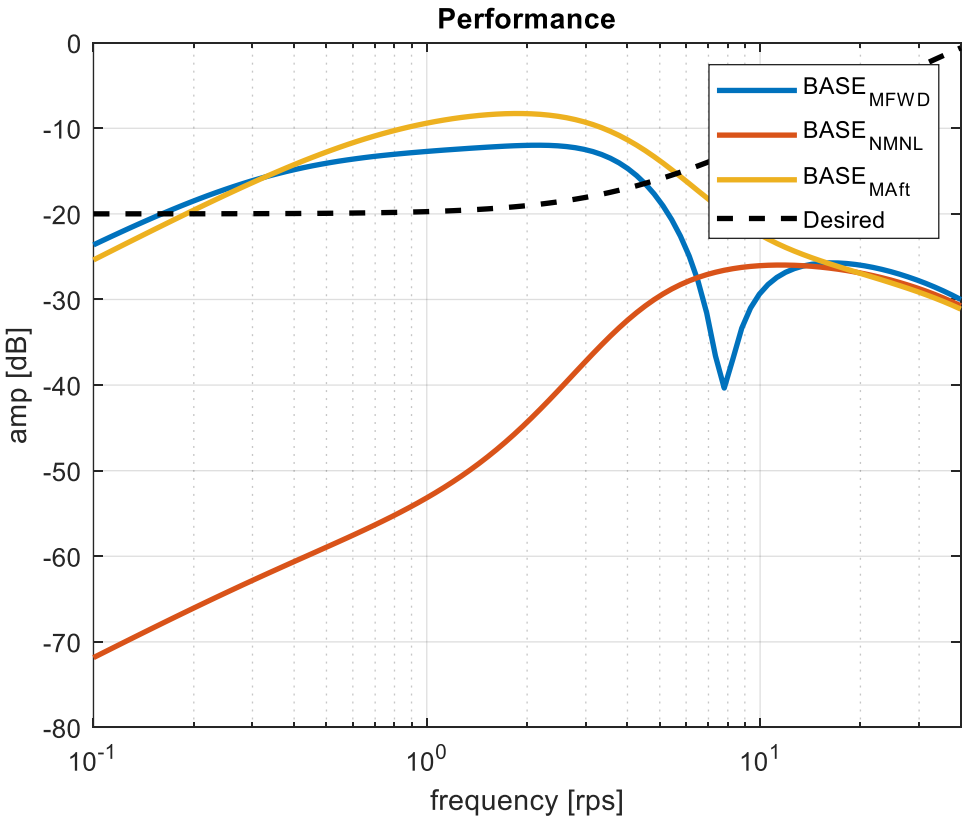

Figure 61. Base controller reference model mismatch

According to the Figure 61 model mismatch is above the allowable limit for off design points, which indicates poor reference model tracking in case of CG_X position information fault.

Disturbance rejection capability of the base controller is also tested. In the scope of disturbance rejection capability analysis, a pitch tracking task is performed where reference pitch rate values vary with time. Linear parametric varying model for specific flight condition, which is defined for performance assessment (10kft, 0.7 Mach), is used in the scope of this analysis. During the task, CG_X position of the aircraft is initially set to nominal configuration and varies with time between

most forward and most aft configurations. It is assumed that CG_X position information is not provided to base longitudinal flight control algorithm because of an error occurred in configuration management computer. Complete pitch tracking task is performed with mid CG_X position configuration parameters, according to the procedure defined for CG_X position information fault.

In the scope of the analysis, disturbance is defined as variation of aircraft longitudinal dynamics characteristics because of change in CG_X position. In other words, disturbance is defined implicitly. Satisfactory disturbance rejection capability requires minimum deviation from desired pitch rate tracking characteristics in case of variation in CG_X position.

Variation of CG_X position during pitch tracking task is given in Figure 62.

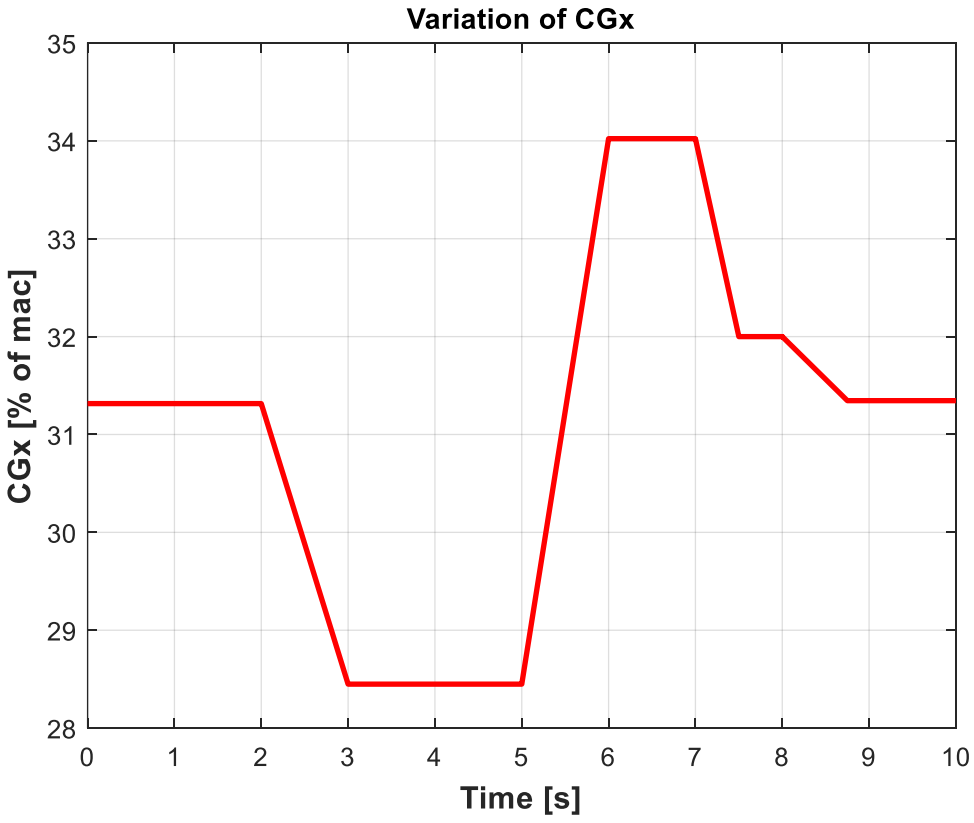

Figure 62. Variation of CG_X position during pitch tracking task

In real life, CG_X position does not change in such dramatic way within 10s period. To test disturbance rejection capability of base controller such significant changes in CG_X position is considered.

Base controller pitch tracking task is given in Figure 63.

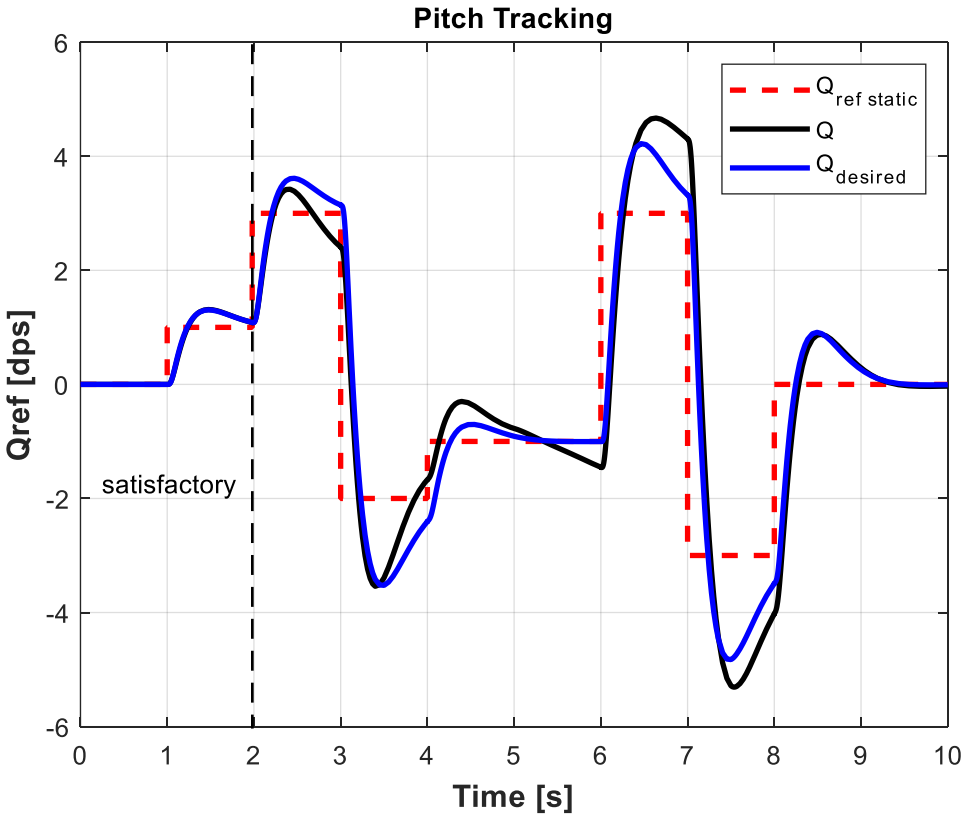

Figure 63. Base controller pitch tracking task

According to Figure 63, pitch tracking response matches desired pitch rate handling quality model when CG_X position is in nominal configuration. As CG_X position varies from nominal configuration, difference between desired pitch tracking response and current pitch tracking responses increases. It shows that disturbance rejection capability of base controller is not satisfactory.

5.1.1.2 Handling Qualities Requirements

Selected handling qualities requirements are checked in the scope of performance assessment. The first handling qualities requirement is pitch attitude bandwidth criterion, which is given in Figure 64.

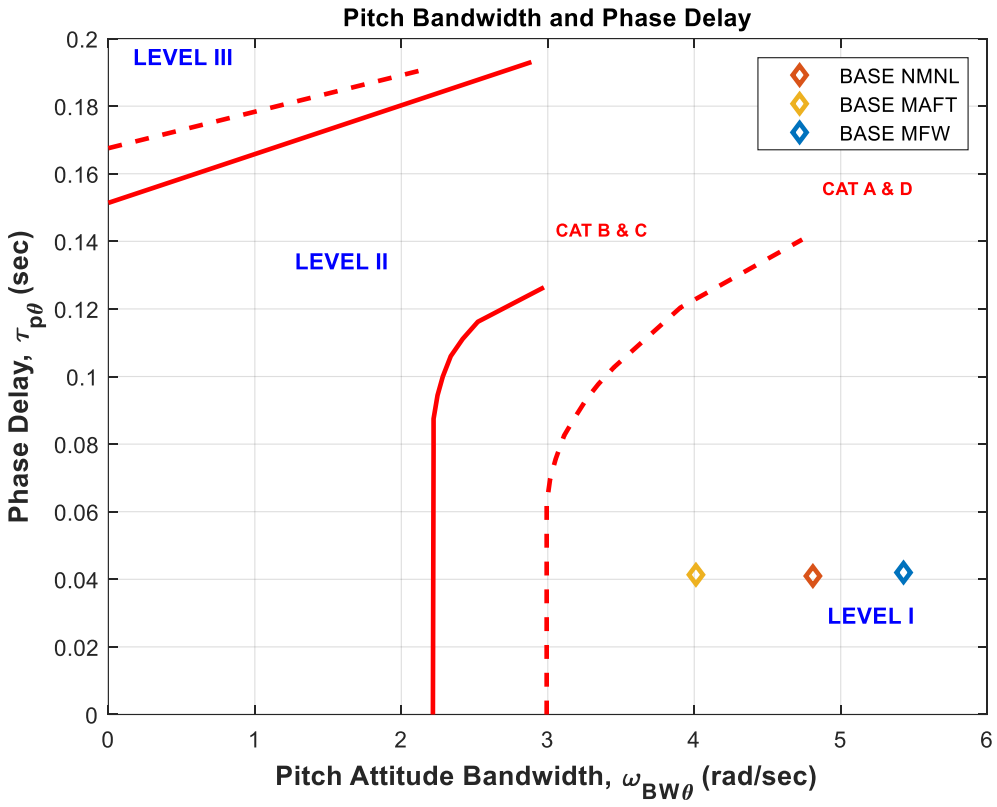

Figure 64. Base controller pitch attitude bandwidth results

According to the Figure 64 pitch attitude bandwidth results are in level 1 region for three CG_X position configurations. Base controller is successful in terms of pitch attitude bandwidth in case of CG_X position information fault.

Second handling qualities requirement which is selected in the scope of performance robustness requirement is TPR. Effective time delay, effective rise time and transient peak ratio results are given in Figure 65.

*Green color indicates that this point satisfies effective rise time requirement.

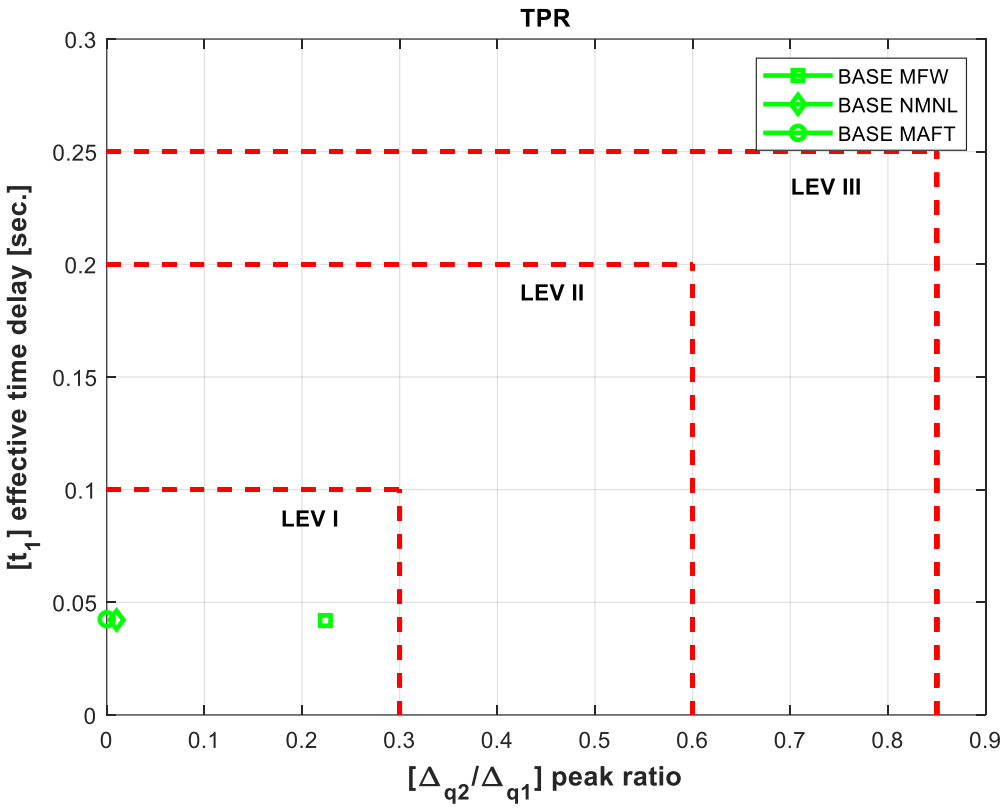

Figure 65. Base controller TPR results

According to the Figure 65 TPR requirement is satisfied for three CG_X position configurations. Base controller is successful in terms of TPR in case of CG_X position information fault.

Transient peak ratio results of nominal and most aft CG_X positions are so close to each other. Most forward CG_X position configuration result falls apart from them. The reason of this separation is time response with significant undershoot for most forward CG_X position configuration. This kind of variation in pitch response may disturb pilot during the task.

Drop-back is the third handling qualities requirement which is checked in the scope of performance assessment. Base controller drop-back result is given in Figure 66.

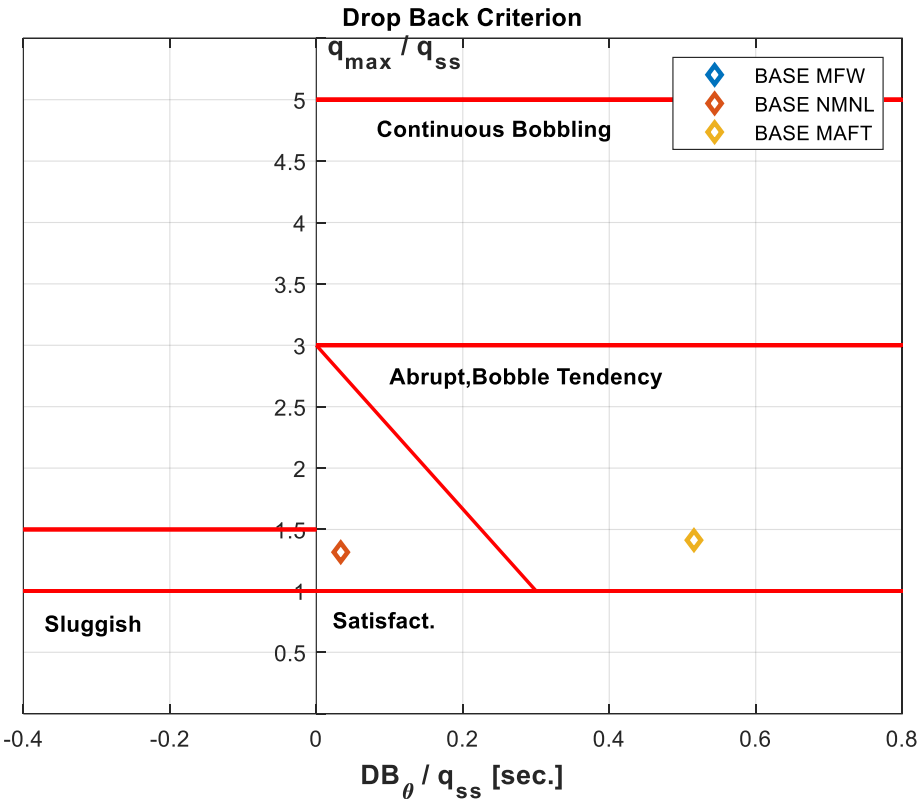

Figure 66. Base controller drop-back results

According to Figure 66 drop-back criteria is satisfied for only design point, in other words base controller fails in terms of drop-back criterion when there is no scheduling w.r.t CG_X position information. Most forward CG_X position configuration drop back result is in far sluggish region, therefore it is not seen on the figure.

5.1.1.3 PIO Requirements

Selected level I PIO criteria are checked in the scope of PIO requirements. The first PIO requirement is pitch attitude bandwidth and pitch rate overshoot. This criterion is based on pitch attitude bandwidth criterion with addition of pitch rate overshoot term. Base controller pitch attitude bandwidth and pitch rate overshoot result is given in Figure 67.

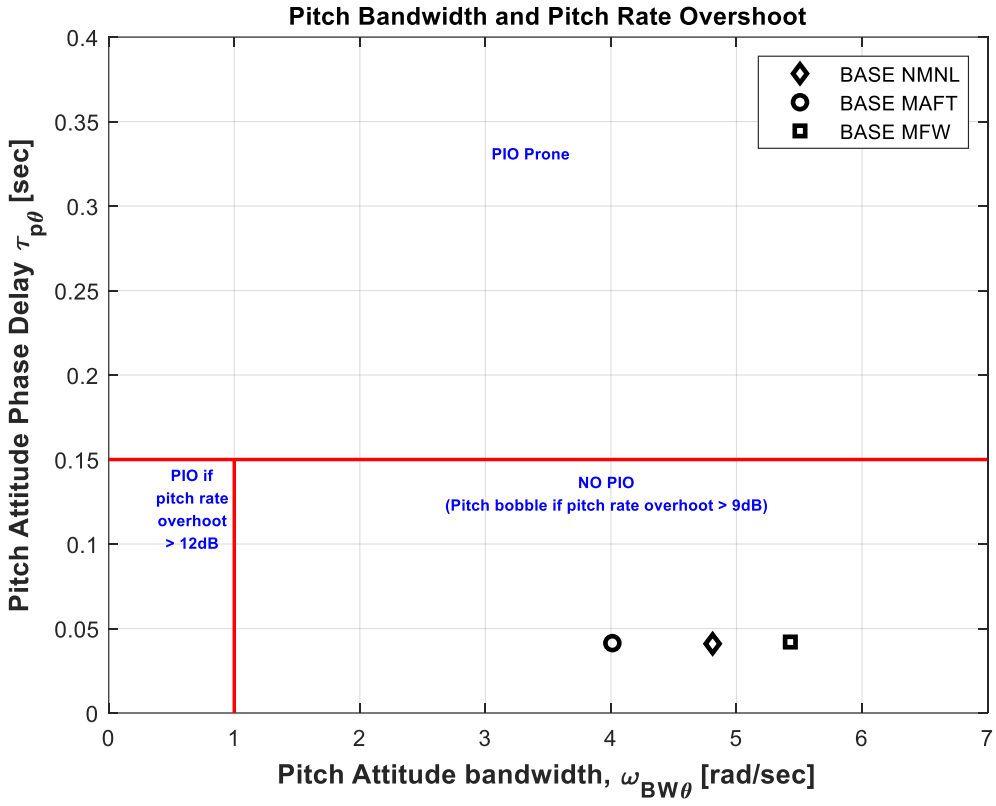

Figure 67. Base controller pitch attitude bandwidth and pitch rate overshoot results

According to Figure 67 base controller satisfies this requirement for three CG_X position configurations without any adaptation w.r.t CG_X position information.

The second PIO requirement is Gibson average phase rate and gain-phase template. Base controller Gibson average phase and gain-phase template results are given in Figure 68.

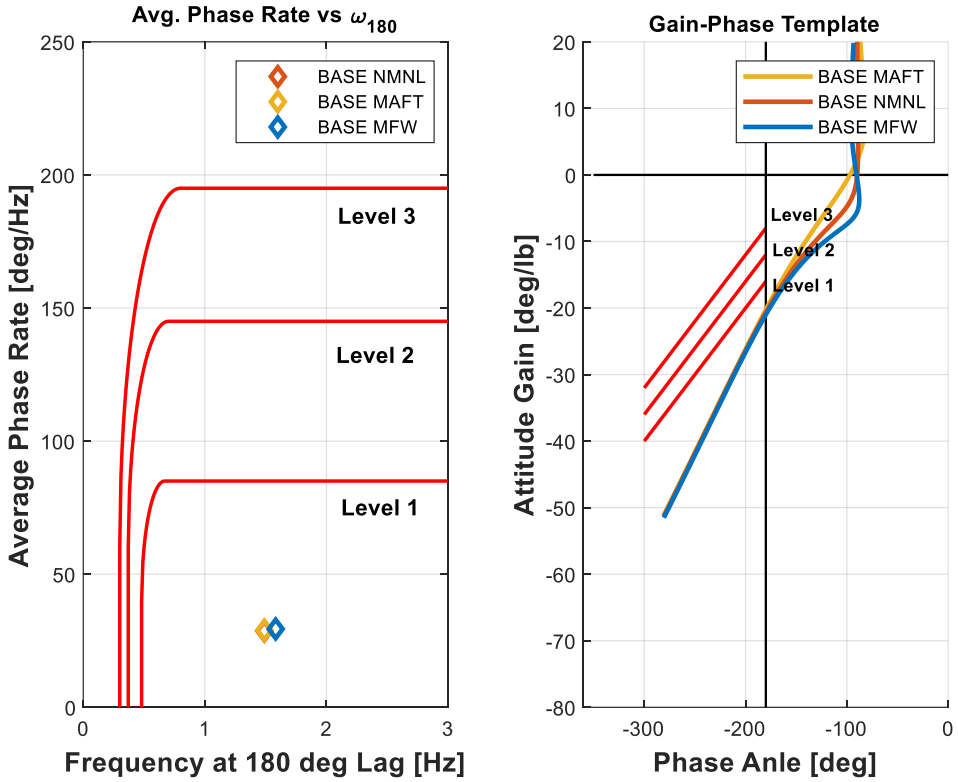

Figure 68. Base controller Gibson average phase rate and gain-phase template results

According to Figure 68 base controller is level 1 PIO free in terms of Gibson average phase rate and gain-phase template, for three CG_X position configurations without any adaptation w.r.t CG_X position information.

5.1.2 Stability Assessment

Base controller relative stability is investigated with Nichols exclusion zone which is given in Figure 69. Absolute stability is assessed with Nyquist diagram, it is given in Figure 70.

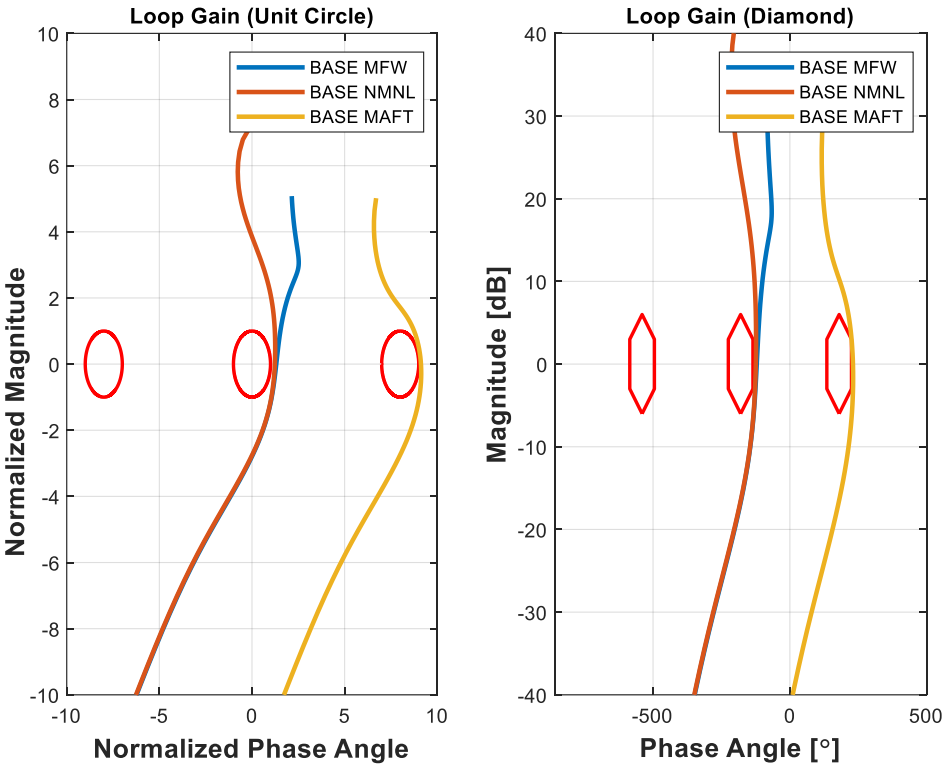

Figure 69. Base controller relative stability assessment

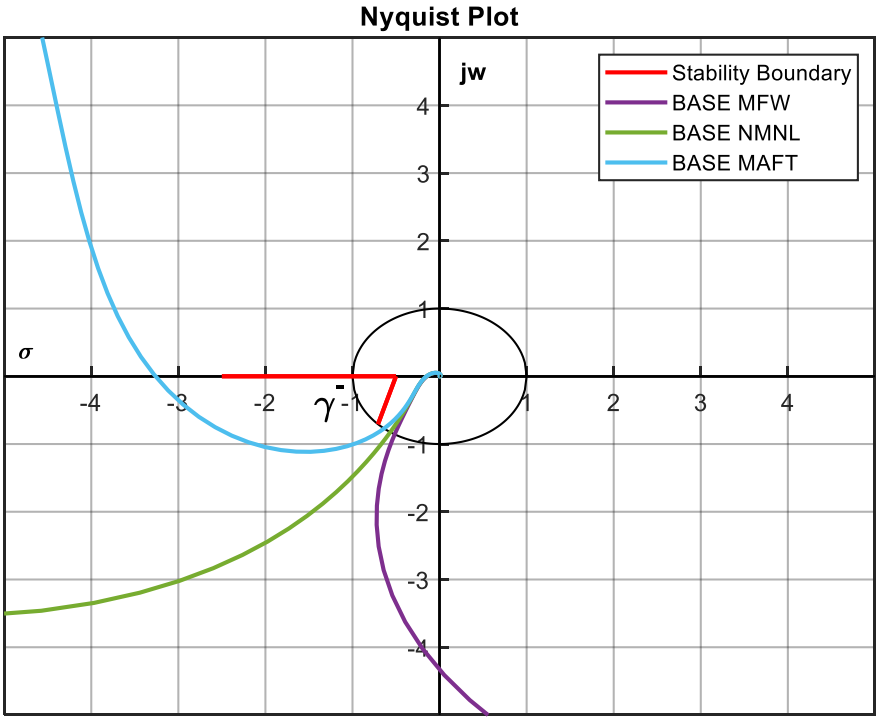

Figure 70. Base controller absolute stability assessment

Classical stability margins are given in Table 25 .

Table 25. Base controller relative and absolute stability margins

Configuration	GM	PM	SM
MFW	16.2581	58.9711	0.7551
NMNL	16.0912	55.5298	0.7505
MAFT	16.0440	50.3916	0.7473

According to Figure 69 it is obvious that Nichols exclusion zone is not violated by the Base controller for three different CG_X position configurations without any adaptation w.r.t CG_X position information. Critical point is also not encountered in clockwise direction by frequency loci, so; absolute stability is also succeeded. In other words, base controller satisfies relative and absolute stability requirements in case of CG_X position information fault.

5.2 Alternative Controller No1

Performance and stability assessment results for the first alternative controller are given in this chapter.

5.2.1 Performance Assessment

Reference model tracking capability analysis, handling qualities requirements and PIO requirements checks are performed in the scope of performance assessment.

5.2.1.1 Reference Model Tracking Capability

Time response comparison, frequency response comparison and error between desired pitch rate handling quality model and current pitch rate response are given in Figure 71.

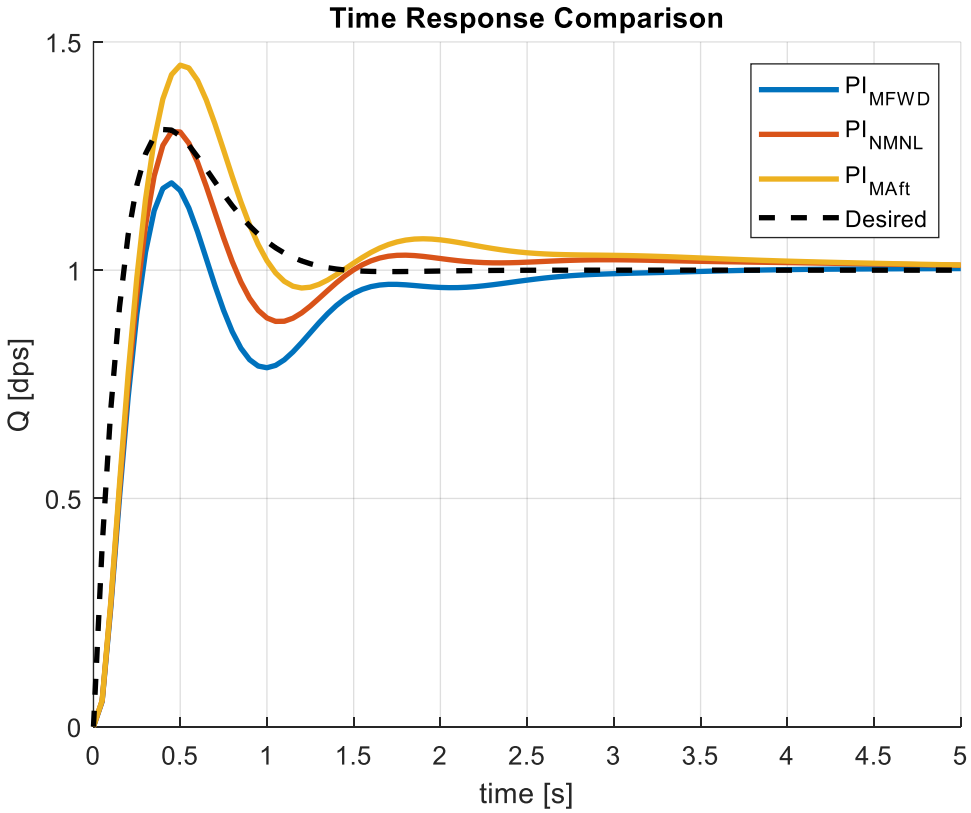

Figure 71. First alternative controller time response comparison

According to Figure 71 the first alternative controller time response does not match with the desired pitch rate handling quality model even for the design point. Time responses are close to each other on the other hand. Most aft CG_X position configuration has the maximum overshoot as expected and most forward CG_X position configuration is the most sluggish one. Undershoot to overshoot ratio is high for most forward CG_X position configuration.

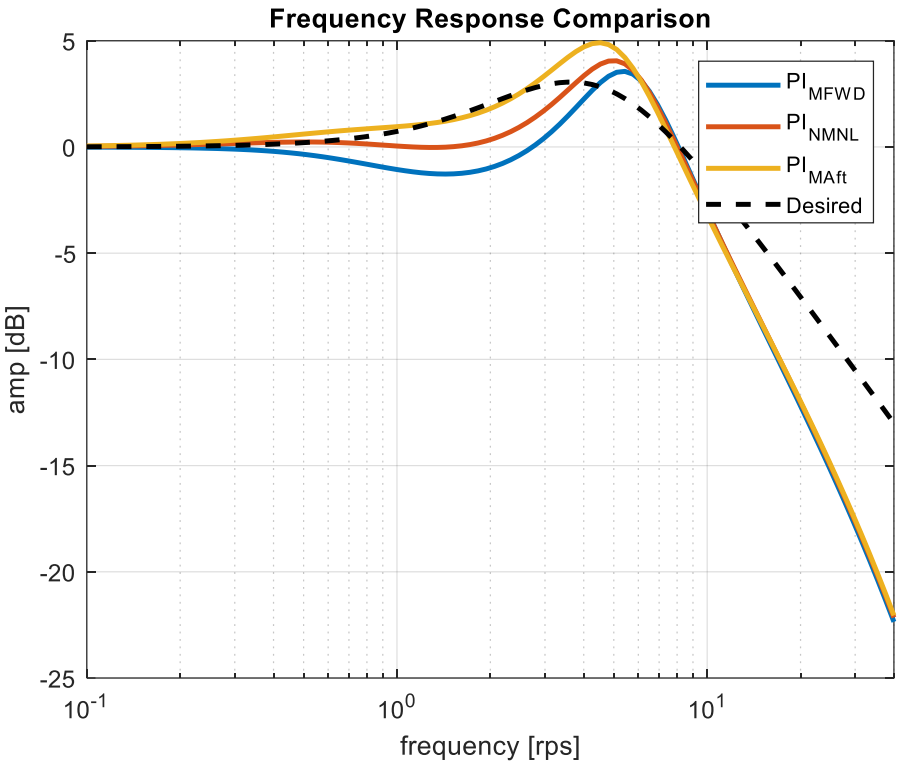

Figure 72. First alternative controller frequency response comparison

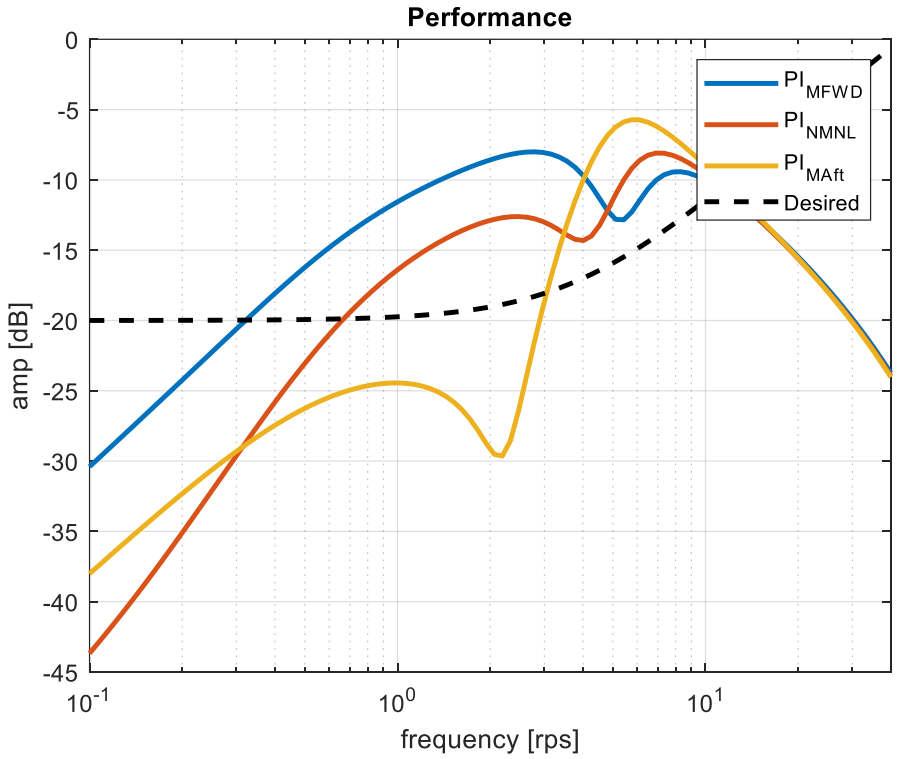

Figure 73. First alternative controller reference model mismatch

According to Figure 72 & Figure 73 first alternative controller is unsuccessful to track reference model in case of CG_X position information fault.

Disturbance rejection capability of the first alternative controller is also tested. In the scope of disturbance rejection capability analysis, a pitch tracking task is performed where reference pitch rate values vary with time. Linear parametric varying model for specific flight condition, which is defined for performance assessment (10kft, 0.7 Mach), is used in the scope of this analysis. Variation of CG_X position during the pitch tracking task and comparison of pitch rate responses are given in Figure 74 and Figure 75, respectively.

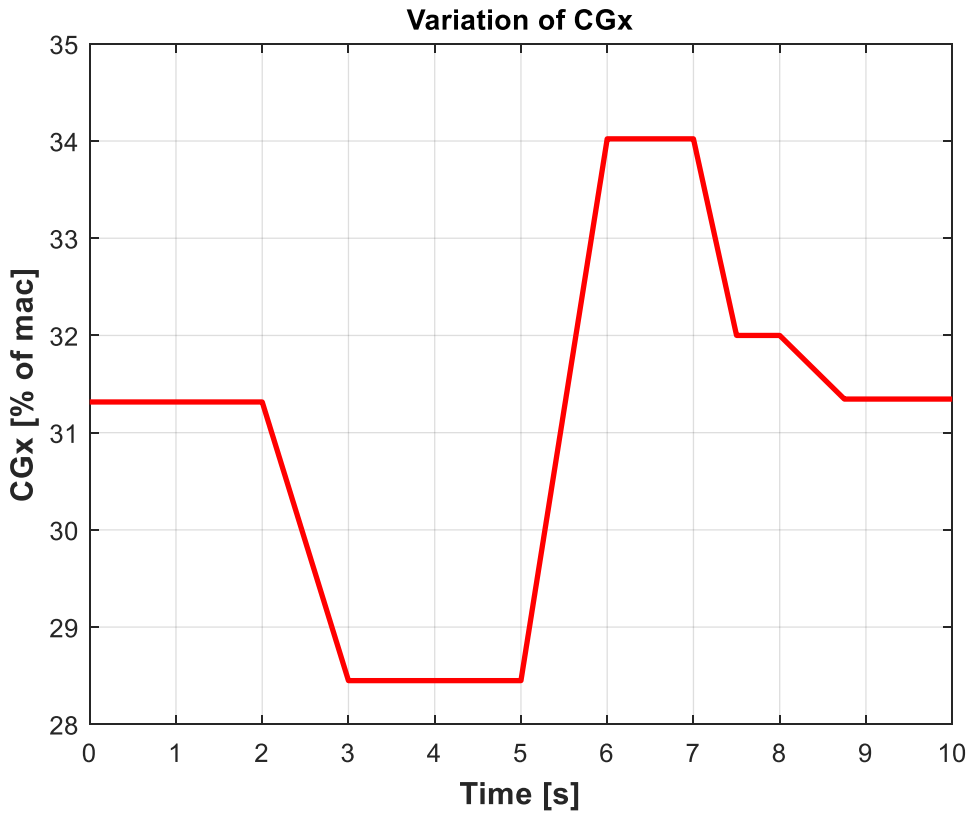

Figure 74. Variation of CG_X position during pitch tracking task

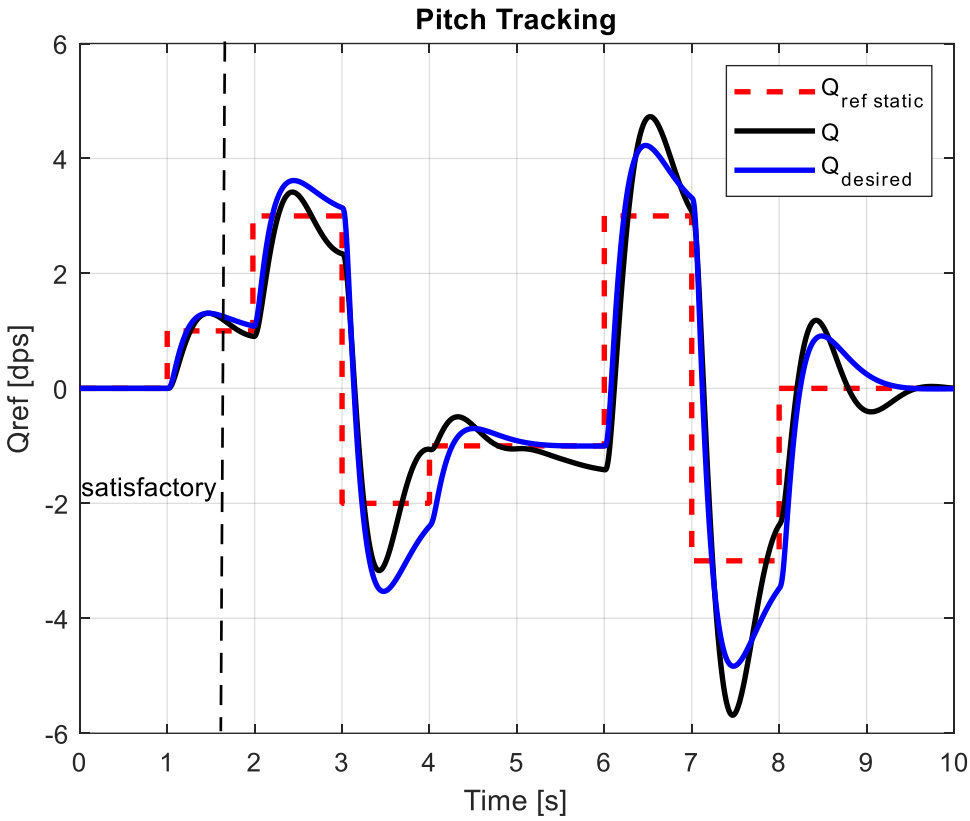

Figure 75. First alternative controller pitch tracking task

According to Figure 75 desired pitch tracking response is only reached when CG_X equals to nominal configuration. As difference between nominal and current position of CG_X increases, deviation from desired pitch tracking is also increases.

5.2.1.2 Handling Qualities Requirements

Pitch attitude bandwidth criterion, TPR, and drop-back criterion results for first alternative controller are given in the scope of handling qualities assessment.

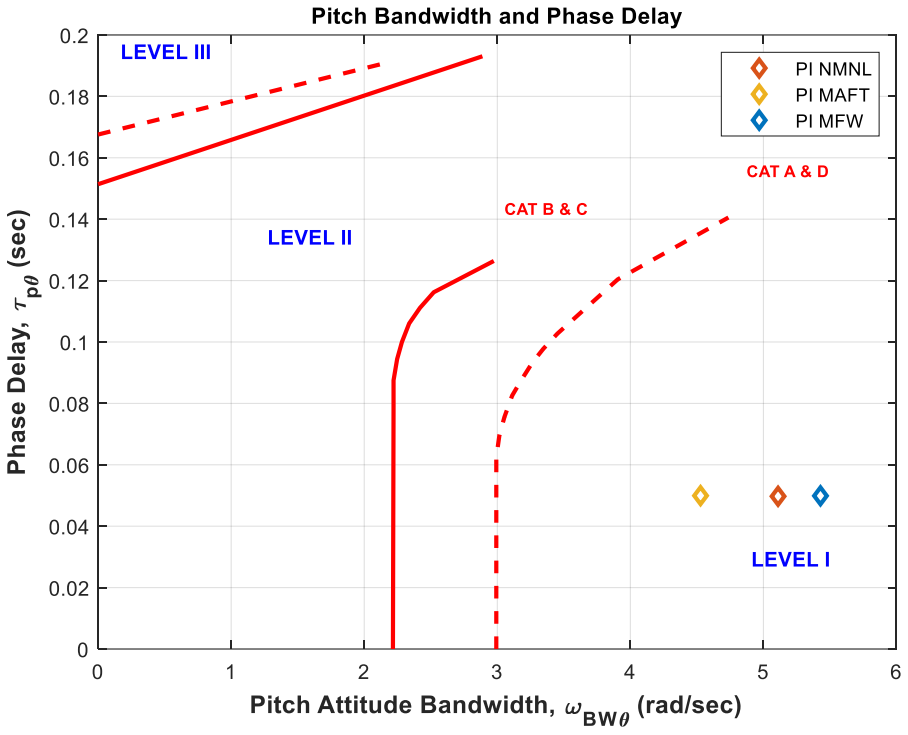

Figure 76. First alternative controller pitch attitude bandwidth results

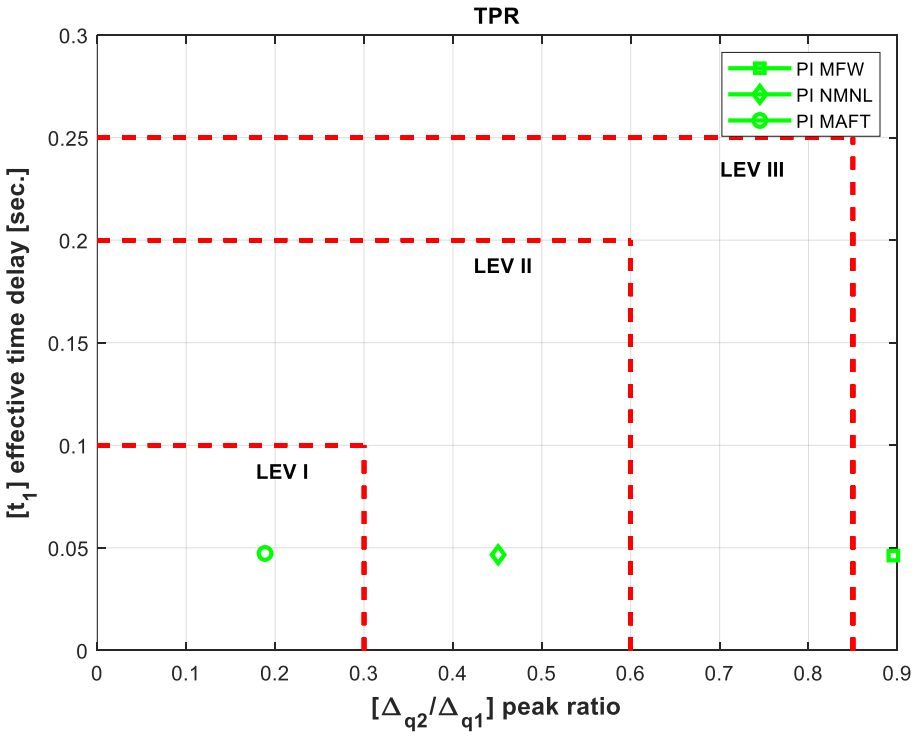

Figure 77. Fist alternative controller TPR results

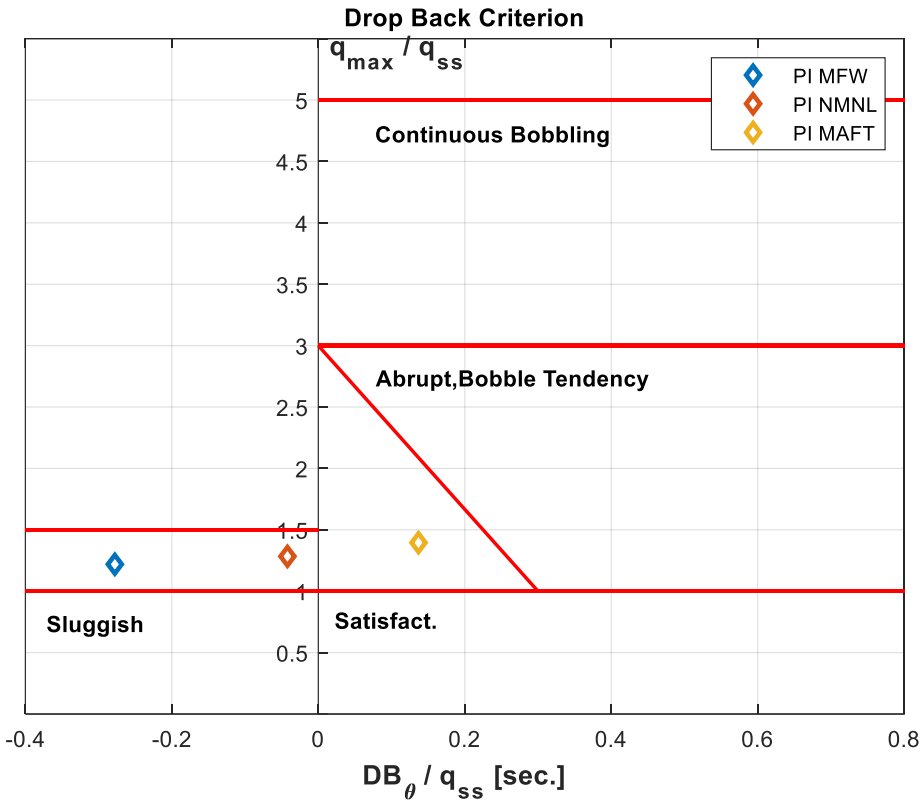

Figure 78. First alternative controller drop-back results

According to Figure 76 pitch attitude bandwidth results are in level 1 region for three CG_X position configurations without controller parameter scheduling w.r.t CG_X position information.

Effective time delay and effective rise time results are satisfactory for three CG_X position configurations. Transient peak ratio results vary from level 1 region to beyond level 3 region as CG_X moves forward.

5.2.1.3 PIO Requirements

Pitch attitude bandwidth and pitch rate overshoot, Gibson average phase rate and gain phase templates for first alternative controller are given to determine level I PIO susceptibility.

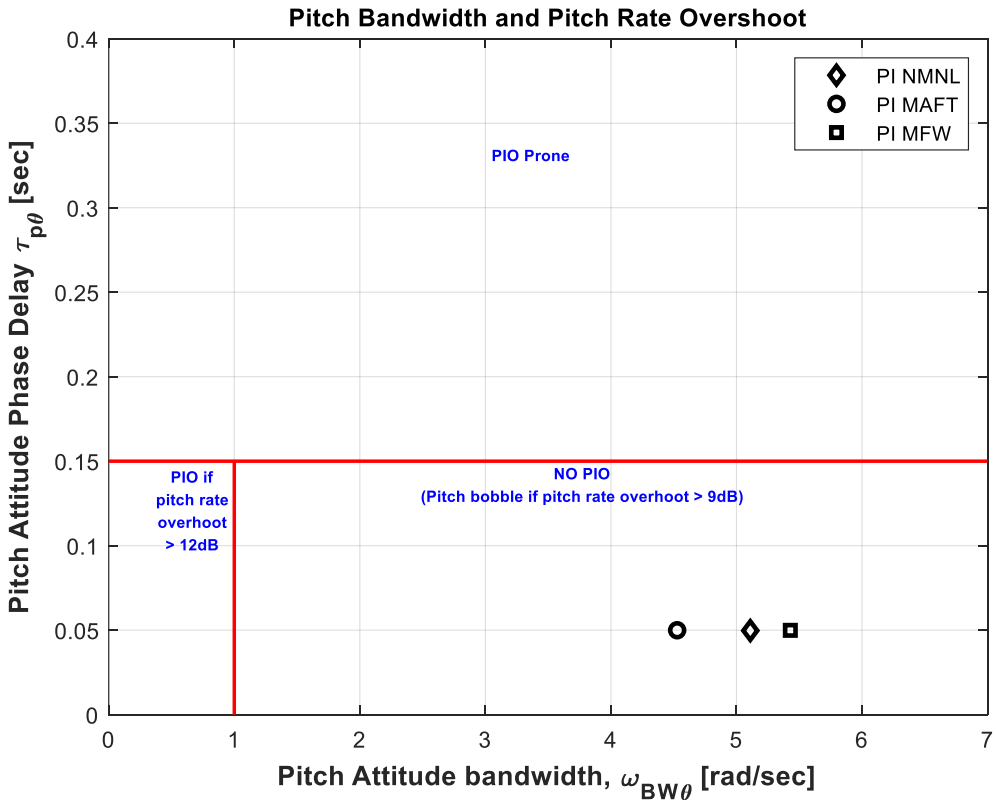

Figure 79. First alternative controller pitch attitude bandwidth and pitch rate overshoot results

According to Figure 79 first alternative controller satisfies pitch attitude bandwidth and pitch rate overshoot requirement in case of CG_X position information fault.

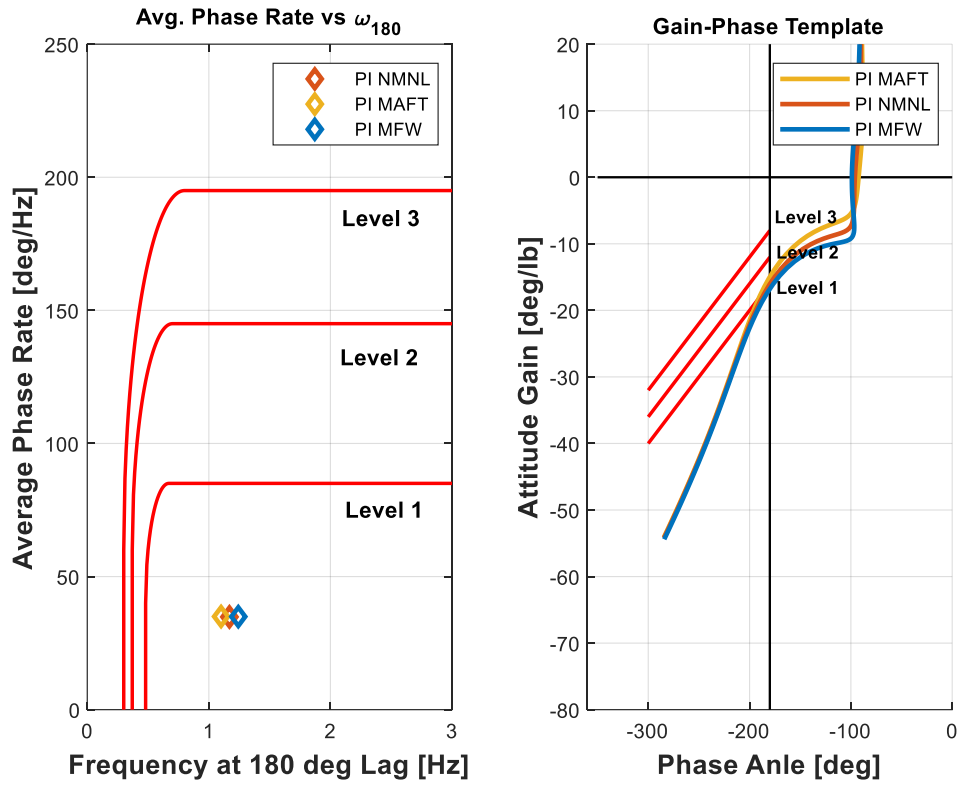

Figure 80. First alternative controller Gibson average phase rate and gain-phase template results

According to Figure 80 first alternative controller is level I PIO free in terms of Gibson average phase rate and gain-phase template. Pitch attitude frequency loci intersects with level 2 region around PIO frequency, where $\varphi = -180\, deg$, but after than moves toward level1 region.

*φ represents phase angle of pitch attitude to stick transfer function.

5.2.2 Stability Assessment

Stability robustness is defined with respect to the classical stability margins. Nichols exclusion zone is used to investigate relative stability. Absolute stability, Hurwitz Stability, is assessed with Nyquist diagram. Relative and absolute stability results are given in Figure 81 and Figure 82 for first alternative controller, in case of CG_X position information fault.

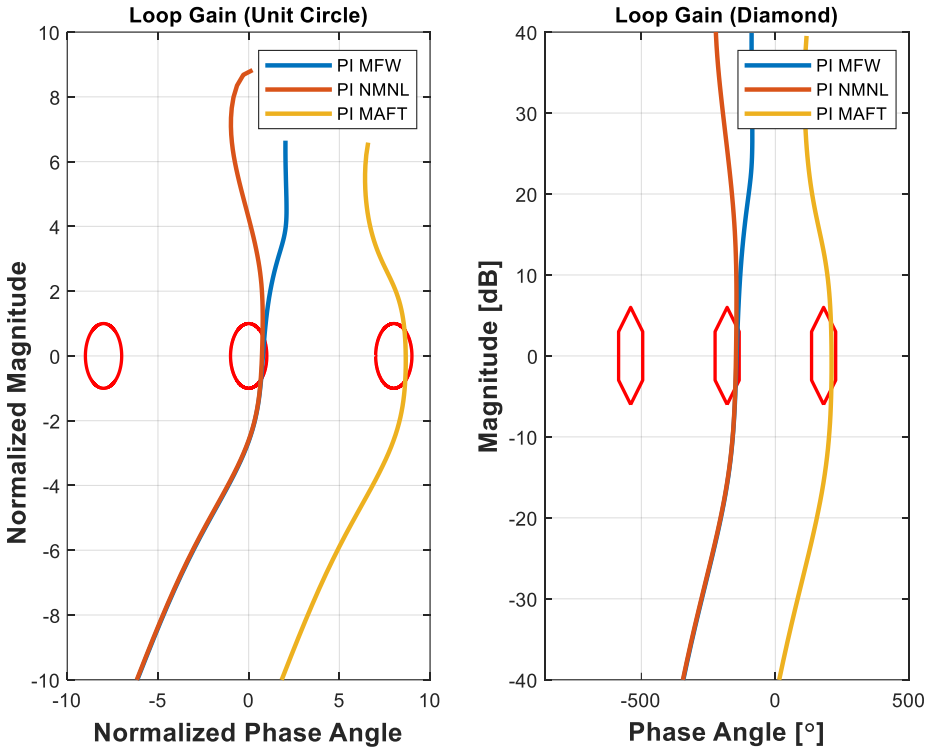

Figure 81. First alternative controller relative stability assessment

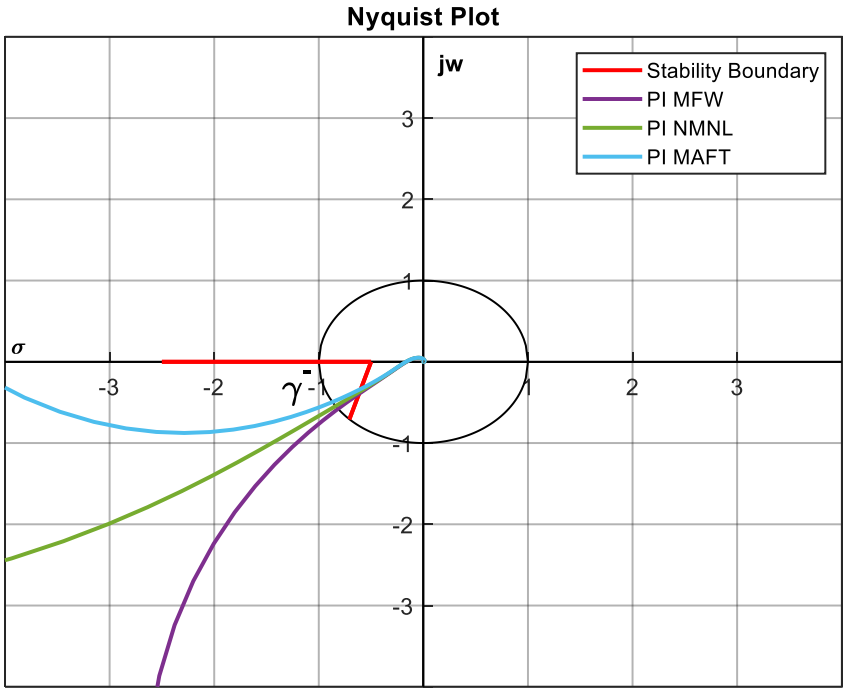

Figure 82. First alternative controller absolute stability assessment

According to Figure 81 & Figure 82 relative stability requirements are not satisfied by the first alternative controller without controller parameters scheduling w.r.t CG_X position information. Absolute stability is ensured but stability margin is not satisfied for most aft CG_X position. Classical stability margins are given in Table 26.

Table 26. First alternative controller relative and absolute stability margins

Configuration	**GM**	**PM**	**SM**
MFW	14.7811	35.3491	0.5506
NMNL	14.6344	32.9703	0.5326
MAFT	14.6158	29.6470	0.4965

5.3 Alternative Controller No2

Performance and stability assessment results for the second alternative controller are given in this chapter.

5.3.1 Performance Assessment

Reference model tracking capability analysis, handling qualities requirements and PIO requirements checks are performed in the scope of performance assessment.

5.3.1.1 Reference Model Tracking Capability

Reference model tracking capability is assessed in both time and frequency domain.

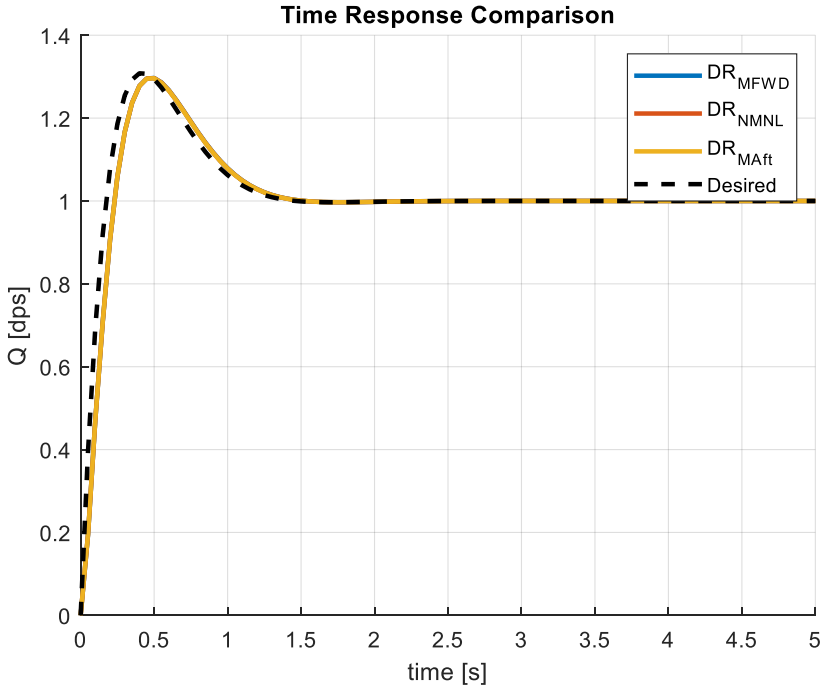

Figure 83. Second alternative controller time response comparison

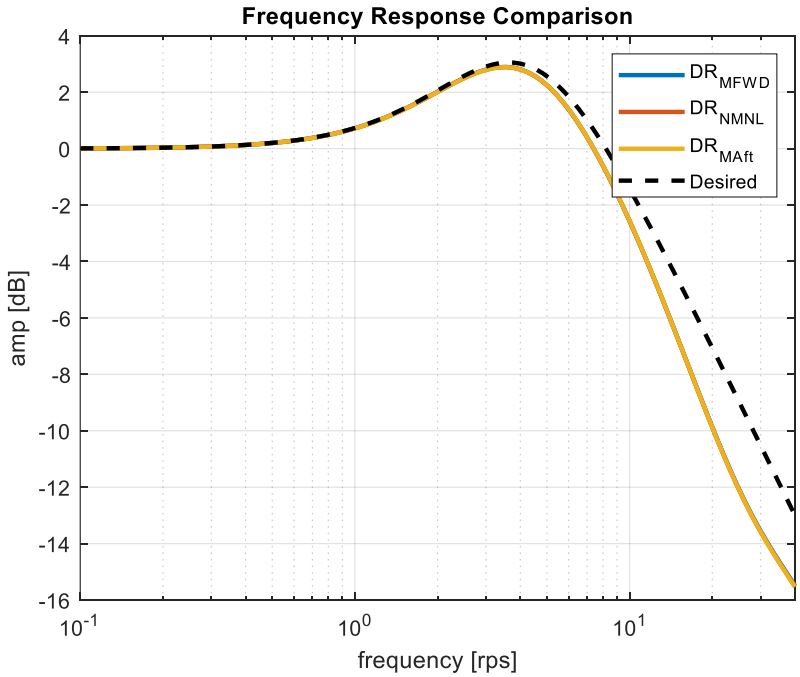

Figure 84. Second alternative controller frequency response comparison

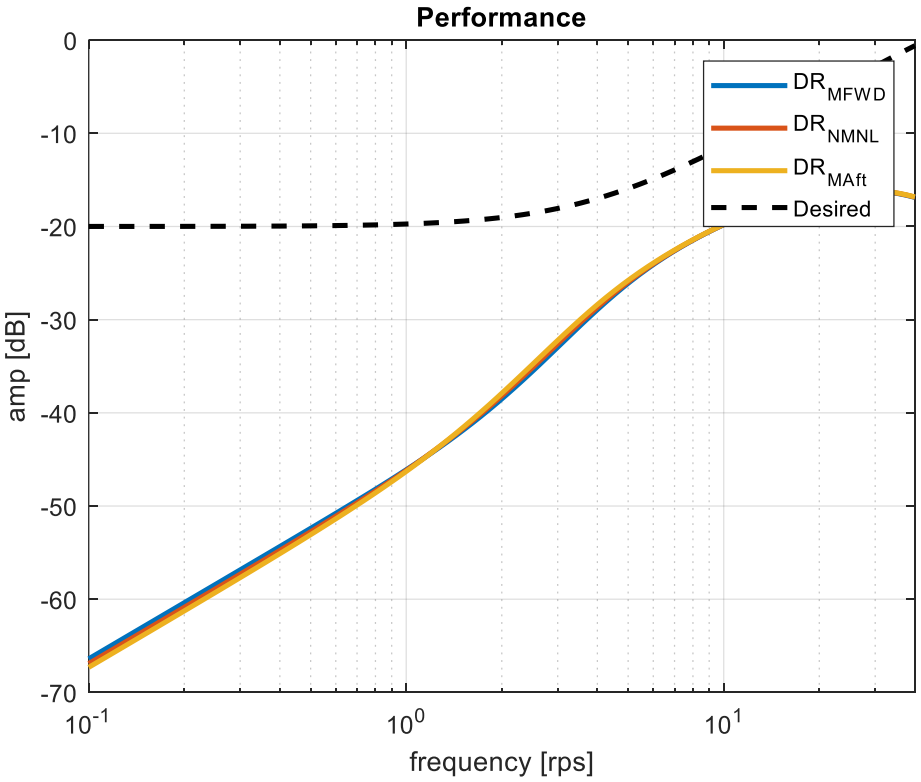

Figure 85. Second alternative controller reference model mismatch

According to Figure 83, Figure 84, and Figure 85 exact reference model tracking is succeeded with the second alternative controller in case of CG_X position information fault.

Disturbance rejection capability of the second alternative controller is also tested. In the scope of disturbance rejection capability analysis, a pitch tracking task is performed where reference pitch rate values vary with time. Linear parametric varying model for specific flight condition, which is defined for performance assessment (10kft, 0.7 Mach), is used in the scope of this analysis. Variation of CG_X position during the pitch tracking task and comparison of pitch rate responses are given in Figure 86 and Figure 87, respectively.

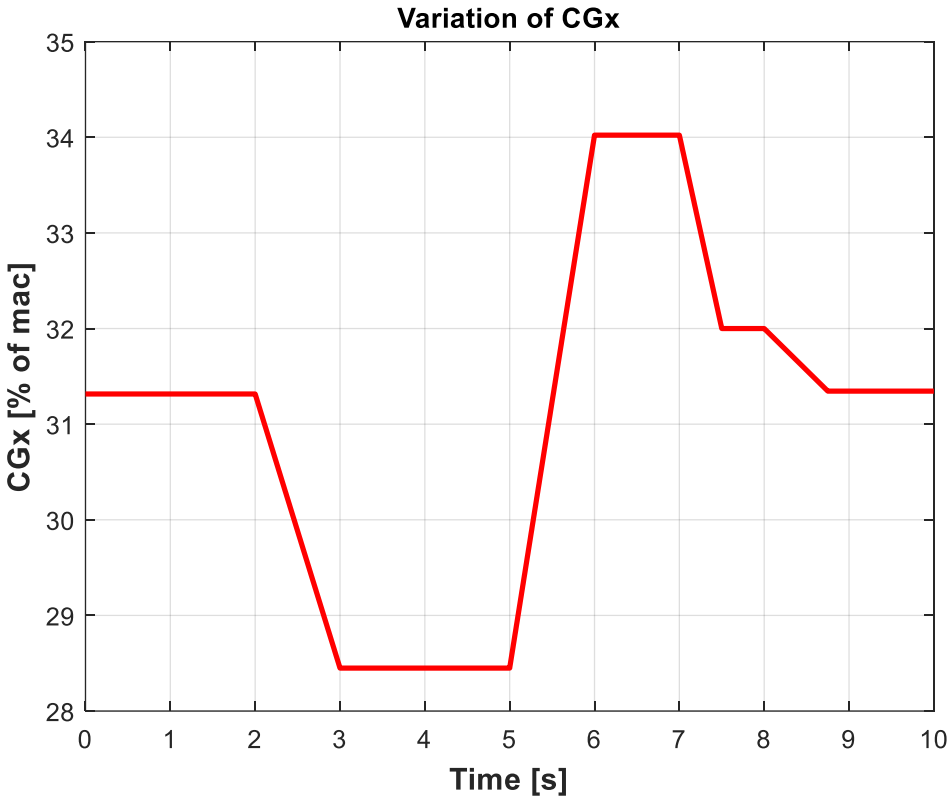

Figure 86. Variation of CG_X position during pitch tracking task

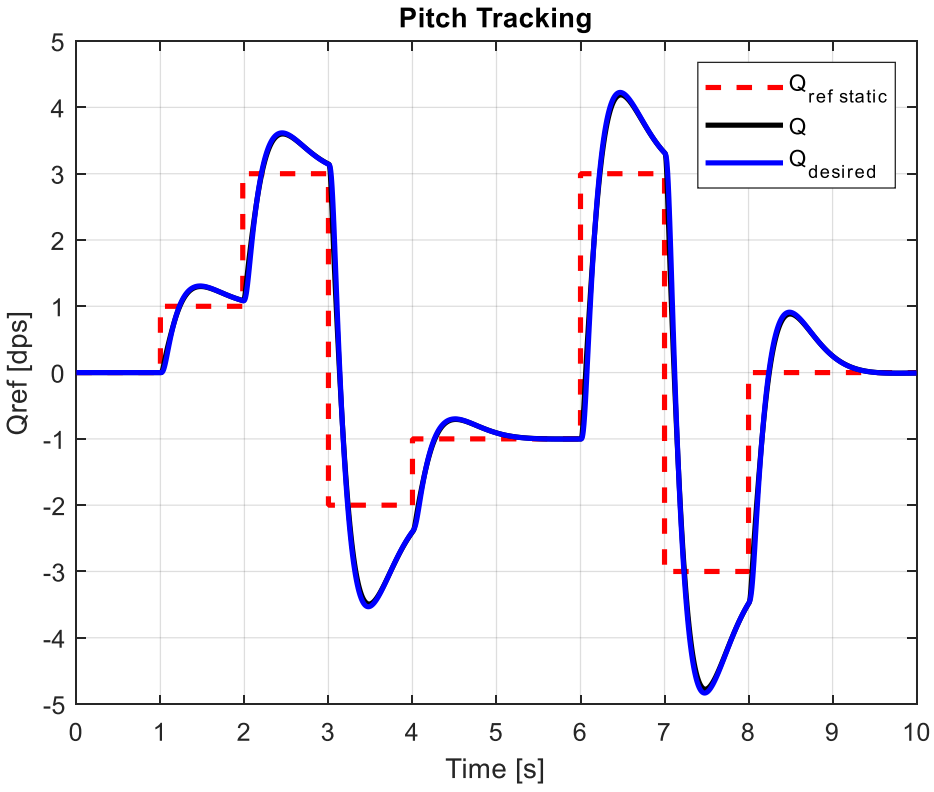

Figure 87. Second alternative controller pitch tracking task

According to Figure 87 desired pitch tracking response is reached in case of varying CG_X position without any controller parameter adaptation mechanism, which is a result of satisfactory disturbance rejection capability.

5.3.1.2 Handling Qualities Requirements

Pitch attitude bandwidth, TPR, and drop-back requirements results are given in the scope of second alternative controller handling qualities assessment.

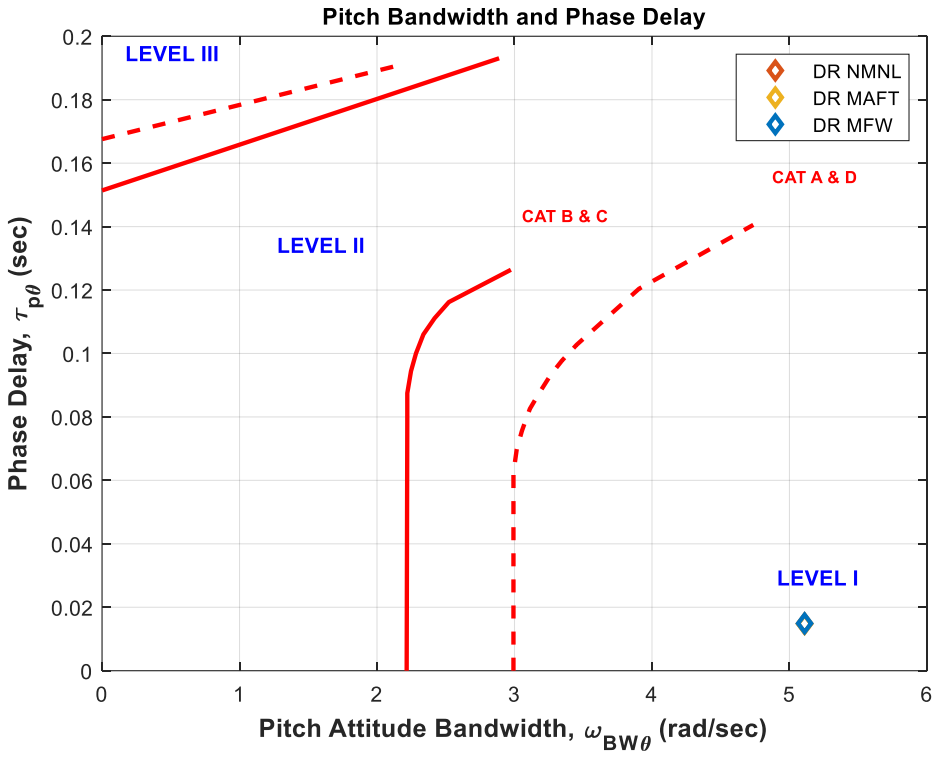

Figure 88. Second alternative controller pitch attitude bandwidth results

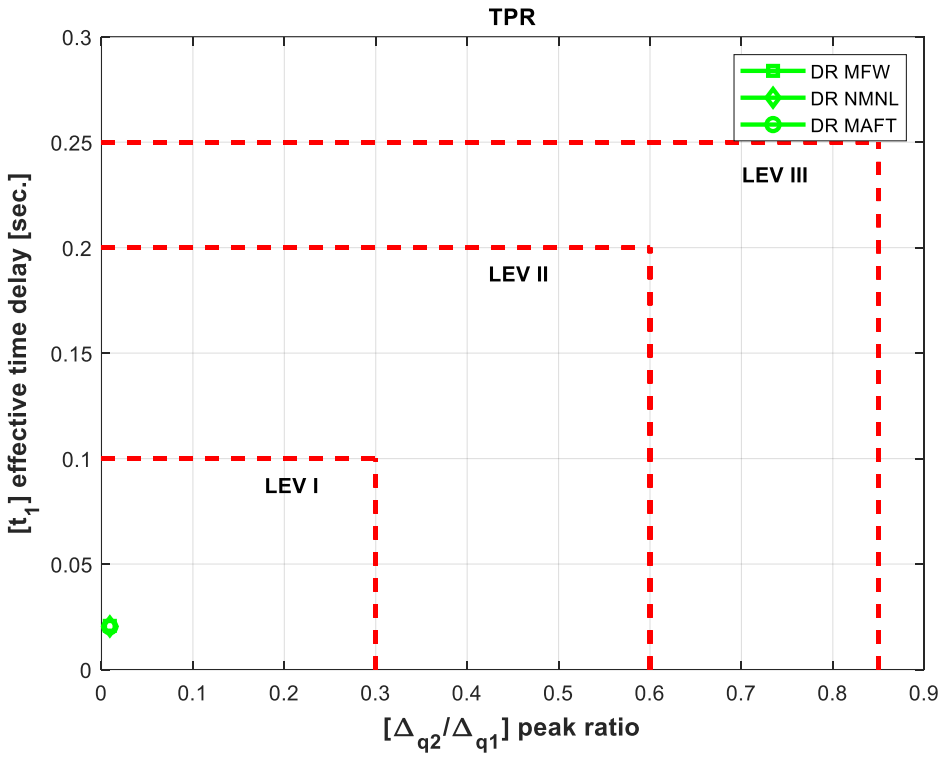

Figure 89. Second alternative controller TPR results

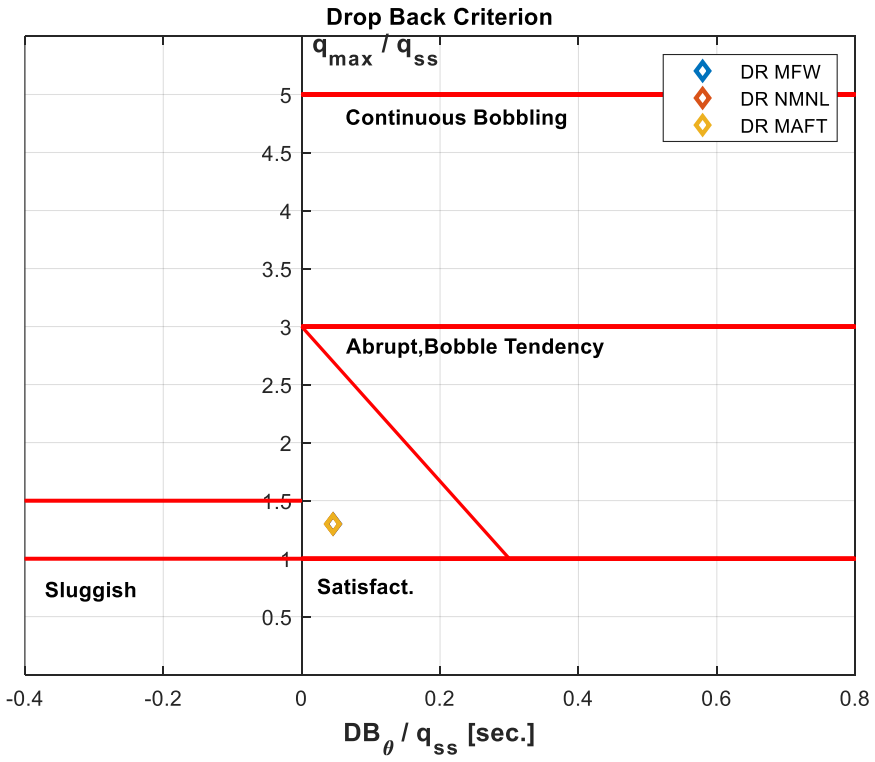

Figure 90. Second alternative controller drop-back results

According to Figure 88,Figure 89, and Figure 90 handling qualities requirements are satisfied for CG_X position configurations. It is obvious that exactly same values are reached for both time domain and frequency domain requirements. This is another indication of exact match with reference model in both time and frequency domain.

5.3.1.3 PIO Requirements

Pitch attitude bandwidth - pitch rate overshoot, Gibson average phase rate and gain phase templates for the second alternative controller are given to determine level I PIO susceptibility.

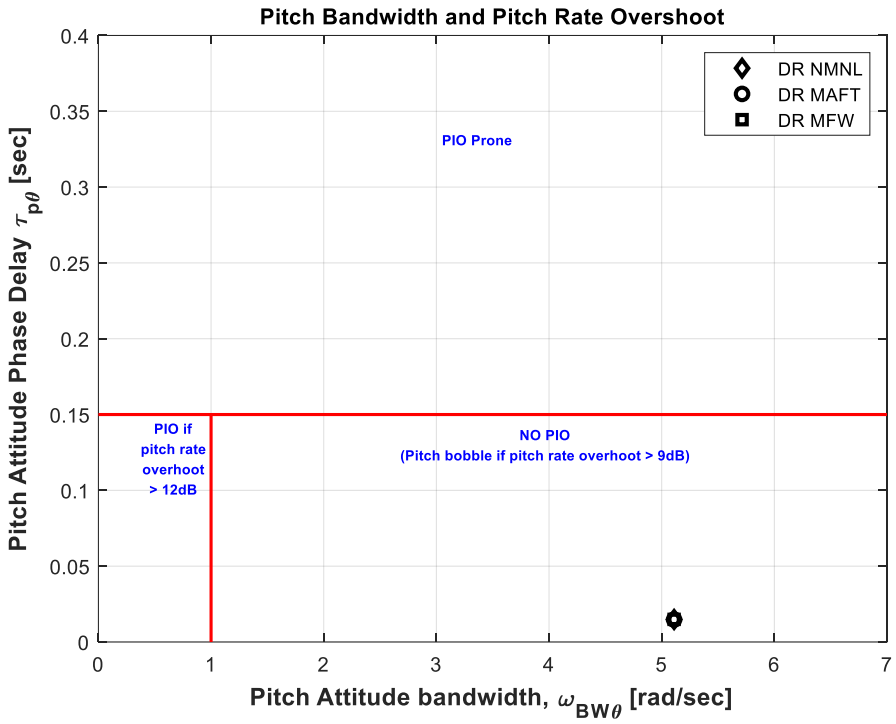

Figure 91. Second alternative controller pitch attitude bandwidth and pitch rate overshoot results

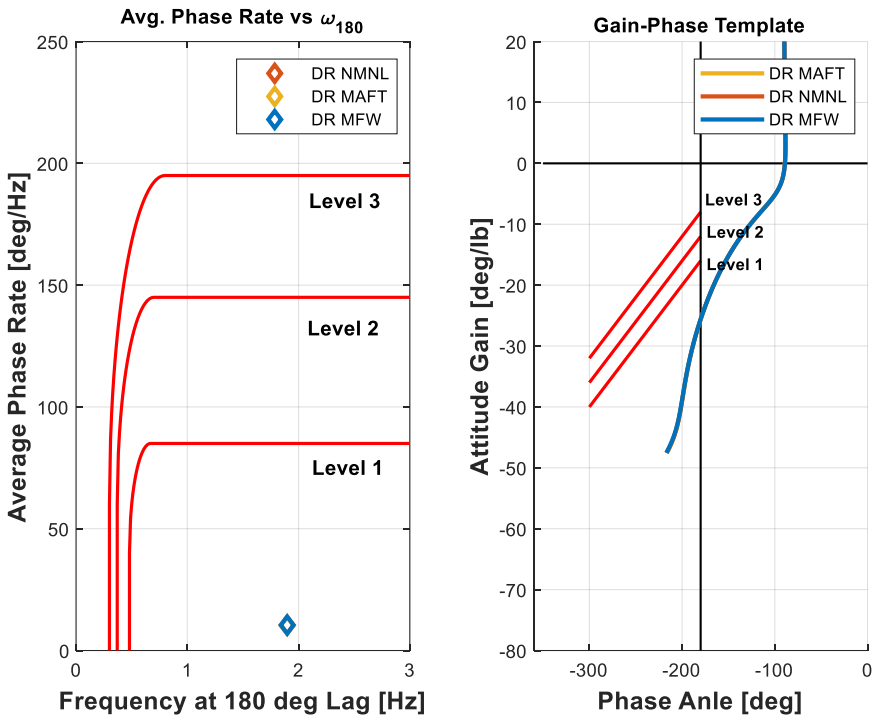

Figure 92. Second alternative controller Gibson average phase rate and gain-phase template results

According to Figure 91 and Figure 92 the second alternative controller is level I PIO free in terms of selected PIO requirements. The exact same characteristics in terms of selected PIO requirements are observed for three CG_X position configurations. It is a proof of exact reference tracking in frequency domain.

5.3.2 Stability Assessment

Nichols exclusion zone and Nyquist diagram are used to assess relative and absolute stability of the second alternative controller.

Result of relative and absolute stability assessments of the second alternative controller are given in Figure 93 & Figure 94.

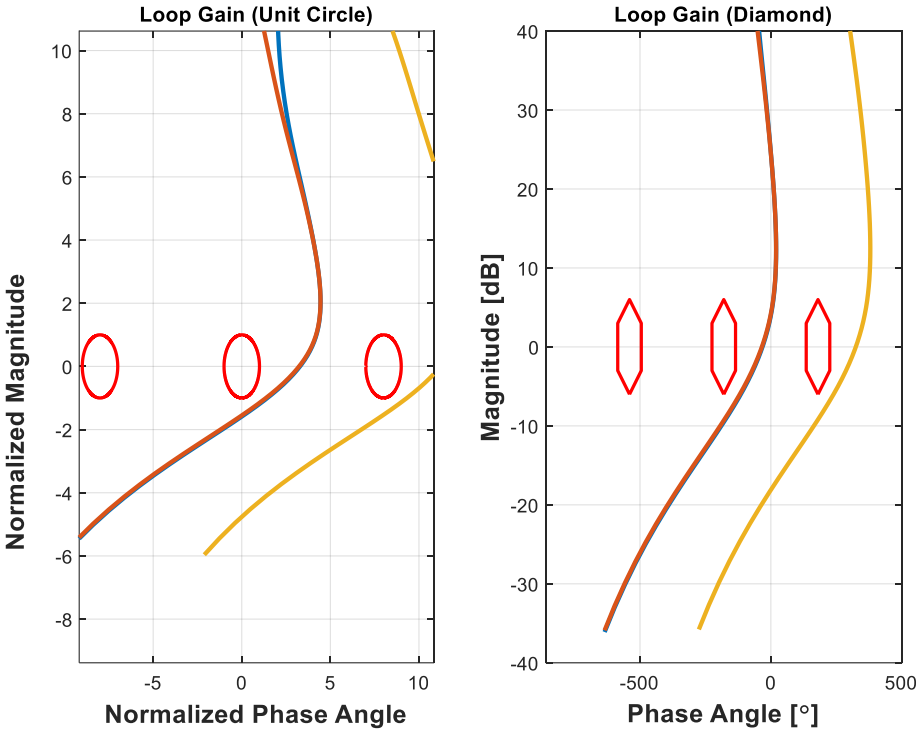

Figure 93. Second alternative controller relative stability assessment

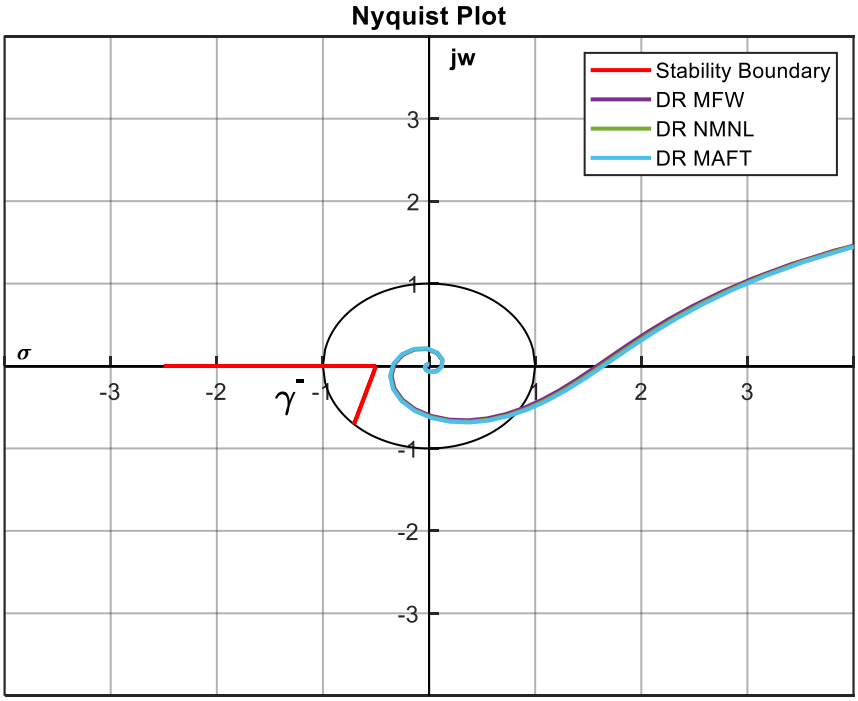

Figure 94. Second alternative controller absolute stability assessment

According to Figure 93 and Figure 94 stability robustness requirements are satisfied by the second alternative controller without parameters scheduling w.r.t CG_X position information. Classical stability margins are given in Table 27.

Table 27. Second alternative controller relative and absolute stability margins

Configuration	GM	PM	SM
MFW	8.5649	147.7618	0.6572
NMNL	8.3526	145.5068	0.6491
MAFT	8.2399	144.2980	0.6447

6. CONCLUSION

In the scope of the thesis, design of a longitudinal flight control algorithm which satisfies predefined stability and performance robustness requirements in case of CG_X position information fault is aimed.

Anatomy of the nonlinear aircraft model which is used in scope of the thesis was explained. Definition of fault and detection mechanism were made. Control algorithm design requirements in terms of stability and performance were given. Design methodology of base controller, which suffers stability and performance robustness in case of CG_X position information fault, and two alternative controllers were explained.

Finally designed controllers, base controller and two alternative ones were assessed in terms of performance and stability, in case of CG_X position information fault at specific flight condition. In case of CG_X position information fault, base controller parameters are not scheduled w.r.t CG_X position information anymore, nominal CG_X position configuration parameters are used. Alternative controllers were designed such that they don't require CG_X position information.

Reference model tracking capability of the base controller is not sufficient at off design points. Slow tail like response is observed at off design points. Error

between reference model and the response at off design points are above the predefined mismatch limit.

Handling qualities requirements are satisfied expect drop-back requirement, by the base controller. Most forward CG_X position configuration drop-back result is in sluggish region and most aft CG_X position configuration result is suffering from pitch bobbling.

The base controller is level I PIO free w.r.t predefined PIO requirements. All the PIO requirements are satisfied.

Stability robustness is succeeded by the base controller. Relative and absolute stability requirements are satisfied.

The first alternative controller is based on the same architecture with the base controller. A different design methodology is followed with this structure. The purpose is to improve reference tracking capability.

Although improvement in slow tail like response observed, pitch rate response reaches to steady state value faster, required reference tracking capability is not reached.

Handling qualities requirements, except pitch attitude bandwidth requirement, are not satisfied by the first alternative controller. Moreover, improvement in slow tail like response causes pitch rate damping ratio to decrease. Transient peak ratio of the pitch rate response at off-design points, most forward and most aft CG_X positions respectively, are in level II region and level III region. Drop-back requirement is not satisfied also, the results for off-design points are in sluggish and pitch bobbling regions respectively.

The first alternative controller is level I PIO free w.r.t predefined PIO requirements.

Relative stability is not satisfied by the first alternative controller. Phase margins are below the predefined limits. The main reason of this situation is that; in first alternative controller integrator mode is assigned to higher value as compared to the base controller. Phase lag comes with integration action increases and phase

margin decreases. Optimization algorithm follows a design methodology such that increasing disturbance rejection capability by increasing integrator mode. This methodology improves slow tail like response but disturbs transition response on the other hand.

The second alternative controller satisfies all the performance requirements. Exact refence model tracking is reached via disturbance rejection controller. Desired handling qualities are satisfied with exact reference model tracking. Gain crossover frequency of the second alternative controller loop gain is higher as compared to base and the first alternative controllers. High gain crossover frequency enables disturbance rejection up to higher frequencies , it also helps to explain disturbance rejection capability of the second alternative controller.

The second alternative controller is level I PIO free in terms of predefined PIO requirements.

Relative and absolute stability is sustained by the second alternative controller in case of CG_X position information fault.

By taking all the result into the consideration the second alternative controller is the most successful one in terms of both stability and performance. The power of the second alternative controller comes from parameter space approach and disturbance rejection capability. Stability is enhanced via parameter space approach for three CG_X position configurations. Eigen values which satisfy stability robustness requirements for three CG_X position configurations are found and assigned via stability augmentation system for nominal CG_X position configuration. A desired pitch rate handling quality model with these selected Eigen values is generated after then. The purpose is to sustain desired pitch rate characteristics for three CG_X position configurations without controller parameter scheduling w.r.t CG_X position. Finally reference model tracking is reached with disturbance rejection controller. In this way desired handling qualities are directly assigned.

Explicit model following with disturbance rejection controller structure is efficient for flight control algorithm design problem. Desired handling qualities can be directly assigned in case of uncertainties. Varying flight condition parameters,

varying aircraft configuration, and various failures can be accepted as uncertainty or disturbance. Flight control algorithm requires scheduling or adaptation to provide nominal performance in case of these uncertainties and disturbances. These uncertainties and disturbances can be rejected with disturbance rejection controller architecture and flight control algorithm that satisfies predefined handling qualities requirement can be designed without controller parameter scheduling or adaptation mechanism.

6. REFERENCES

[1] W. Wright, H.P. Dayton, O. Susan, M.W. Dayton, The Wright Way: The Process of Invention, (n.d.).

[2] R. Storm, T. Benson, C. Galica, P. McCredie, Learning to Fly: The Wright Brothers' Adventure A Guide for Educators and Students with Activities in Aeronautics, (n.d.).

[3] H. Al-Lami, A. Aslam, T. Quigley, J. Lewis, R. Mercer, P. Shukla, The Evolution of Flight Control Systems Technology Development, System Architecture and Operation, 2015.

[4] Bjorn's Corner: Flight control - Leeham News and Analysis, (n.d.). https://leehamnews.com/2016/03/11/bjorns-corner-flight-control/ (accessed January 15, 2023).

[5] R. Islam, W.: Www, G. Capt, A. Garg, R.I. Linda, T. Chowdhury, Evolution of aircraft flight control system and fly-by-light flight control system International Journal of Emerging Technology and Advanced Engineering, 2008.

[6] C.R. Jarvis, Description and Flight Test Results of The NASA F-8 Digital Fly By Wire Control System, California, 1974.

[7] L. Zhong, M.C. Félix, A two-stage approach for managing actuators redundancy and its application to fault tolerant flight control, Chinese Journal of Aeronautics. 28 (2015) 469–477. https://doi.org/10.1016/j.cja.2015.02.004.

[8] A. Smerlas, I. Postlethwaite, D. Walker, M. Strange, J. Howitt, R. Horton, A. Gubbels, S. Baillie, Design and flight testing of an H-infinity controller for the NRC Bell 205 experimental fly-by-wire helicopter, Guidance, Navigation, and Control Conference and Exhibit. (1998). https://doi.org/10.2514/6.1998-4300.

[9] N. Singh, Reduction of linear dynamic systems using hankel norm approximation, Control and Intelligent Systems. 41 (2013) 189–196. https://doi.org/10.2316/Journal.201.2013.4.201-2265.

[10] P. Gahinet, P. Apkarian, Structured H∞ synthesis in MATLAB, in: IFAC Proceedings Volumes (IFAC-PapersOnline), IFAC Secretariat, 2011: pp. 1435–1440. https://doi.org/10.3182/20110828-6-IT-1002.00708.

[11] E. Prempain, I. Postlethwaite, Static $\mathcal{H}\infty$ loop shaping control of a fly-by-wire helicopter, Automatica. 41 (2005) 1517–1528. https://doi.org/10.1016/j.automatica.2005.04.001.

[12] K.M. Sobel, w. Yu, J.E. Piou, J. Cloutier, R. Wilson, Robust Eigenstructure Assignment with Structured State Space Uncertainty and Unmodelled Dynamics, Proceedings of American Control Conference. 3 (19991) 3137–3141.

[13] J. Ackerman, P. Blue, T. Bünte, L. Güvenç, D. Kaesbauer, M. Kordt, M. Muhler, D. Odenthal, Robust Control The Parameter Space Approach, Springer - Verlag, 2002.

[14] M.L. Kerr, C.Y. Lan, S. Jayasuriya, Non-sequential MIMO QFT control of the X-29 aircraft using a generalized formulation, International Journal of Robust and Nonlinear Control. 17 (2007) 107–134. https://doi.org/10.1002/RNC.1106.

[15] O.R. Reynolds, Design of A Subsonic Envelope Flight Control System for The F16 Vista Using Quantitative Feedback Theory, Air Force Institute of Technology, 1993.

[16] B.L. Stevens, F.L. Lewis, E.N. Johnson, Aircraft control and simulation: Dynamics, controls design, and autonomous systems: Third edition, 2016.

[17] Basic Air Data, (2022). https://www.basicairdata.eu/knowledge-center/background-topics/coordinate-system/ (accessed November 9, 2022).

[18] EXO, (2022). https://dodlithr.blogspot.com/2011/09/airplanes-stability-axis.html (accessed November 9, 2022).

[19] Earth Atmosphere Model - Metric Units, (n.d.). https://www.grc.nasa.gov/www/k-12/airplane/atmosmet.html (accessed November 11, 2022).

[20] Similarity Parameters, (n.d.). https://www.grc.nasa.gov/www/k-12/airplane/airsim.html (accessed November 11, 2022).

[21] L.T. Nguyen, M.E. Ogburn, W. p. Gilbert, K.S. Kibler, P.W. Brown, P.L. Deal, Simulator Study of Stall/Post-Stall Characteristics of a Fighter Airplane With Relaxed Longitudinal Static Stability, 1979.

[22] Boeing Co., Background Information and User's Guide for MIL-F-9490, 1975.

[23] G.E. Cooper, R.P. Harper, The Use of Pilot Rating in the Evaluation of Aircraft Handling Qualities, 1969.

[24] D.G. Mitchell, D.H. Hoh, B.L. Aponso, D.H. Klyde, MIL STD 1797A, 1994.

[25] R.C. Nelson, Flight Stability and Automatic Control, McGraw-Hill, 1989.

[26] T.J.J. Lombaerts, Q.P. Chu, J.A. Mulder, D.A. Joosten, Modular flight control reconfiguration design and simulation, Control Eng Pract. 19 (2011) 540–554. https://doi.org/10.1016/j.conengprac.2010.12.008.

[27] J. Gibson, Development of a Design Methodology for handling Qualities Excellence in Fly by Wire Aircraft, 1999.

[28] J.B. Witte, An Investigation Relating Longitudinal Pilot-Induced Oscillation Tendency Rating to Describing Function Predictions for Rate-Limited Actuators, Air Force Institute of Technology, 2004.

[29] D.J. Moorhouse, R.J. Woodcock, MIL STD 8785C, 1982.

[30] B. Gökçeaslan, O. Albostan, Fault Tolerant Longitudinal Robust Flight Control Algorithm Design with All Stabilizing Multi Objective Parameter Synthesis, SCITECH . (2022). https://doi.org/10.2514/6.2022-2035.